Yong-Su Na

Modelling of Current Profile Control
in Tokamak Plasmas

Technische Universität München

Max-Planck-Institut für Plasmaphysik

Modelling of Current Profile Control in Tokamak Plasmas

Yong-Su Na

Abstract

In thermonuclear fusion research using magnetic confinement, the tokamak shows the best results today. However, tokamak operation is inherently pulsed. Recently, so-called advanced scenarios are being developed for steady state operation of tokamak experiments by maximising the self-generated current in the plasma at high plasma pressures. The control of the shape of the current density profile in the plasma is key to improve confinement and stability in these advanced scenarios.

This thesis focuses on the modelling of the evolution of the current profile in advanced scenarios at the ASDEX Upgrade tokamak and the JET tokamak. This is used to prepare a model for real-time feedback control of the current density profile. These models are verified by simulations and dedicated experiments in ASDEX Upgrade using current drive by neutral beam injection.

The majority of the work presented here is based on simulations with a transport code (ASTRA), which includes a model for the ohmic current, a model for bootstrap current, a model for the current driven by external actuators (neutral beam injection). In addition, a model for energy transport (Weiland transport model) is employed. Simulations are performed for advanced scenarios to validate the models used by comparing to experimental observations. The results show that ASTRA simulations describe the evolution of current density profile and temperature profiles appropriately in advanced scenarios.

For modelling of a system used for real-time control, a database is required to calculate transfer functions that describe relationship between input signals (neutral beam power from different beam sources) and output signals (total plasma pressure and current density profile). The ASTRA code is used for the simulations to create the database. Model structures suited for systems with many input and output signals are used to calculate a model for current profile control in ASDEX Upgrade and JET.

A validation of identified models is carried out using a simulated step response of the neutral beam sources with ASTRA and dedicated experiments with measurements of the current density profile. Both confirm the validity of the models obtained for current density profile control. However, the observations that with neutral beam injection, in some plasma condition, the changes of the current density profile are not in agreement with model calculations are discussed.

The approach developed here is applicable to different actuators for current profile or pressure profile control in existing and future experiments.

Acknowledgements

I would like to give some appreciation to those who contributed to this thesis.

First of all, I would like to express my deep gratitude to my scientific advisor, Dr. George Sips, who not only gave me freedom during the research but also guided me with valuable discussions and provided me with helpful advice.

I would like to express my heartfelt thanks to my academic advisor, Prof. Dr. Rolf Wilhelm, for his kindness and understanding throughout my thesis work. I am deeply grateful to my friend, Dr. Gerhard Raupp, for providing me the opportunity to work with the ASDEX Upgrade team and for making my stay in Germany comfortable.

I am also grateful to the people at ASDEX Upgrade, especially Dr. Jörg Hobirk for his guidance on ASTRA simulations and his useful advice. In addition, I would like to thank both Dr. Grigory Pereverzev for guidance on the ASTRA code and Dr. Wolfgang Treutterer for guidance on system modelling and controller design using MATLAB. I would like to thank Prof. Dr. Michael Kaufmann, Prof. Dr. Hartmut Zohm, Prof. Dr. Sibylle Günter and Dr. Otto Gruber for their valuable suggestions and fruitful discussions. I would like to express my appreciation to my colleagues Dr. Giovanni Tardini, Doris Merkl, Jasmine Shirmer and Dr. Si-Woo Yoon.

I thank my colleagues working in Task Force S2 and T at JET, particularly Dr. Xavier Garbet, who helped me become very quickly accustomed to the environment of JET and gave me useful suggestions. In addition, I would like to thank Dr. Xavier Litaudon, Dr. Didier Moreau, Dr. Tuomas Tala and Dr. Emmanuel Joffrin for valuable discussions.

A special thanks I would like to give to the secretaries in IPP, especially Frau Gabriele Daube and Lucy Scoones who helped me with administrative work.

In addition, I would like to express my gratitude with all my heart for the support of my family over the years. Finally and most of all, I thank you, God, from the bottom of my heart who allows me to breathe in this world and allows me to meet and to fall in love with my fiancée, Hey-Won whom I cannot exchange with anything in the universe.

Contents

petite et dabitur vobis quaerite et invenietis pulsate et aperietur vobis

omnis enim qui petit accipit et qui quaerit invenit et pulsanti aperietur

Matthew 7:7-8
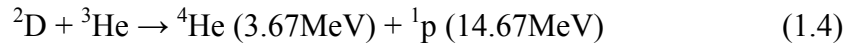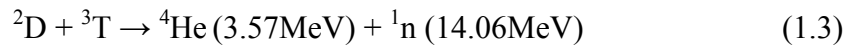
Chapter 1

Introduction

The world's energy consumption increases significantly due to the population explosion and an increasing standard of living. It is anticipated to double or even to triple within the next 50 years. There are many different ways to face this need. However, conventional energy sources entail several problems; resources of fossil fuels are being depleted and they pose a serious environmental threat.

Nuclear energy through fission can provide energy and has minimal emissions to air and water. However, long term, safe disposal of nuclear waste and nuclear weapons proliferation are the main obstacles for widespread use of nuclear fission. Renewable energy sources, such as solar, wind, geothermal energy, are under intensive research investigation. However, they have also limitations due to strong daily and seasonal variations in the primary source of the energy until a proper method for energy storage is found.

Consequently, it is necessary to develop an alternative abundant energy source, which is able to overcome all these drawbacks. It is considered that nuclear fusion meets these rigorous requirements. Nuclear fusion has potentially nearly inexhaustible resources, is environment friendly, inherently safe since any malfunction results in a rapid shutdown (the worst possible accident in a fusion reactor would not lead to evacuation of people living nearby). Long-term waste disposal can be avoided as the radioactivity of the reactor structure, caused by the neutrons, could decay within several tens of years by careful selection of low activation construction materials. However, to exploit the reaction, high technology is required, which makes nuclear fusion expensive compared to conventional energy sources.

1.1 Thermonuclear Fusion

The goal of controlled nuclear fusion research is to generate energy by combining two low-mass nuclei to form a more massive nucleus. This reaction is the power source of the sun and other stars, where confinement and heating occurs through compression under enormous gravitational forces. Possible candidates for using fusion energy on earth are the following reactions (the energy released is given in parentheses):

$$^2D + {}^2D \rightarrow {}^3T \ (1.01 \text{Mev}) + {}^1p \ (3.03 \text{MeV}) \qquad (1.1)$$
$$^2D + {}^2D \rightarrow {}^3He \ (0.82 \text{MeV}) + {}^1n \ (2.46 \text{MeV}) \qquad (1.2)$$
$$^2D + {}^3T \rightarrow {}^4He \ (3.57 \text{MeV}) + {}^1n \ (14.06 \text{MeV}) \qquad (1.3)$$
$$^2D + {}^3He \rightarrow {}^4He \ (3.67 \text{MeV}) + {}^1p \ (14.67 \text{MeV}) \qquad (1.4)$$
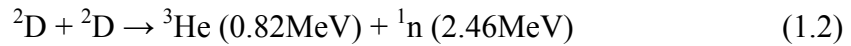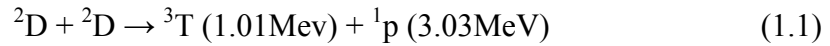
By far the most accessible and promising reaction for fusion reactors is a reaction in which Deuterium (D) and Tritium (T) fuse, producing a Helium nucleus (He) and a neutron (n). This reaction has the largest cross section at the lowest energy as shown in figure 1.1.
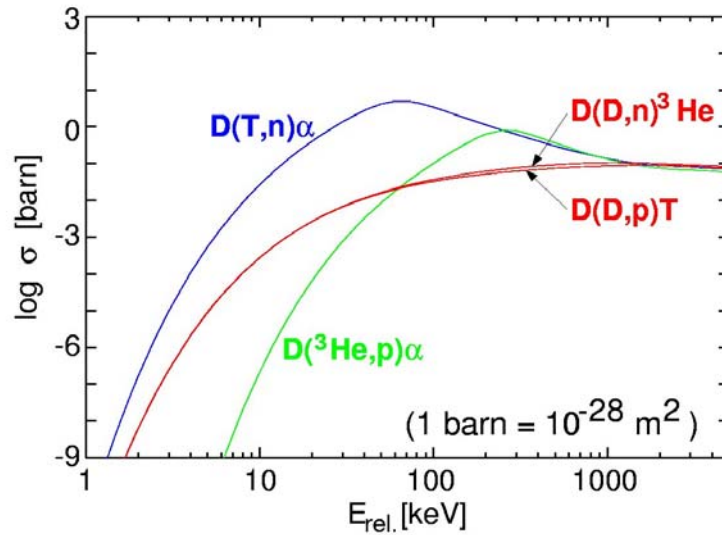

Figure 1.1. Cross section for the reactions D-T, D-D and D-^{3}He.
The two D-D reactions have similar cross sections.

For a fusion reaction to occur, however, the two nuclei have to overcome the prevailing repulsive Coulomb force. The nuclear force (strong interaction) is active only for

distances in the order of the nucleus dimensions (10^{-15}m). For larger distances, the repulsive Coulomb force dominates where potential wall is several 100keV. For example, a Deuterium and Tritium fuel mix must be confined for a sufficient period at a sufficiently high temperature in a state where ions and electrons are separated, called a plasma. For break-even, so-called Lawson criterion, the fusion energy released equals the amount of energy applied to heat the plasma; fusion gain $Q = 1$ (where $Q = P_{fus} / P_{in}$, in which P_{fus} and P_{in} are the fusion and input heating power, respectively) [1]. A step further is the fusion ignition, where the auxiliary heating can be turned off. For the Deuterium/Tritium reaction a necessary requirement, the so-called fusion triple product [1], for the ignition is:

$$n T \tau_E > 3 \times 10^{21}\, \text{m}^{-3}\text{keVsec} \qquad (1.5)$$

where n is the average density over the plasma volume, T the average temperature and τ_E is the energy confinement time; ratio between the energy in the plasma $W = 3/2(nT)$ and the input heating power P_{in}, i.e. $\tau_E = W/P_{in}$. The required temperature is in the order of $T=10^8$K, i.e. corresponding to about 100-200 million °C.

1.2 Tokamaks

Since an extremely high temperature is needed for confinement of a hot plasma is not a trivial problem. At present, two main approaches exist; inertial and magnetic fusion.
In inertial fusion, dense, hot plasma is produced and confined only for a very short time (nanoseconds) dictated by its inertia. For fusion reaction, powerful lasers or particle beams simultaneously converge on a tiny target (D-T fuel pellet), intensely heating the outside and squeezing the fuel into the centre of the pellet. The intense heat and pressure force the fuel to fuse, much like inside a star. The fuel pellet reaches the required temperature and finally the burning pellet ignites.
In magnetic fusion, hot plasmas are confined with magnetic fields. Contrary to inertial fusion, plasma densities are moderate, but the energy confinement time can be much longer, of the order of 1sec in the present fusion devices. Magnetic fusion exploits the fact that the charged particles in a magnetic field are tied to the field lines. In a toroidal device, the magnetic field lines are closed. However, in addition to the motion of particles along the field lines and the gyromotion around the field lines, the particles have a drift velocity in the direction perpendicular to the magnetic field and its gradient.

For this reason, additional magnetic field components are added, forming helically winding field lines around the centre of the torus. The helicity of the magnetic field lines prevents the particles from escaping confinement due to the perpendicular drift. In order to twist the magnetic field lines, two different principles are used; the stellarator and the tokamak.

In a stellarator, external coils produce both the toroidal and the poloidal magnetic field components, as shown in figure 1.2 (a). All the magnetic fields are controlled from outside and can flow continuously, thus steady state conditions are inherently present.
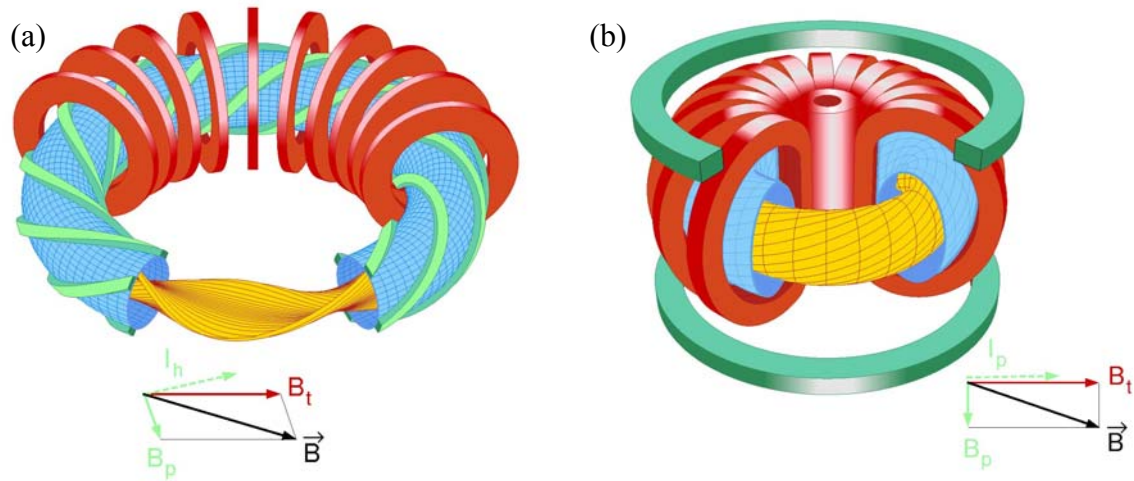
Figure 1.2. Schematic picture of a stellarator(a) and a tokamak (b), where B_t, B_p are toroidal, poloidal magnetic field, respectively. I_h, I_p are helical and plasma current, respectively.

In a tokamak, external coils produce the toroidal field component, while a toroidal current flowing within the plasma itself produces a poloidal field component. This current is produced by induction, the plasma acting as the secondary winding of a transformer with the primary winding in the centre of the torus. A schematic of a tokamak is shown in figure 1.2 (b). The magnetic field is axisymmetric in toroidal direction.

Tokamaks have proved to be very successful in improving the desired fusion plasma conditions in today's experiments, for example, in ASDEX Upgrade, at the Max-Planck-institute for plasmas physics in Garching, Germany and in JET, a European experiment, the largest experiment worldwide, sited in Culham, United Kingdom (both are described in §1.6).

1.3 Motivation and Background of the Thesis

As mentioned in previous section, a tokamak has an inherent drawback; pulsed operation. While a stellarator may principally run steady state, in a tokamak a transformer can induce the (dc-) plasma current only during a finite time. For steady state operation of a tokamak, full non-inductive current drive is required. However, present external current drive tools such as Radio-Frequency (RF) resonance heating or Neutral Beam Injection (NBI) have such a low current drive efficiency (ratio of driven current and applied power) that when used to sustain the plasma current, the electrical power requirements for the current drive systems would be comparable to the electrical output power of typical fusion power plant. Therefore, a high fraction of the plasma current should be provided by self-generated current (the neoclassical bootstrap current [2]) in the plasma for steady state operation. A bootstrap fraction of over 90% of the plasma current, together with current drive by external heating such as NBI, would allow an economically viable, steady state (not pulsed) operation of the tokamak [3]. Consequently, advanced scenarios with high pressure gradients such as Internal Transport Barrier (ITB) discharges or improved core confinement have been proposed where high bootstrap current fractions can be obtained. However, the experimental conditions required for these advanced scenarios with high pressure gradient cannot be sustained in long pulse duration without (some) control of the pressure profile and current density profile. This is because the shape of plasma current density profile, closely linked with stability and fusion performance of the plasma, evolves (away from the optimum conditions, described in §1.4) due to the inherent diffusion of the plasma current to the central region. Therefore, the shape of current density profile should be kept and modified as required (active control) to sustain these regimes with high pressure gradient.

To control the current density profile, pre-programmed feedforward control is not sufficient since the current density profile with contribution from the externally driven current, ohmic and bootstrap current also determines the transport in the plasma, which changes the profiles and the contributions to the current density profile. Hence, they form a closed non-linear internal feedback loop.

External current drive tools are used for feedback control of the current density profile. Particularly, NBI with tangential off-axis beam sources can be applied with reasonable current drive efficiency [4].

In the following sections, the background of the thesis will be described more detail.

1.4 Tokamaks: Standard and Advanced Scenarios

1.5 Current Drive

1.6 Tokamak Experiments: ASDEX Upgrade and JET

1.7 Identification of Current Density Profile Using Motional Stark Effect Diagnostics

1.4 Tokamaks: Standard and Advanced Scenarios

As described above, advanced scenarios in tokamaks are being developed to accomplish the ultimate objective of fusion energy research; the demonstration of a steady state, high gain fusion plasma producing reactor-level fusion power. Advanced scenarios are developed with an aim of improving the confinement and stability over standard discharges in tokamaks called H-modes [5]. First, the background for this standard scenario is given, followed by a description of several types of advanced scenarios.

Standard Scenario: H-mode

H-modes have already improved confinement over so-called L-mode plasmas due to a transport barrier at the edge of the plasma. This is achieved by modifying the magnetic fields nearest the walls to guide the particles escaping away from the main plasma to localised targets known as divertors. By combining results from several experiments, scaling laws for the measured energy confinement of tokamaks have been devised [6]. One of them is the so-called "ITER89-P scaling" for L-mode plasmas. For H-mode plasmas the enhancement factor H over the predicted energy confinement time using this scaling law is typically 2 ($H_{ITER89-P} \sim 2$). Alternately, a scaling law for H-mode was obtained called "ITER98(y,2) scaling" for which the enhancement factor of the energy confinement is typically 1 for stationary H-modes ($H_{98}(y,2) \sim 1$). In the edge region of stationary H-mode discharges, Edge Localised Modes (ELM's) are observed, periodic relaxations of the edge pressure gradient [7]. H-mode confinement is observed over a range of plasma densities and input powers. Sufficient input power needs to be applied to the plasma to access the H-mode, while H-mode conditions have an empirical upper limit for the average electron density in the plasma; the Greenwald density limit, $n_{GW}=10^{20} \cdot I_p / \pi a^2$ in MAm^2 with the I_p plasma current and the a minor radius [8]. The current profile for standard H-modes is peaked in the central region with positive

magnetic shear (where magnetic shear $s = (r/q)dq/dr$, $q = d\Phi/d\Psi$ with q the safety factor, the rate of change of toroidal flux (Φ) with poloidal flux (Ψ)). Therefore, q in the centre (q_0) is just below 1 while q at the plasma boundary (q_{95}, the safety factor at 95% of the plasma minor radius) is 3 or above.

Advanced Scenarios

The improvement in confinement and stability of advanced tokamak discharges is associated with modifications of the current density profile in most experiments [9-18]. In order to obtain a different current density profiles for advanced scenarios, the initial skin current profile of a tokamak plasma is utilised when the plasma current is build up. Furthermore, additional heating is used to slow down the current diffusion to the centre in the plasma. Consequently, current profiles with zero or negative (reversed) central magnetic shear can be produced. There are two types of advanced scenarios:
i) Plasmas with negative magnetic shear in the centre, in which ITB's can be formed for ions or electrons depending on the type of heating applied or both can be obtained simultaneously.
ii) Plasmas with low or zero magnetic shear in the centre, which have a moderate but significant increase of the plasma pressure in the core over standard H-modes.

i) Plasmas with Negative Magnetic Shear in the Centre

A hollow current density profile, i.e. a reversed q-profile (negative magnetic shear), is one of the key conditions that give rise to improved core confinement. Many tokamak experiments have reported favourable conditions for the formation of ITB's (see refs [9] to [13]). Central heating of the plasma is a pre-requisite for the formation of transport barriers in negative shear plasmas. In the case of ion ITB formation with NBI heating, this provides $T_i > T_e$, a peaked density profile, and strong variation of the toroidal rotation of the plasma from the centre to the edge, due to the momentum input of the NBI. These conditions reduce the turbulent radial transport for the ions. A positive feedback loop is created in which the reduction in transport allows the pressure gradient to build up, providing conditions for further reduction of the turbulent transport.
In spite of the increase in core pressure of ITB discharges, they have several drawbacks, namely, (i) a susceptibility to confinement-limiting MHD instabilities caused by a lack of current and pressure profile control both in the core and at the edge of the plasma,

which prevent the discharges reach steady state at high $\beta_N > 2.5$ (where β_N is normalised beta defined as $\beta_N = <\beta>aB_t/I_p$ in %mT/MA with $<\beta>$ the ratio of the average plasma pressure to the total magnetic pressure and B_t the toroidal field), (ii) they typically operate at low electron density not compatible with reactor requirements to limit the erosion of wall materials [19] and (iii) impurity accumulation in the plasma core is often observed, which implies a dilution of the fuel and hence a reduction of the potential fusion power for a given plasma pressure. Moreover, without sufficient external current drive, the current density profile continues to evolve to a profile without reversed shear, losing the ITB. Therefore, current profile control is essential for ITB discharges.

ii) Plasmas with Low or Zero Magnetic Shear in the Centre

These conditions are created by heating during the current rise phase. The heating reduces the current diffusion and delays formation of a $q = 1$ resonant surface. When q reaches unity in the centre, strong ($m=1$, $n=1$) fishbones occur, driven by NB injection, a consequence of the interaction of energetic particles with the resonant kink mode within the $q = 1$ surface. These fishbones prevent sawtooth activity (a periodic flattening of the pressure profile) by keeping q near or above 1 in the centre. This is a prerequisite for obtaining steady state and the good confinement properties of this scenario. For example, at ASDEX Upgrade this is called an improved H-mode scenario [20].

Similar improved core confinement can be obtained at high average densities of 80% to 90% of the Greenwald density limit. These discharges also have zero magnetic shear at the centre with $q(0)$ near 1 and typically have fishbones and applying high NB power. At ASDEX Upgrade, these discharges are called high β_N discharges [21].

Both low density and high density scenarios described above rely on MHD activity to sustain the q-profile. For reactor application of these regimes, the use of external current drive (< 20% of the total current) would be desirable to sustain q-profile as the occurrence of the MHD with dominant α-power heating in a reactor is uncertain.

The non-inductive drive of the plasma current can be optimised at low plasma current and high toroidal magnetic field. Although not directly relevant for fusion reactor application, these discharges obtain high bootstrap current fractions while relatively high values for β_p are achieved (called high β_p discharges in ASDEX Upgrade, where $\beta_p=2\mu_0<p>_A/<B_p>^2$ with $<p>_A$ the poloidal cross section averaged plasma pressure and $<B_p>$ the average poloidal magnetic field on the plasma boundary).

In this thesis, discharges with zero magnetic shear in the centre and discharges at low plasma current will be used to study current drive and current profile control.

1.5 Current Drive

In a tokamak, the toroidal plasma current (I_p) is driven inductively so that the plasma operates as secondary circuit of a transformer as shown in figure 1.2 (b). When a current flows in the primary circuit, it induces an electric field in the plasma and further the electric field creates the toroidal plasma current. The plasma current produced by this method (called induction) is called ohmic current. In order to maintain the electric field by means of induction, the current in the primary circuit system should be changed continuously. Since this is not possible in reality, a tokamak has to be driven in a pulsed mode. However, the pulsed tokamak operation mode has substantial drawbacks related to the fatigue stress produced by thermal cycling and the interruption of the fusion power output. Therefore, large efforts are devoted to developing non-inductive current drive methods that would enable a tokamak fusion reactor to operate continuously. In addition, such a system could be used to control the radial profile of the current density because the current density profile and safety factor q play a key role in plasma stability and confinement (MHD instabilities are observed at or near rational values of q).

In a tokamak plasma, the current drive methods are closely related to the heating methods. In general, the difference between the external plasma heating and the external current drive is that in heating, both toroidal directions are treated in an equal manner whereas in current drive, one toroidal direction is favoured over the other, though the current drive always contributes to heating. The basis for current drive is to introduce an asymmetry in the velocity distribution of the electrons or ions in the toroidal direction leading to a toroidal current.

There are several ways to generate this asymmetry. The methods to modify the current density profile can be divided into two different ways; (i) using external current drive with NB current drive or Radio-Frequency (RF) current drive and (ii) using inherently present current in the tokamak operation such as bootstrap current.

A current drive efficiency, γ_{th}, can be defined as the ratio of local parallel current density, j, and the local absorbed power density, p: $\gamma_{th} = j/p$. Different experiments are often compared using a scaled figure of merit, γ_{ex}, defined as $\gamma_{ex} = n_eRI / P$ in 10^{20}m^{-2} A/W, where n_e is the line-averaged density, R is the major radius of the plasma, I is the driven plasma current and P is the total absorbed power. For a large aspect-ratio (R/a) tokamak of circular cross section, $I \approx \pi a^2 j$ and $P = \pi a^2 \cdot 2\pi R \cdot p$ and j/p is proportional to $1/n_e$, hence γ_{th} is proportional to γ_{ex}.

The properties and current drive efficiencies of current drive methods mentioned above are described briefly as following:

● NB current drive: Current drive by tangential neutral particle injection. Good penetration, but would be limited by high core density in a fusion reactor. Expensive. γ_{ex} ~ 0.2 at T_e = 10keV with a linear increase with T_e [22]. The principle of NB current drive will be described further detail below.

● RF current drive: Current can be driven by asymmetric wave launching in the plasma. Energy is given to the plasma at the precise location where the radio waves resonate with the ion rotation, accordingly accelerate the plasma electrons to generate a plasma current [23].

a) Lower Hybrid (LH) current drive: Coupling the lower hybrid waves to electrons rather than to ions. Accessibility to high density regime is major concern. Useful for low density operation and start-up, widely used. For this technique, typically radio frequencies in the range 1-8GHz are used. γ_{ex} ~ 0.35-0.4.

b) Electron Cyclotron (EC) current drive: The simplest of the RF heating methods. Electrons heated directly. Attractive for start-up. Bootstrap current through electron heating. Accessibility should be checked. For this technique, typically radio frequencies in the range 100-200GHz are used. γ_{ex} < 0.1 at T_e = 10keV with a linear increase with T_e.

c) Fast Wave (FW) current drive: Fast magnetosonic (compressional Alfvén) wave to transport energy from the antenna to the absorption region of the plasma. Good penetration for high density region, however need more research for applying to the experiment. For this technique, typically radio frequencies in the range 20-80MHz are used. γ_{ex} ~ 0.1 at T_e = 10keV with a linear increase with T_e.

● Bootstrap current [2]: Generally proportional to β_p and pressure gradient. Need high β_p and low collisionality.

Neutral Beam Current Drive

For this thesis, the main current drive tool used is NB current drive. NBI heating is based on the interaction of fast neutral atoms with a plasma. Since ions would be deflected by the magnetic fields required for confinement of the plasma, neutral particles are used as injecting particles to the plasma. NBI heating comprises the following physical processes (the last three occur simultaneously):

● Ionisation of the fast neutral atoms by collisions with electrons and ions in the plasma.
● The drift motion of the fast ions in the magnetic field.

● The collisions of the fast ions with electrons and ions in the plasma, giving rise to slowing down and scattering.

● The charge exchange collisions of the fast ions with background neutral atoms.

In addition to heating of the plasma, NBI produces a current of fast ions circulating around the torus. The slowing down of these fast ions by collisions with electrons causes the electrons to drift toroidally in the same direction as the fast ions. The electron current owing to this drift is in the reverse direction to the fast ion current, and so there is some cancellation between these two components. The degree of cancellation depends on the charge, $Z_f e$, of the fast beam ions, the effective plasma ion charge $Z_{eff} e$, and the number of magnetically trapped, banana-orbiting electrons in the plasma. In the classical description, i.e., when the tokamak orbits of the electrons are not considered, the collisional electron current will cancel the ion current if $Z_f = Z_{eff}$. When trapped electrons are included, the electron current is reduced and Z_f need not to differ from Z_{eff} in order to drive a net current. In the normal regime, the electron thermal velocity well exceeds the fast ion velocity. The total driven current is given by

$$I / I_f = 1 - Z_f/Z_{eff} + 1.46 \, \varepsilon^{1/2} Z_f A(Z_{eff}) / Z_{eff} \qquad (1.6)$$

Where I / I_f is the ratio of the net current to the fast ion current and $\varepsilon = r/R$ is the inverse aspect-ratio. For fast ion velocities, which are normally much less than the electron thermal velocity, values of the function A range from 1.67 for $Z_{eff} = 1$ to 1.18 for $Z_{eff} = 4$. In above equation, the second term on the right hand side represents the reverse electron current in the absence of trapped electrons and the third term takes their effect into account.

1.6 Tokamak Experiments: ASDEX Upgrade and JET

ASDEX Upgrade is, compared to other international tokamaks, a midsize tokamak experiment. As its predecessor (ASDEX), it uses a divertor concept. Although the magnetic fields in a tokamak prevents the hot plasma streaming directly onto the surrounding material surfaces, the heat produced in the plasma will ultimately fall onto the surfaces of the vacuum vessel walls. This can be controlled by modifying the magnetic fields nearest the walls to guide the particles escaping away from the main plasma to localised targets known as divertors. ASDEX Upgrade, which started

operation in 1991 is designed as a fusion experiment with a reactor relevant plasma cross section, open divertor configuration and poloidal field arrangement, with the coils outside the vacuum vessel and outside the toroidal field coil set. The main parameters of ASDEX Upgrade are listed in table 1.1.

The Joint European Torus (JET) is the largest tokamak in the world. It started operation in 1983. The main parameters of JET are listed in table 1.1. JET is very similar to ASDEX Upgrade, but roughly two times larger in linear dimension. In both experiment the majority of the experiments are performed in Deuterium plasmas. JET is currently the only experiment running with a capability to do experiments with Tritium, although this is not used for the work presented in this thesis.

The main heating for ASDEX Upgrade and JET are NBI systems and RF heating systems (the heating levels are given in table 1.1).

Parameters	ASDEX Upgrade	JET
Major radius (m)	1.65	2.96
Minor radius (horizontal) (m)	0.5	1.25
Minor radius (vertical) (m)	0.8	2.10
Plasma volume (m^3)	14	90
Maximum toroidal magnetic field on plasma axis (T)	3.9	3.45
Maximum plasma current (MA)	1.6 (Single-null configuration)	6.0 (Single-null configuration)
NBI power (MW)	20 (in Deuterium)	24 (in Deuterium)
ICRH power (MW)	8	20
ECRH power (MW)	2	-
LH power (MW)	-	10

Table 1.1. The main parameters of ASDEX Upgrade and JET

Neutral Beam Injection System at ASDEX Upgrade and JET

The beam lines for ASDEX Upgrade are presented in figure 1.3. The four sources of beam box 1 (NI-1) routinely operate at 55kV for Hydrogen or 60kV for Deuterium.
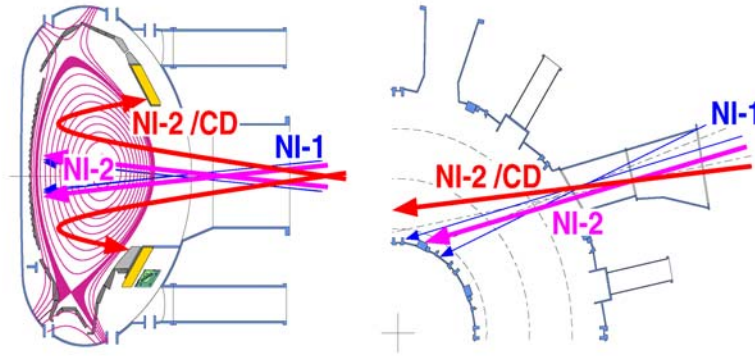
Figure 1.3. The NBI system at ASDEX Upgrade. NI-1, NI-2 represents beam lines from neutral beam box 1 and box 2, respectively. NI-2/CD represents beam lines from current drive beam sources of box 2.

For NBI current drive experiments, the four sources of beam box 2 (NI-2) have been upgraded for operation at 70kV for Hydrogen and 93kV for Deuterium, respectively. Moreover, the positions of two tangential beam sources (source 6 and 7) of box 2 are slightly moved for off-axis beam current drive with higher current drive efficiency, while other sources are used for control of power and particle deposition.

The NBI system in JET is presented in figure 1.4. It consists of two Neutral Injector Boxes (NIBs), octant 4 (80kV) and octant 8 (130kV), and each injector is equipped with eight Positive Ion Neutral Injectors (PINIs). The beam trajectories are the same for both NIBs. They are composed of two groups of four PINIs for each NIB as shown in figure 1.4; (i) tangential injected sources, make two passes through the plasma (ii) normal injected sources, make one pass through the plasma.
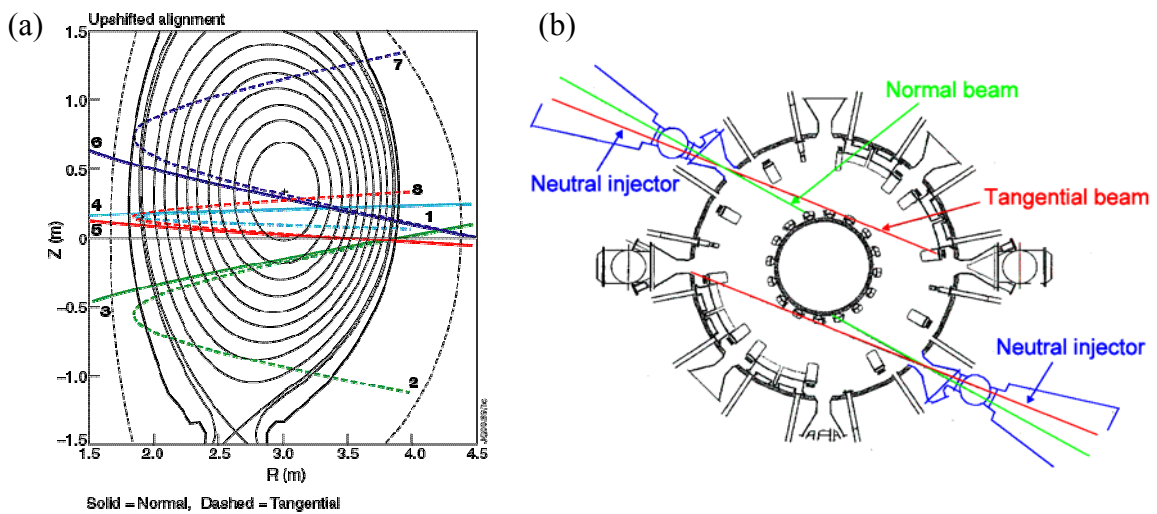

Figure 1.4. Overview of the NBI system at JET. Injection trajectories for upshifted alignment and layout of the neutral injection boxes are shown in (a) and (b), respectively.

1.7 Identification of Current Density Profile Using Motional Stark Effect Diagnostics

As described above, NBI is a main tool for plasma heating and current drive in present tokamaks. In addition to this, it is a very powerful diagnostic tool. An important diagnostic for this thesis also uses a neutral beam; beam emission spectroscopy to determine the internal magnetic field of a tokamak by means of the Motional Stark Effect (MSE) [24]. This diagnostic is described in more detail below.

A neutral atom moving with a constant velocity v_b in a magnetic field B experiences in its own frame of reference a Lorentz electric field E_L induced by its motion: $E_L = v_b \times B$ The splitting and shift of atomic energy levels due to the Lorentz electric field is called motional Stark effect. When NB particles are injected into the plasma, the injected NB particles are excited by collisions with plasma ions and electrons while penetrating the plasma. Since Hydrogen and its isotopes used for NBI exhibit a strong linear Stark effect, the line spectrum of a NB is dominated by the MSE. The beam emission is Doppler shifted if observed at an angle unequal 90°, depending on the velocity of the beam particles and the viewing angle. This separates the beam emission from the edge and charge exchange emission in the spectrum. Measuring both the line splitting and the polarisation properties of the Balmer-α NB emission (H_α, D_α, T_α, $\lambda_0(H_\alpha) = 6563\text{Å}$, transition from $n = 3$ to 2), the magnetic field, its magnitude and orientation can be determined.

The MSE diagnostic provides a determination of the local magnetic field pitch angle $\gamma_p = \tan^{-1}(B_p/B_t)$ which is proportional to γ_m ($\gamma_p \approx \gamma_m$ for simple geometry and $E_r = 0$). The magnetic pitch angle is correlated to the safety factor $q(r)$. The q-profile in simple cylindric case can be represented as $q_{cyl.} = rB_t / RB_p$, where $q_{cyl.}$ is apparently a function of γ_p. With the measured polarisation angle γ_m, the current density profile $j(r)$ can be calculated. Typically the observation geometry of the MSE diagnostic is complex and the current density profile and q-profile can mainly be determined with an equilibrium reconstruction code. ASDEX Upgrade uses CLISTE (CompLete Interpretive Suite for Tokamak Equilibria) [25], which imports the MSE measurements and magnetic probe measurements as input data.

The MSE diagnostic at ASDEX Upgrade uses the 60keV source 3 of box 1 to determine the magnetic pitch angle γ_m by measuring the direction of polarisation and the geometry-dependent polarisation angle from 10 spatial channels.

Scope and Outline of the Thesis

The motivation of the thesis (§1.3) states that stationary operation of fusion experiments using a tokamak would require improvement of the confined plasma pressure or an increase in local pressure gradients over standard experimental conditions. These, so-called advanced scenarios are obtained by modifying the profile of current density in the plasma. To optimise the energy confinement and stability of the advanced scenarios, the current density profile still would require to be controlled by external actuators.

Scope of the thesis

In the ASDEX Upgrade tokamak, current profile control using neutral beams has been proposed. A possible current profile feedback control system at ASDEX upgrade is illustrated in figure 1.5. This control system consists of (i) diagnostic information of the evolution of the current density profile in real-time (MSE measurements), (ii) a tool to identify the current density ($j(r)$, $q(r)$) in real-time (this could be based on a Functional Parameterisation (FP) method [26]), (iii) a control algorithm for an actuator (neutral beams with different injection angles).
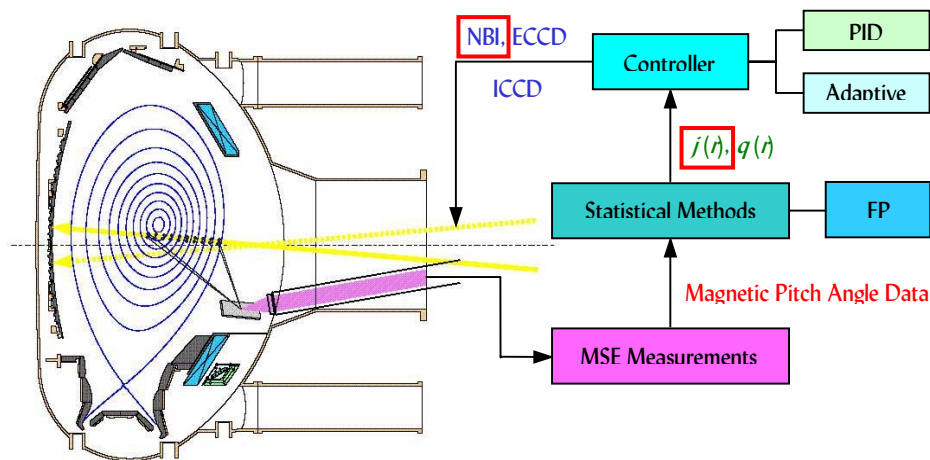

Figure 1.5. Overview of real-time current profile feedback control system at ASDEX Upgrade

The scope of the thesis is (i) to validate the models for the contribution to the current profile in the plasma from the ohmic current, the current generated by pressure gradients and neutral beam driven current, (ii) to obtain a model for the changes of the current density profile when the neutral beam sources are varied, which could be used in the algorithm of the controller, (iii) to validate the models obtained in simulated plasma conditions and specifically designed experiments. These experiments are also used to investigate the physics of neutral beam current drive or contribution of neutral beam driven current, which is not always in agreement with models used in the simulations.

Outline of the thesis

Chapter 2:
In order to document the contribution to the current density profile from the neutral beams, ohmic transformer and the bootstrap current, dedicated transport analyses are performed of advanced scenarios at ASDEX Upgrade. For this, a transport code with models for the different contributions to the current density is used; the so-called ASTRA code. In order to verify the models used, several types of advanced scenarios are studied at ASDEX Upgrade. Also results from other experiments (JET) are modelled using ASTRA.

Chapter 3:
With the successful modelling of advanced scenarios, the ASTRA code is used to model variation of the current density using four neutral beam sources with different injection geometry in the plasma. This is to provide a dataset for system identification to calculate the transfer function (system response) between the actuators (neutral beam sources) and the variables that need to be controlled; current density at different positions in the plasma and the plasma beta (ratio of stored energy in the plasma and magnetic energy used to confine the plasma). For this, a specific type of system identification is proposed and the results are discussed. This response model can then be used for current profile control.

Chapter 4:
In order to verify the model obtained, the transport code ASTRA is used to generate different simulated variations of the neutral beam sources to check if the model calculates the same variation of the current density profile and plasma beta. In addition,

special experiments are made at ASDEX Upgrade, using variation of the beam sources to test the modelling. From this, the contributions of the neutral beam current drive and the diagnostic requirements for control are described. Special attention is given to the understanding of the neutral beam current drive, which in some experiments is in agreement with the models (implemented in ASTRA) and in some experimental conditions is not in agreement with the simulations.

The results, conclusions and recommendations of the thesis are given in Chapter 5.

Chapter 2

Transport Simulations of Advanced Scenarios

Transport in advanced scenarios is investigated with the ASTRA code [27], particularly for discharges with low magnetic shear in the centre of the plasma (these regimes are described in §1.4). The ASTRA code and a model for the energy transport, the Weiland transport model [28] are described in §2.1. Transport simulations for advanced scenarios in ASDEX Upgrade concentrate on the so-called high β_N discharges (§2.2) with emphasis on simulations of the current density profile. In §2.3, transport simulations for another type of advanced scenario with low shear in the centre, the improved H-modes, at ASDEX Upgrade are presented. In addition, similar simulations are performed for an improved H-mode at JET and the results are compared to results from ASDEX Upgrade. A summary of the results is presented and discussed in §2.4.

2.1 Transport Simulations

In general, the evolution of the current density profile is a key to understand improvement of the performance and the occurrence of MHD instabilities in advanced scenarios. In order to simulate this, the ASTRA code is employed for this thesis. It uses kinetic (temperature and density profiles) and geometric data as input as well as models for the bootstrap current and the NB injection current drive. In addition, the energy transport can be simulated by applying the Weiland transport model and the resulting kinetic data can be compared to the experimental measurements.

So two types of simulations are performed with ASTRA for transport simulations. One is a simulation of the current density profile with experimental data assuming neoclassical electrical conductivity [29] (ASTRA in interpretive mode). The other is a simulation of the energy transport and the current density profile using the Weiland transport model (ASTRA in predictive mode). Before presenting simulation results, short description of the ASTRA code and the Weiland transport model will be given in

this section. In addition, diagnostics employed for the simulations will be described briefly.

ASTRA Code

ASTRA is a tool for the study of transport mechanisms in reactor-oriented facilities of the tokamak type such as ASDEX Upgrade and JET. It solves coupled time-dependent 1-D transport equations for particles, heat and current and 2-D MHD equilibrium self-consistently with realistic tokamak geometry, but no divertor geometry. Flexibility is provided within the ASTRA system by a wide choice of standard relationships, functions and subroutines representing various transport coefficients, equilibrium solvers, methods of auxiliary heating (e.g. NBI, ECRH) and other physical processes in the tokamak plasma, as well as by the possibility of pre-setting transport equations and variables for data output in a simple and conceptually transparent form. Therefore a variety of transport models can be imported to ASTRA for transport simulations such as Weiland model [28], IFS/PPPL [30], Current Diffusive Ballooning Model (CDBM) [31], the semi-empirical mixed Bohm/gyroBohm model [32], GLF23 [33] etc.

In this thesis, Weiland model is incorporated for heat transport simulations and NBI heating package is embedded in ASTRA for calculation of additional heating and current drive to the plasma. Kim's bootstrap current model [34] is employed to calculate bootstrap current in the plasma. To compare the MSE angles observed in the experiment, subroutine for calculation of MSE angles is implemented at ASTRA.

Weiland Transport Model

The Weiland transport model is employed for transport simulations with ASTRA since it was demonstrated [35], [36] that the Weiland model yields the most accurate predictions together with GLF23 for standard H-mode discharges at ASDEX Upgrade by comparing different theoretical models: Weiland model, IFS/PPPL, CDBM, the semi-empirical mixed Bohm/gyroBohm model and GLF23.

Weiland model is a fluid model based on Ion Temperature Gradient (ITG) and Trapped Electron Mode (TEM) coupling [28] in addition to the neoclassical transport. It assumes that there are thresholds in both ion and electron temperature gradient lengths; if the gradients are below the critical value, transport is neoclassic. The closure is obtained

taking the heat flux as the diamagnetic heat flux with isotropic temperature. It also assumes that turbulence is suppressed when $E \times B$ shearing rate ($\omega_{E \times B}$) is higher than linear growth rate (γ) [37]. It has a fairly transparent physics among the several transport models mentioned above, based on reactive drift waves described in a fluid approach. Transport is quasi-linear and transport coefficients are derived according to the mixing length estimate. It contains only algebraic equations and the formulas are analytic. Nevertheless, it predicts temperature profiles in good agreement with the measurements in a variety of experimental conditions. In this thesis, electromagnetic effects and collisions for trapped electrons are neglected in the simulations using the Weiland model for simplicity.

Diagnostics Employed for Simulations

For purposes in this thesis, plasma equilibrium as well as several experimental profiles have to be diagnosed, partly as input for the ASTRA simulations or as reference for predictions of the ASTRA simulations using the Weiland transport model. In particular, ion and electron temperature and density profiles measurements are necessary, as well as effective charge of the plasma and the total radiated power. In addition, scalar parameters are required, such as plasma current, toroidal magnetic field, neutral beam power for each source and parameters describing the geometry of the plasma.

The ion temperature profile and the effective charge are measured with the Charge eXchange Recombination Spectroscopy (CXRS) [38]. The basic mechanism of the CXRS diagnostic is the measurement of the Doppler shifted and broadened carbon recombination spectrum, detectable only in presence of NBI.

The electron temperature profiles are measured with the Electron Cyclotron Emission (ECE) [39] and Thomson Scattering (TS) [40]. The ECE in the millimetre wavelength range is measured by using a heterodyne radiometer system, which detects the electron cyclotron radiation. In the case of TS, the electron temperature is determined from the degree of broadening of the spectrum of scattered radiation from an injected laser beam.

The electron density profiles are measured with interferometry sometimes in combination with a Lithium beam diagnostics [41] or TS. In interferometry, the phase difference (change in the phase of a beam of coherent radiation passing through a plasma compared with that of a reference beam) is measured by a Mach-Zehnder interferometer using a DCN laser (wavelength 195μm) as light source. The signals from various observation lines are Abel inverted to compute density profiles.

The radiated power is measured with bolometry [42]. This is made with a wide variety of different sensors often arranged in one or more pinhole camera configurations with a complete view of the plasma cross section. As the observed signals are integrals over a line-of-sight, the total radiated power from the plasma may be found by integrating over the viewing angle of a single camera.

2.2 Simulations for High β_N Discharges

High β_N Discharges

As described in §1.4, the high β_N regime is obtained at a plasma current of 800kA, toroidal magnetic fields from 1.7 to 2T, giving edge safety factors in the range 3.6-4.1 at high plasma density, approaching $n_e \approx 0.9 n_{GW}$ as shown in figure 2.1 [21], [43]. The plasmas are in H-mode with a type I or type II ELMy edge.
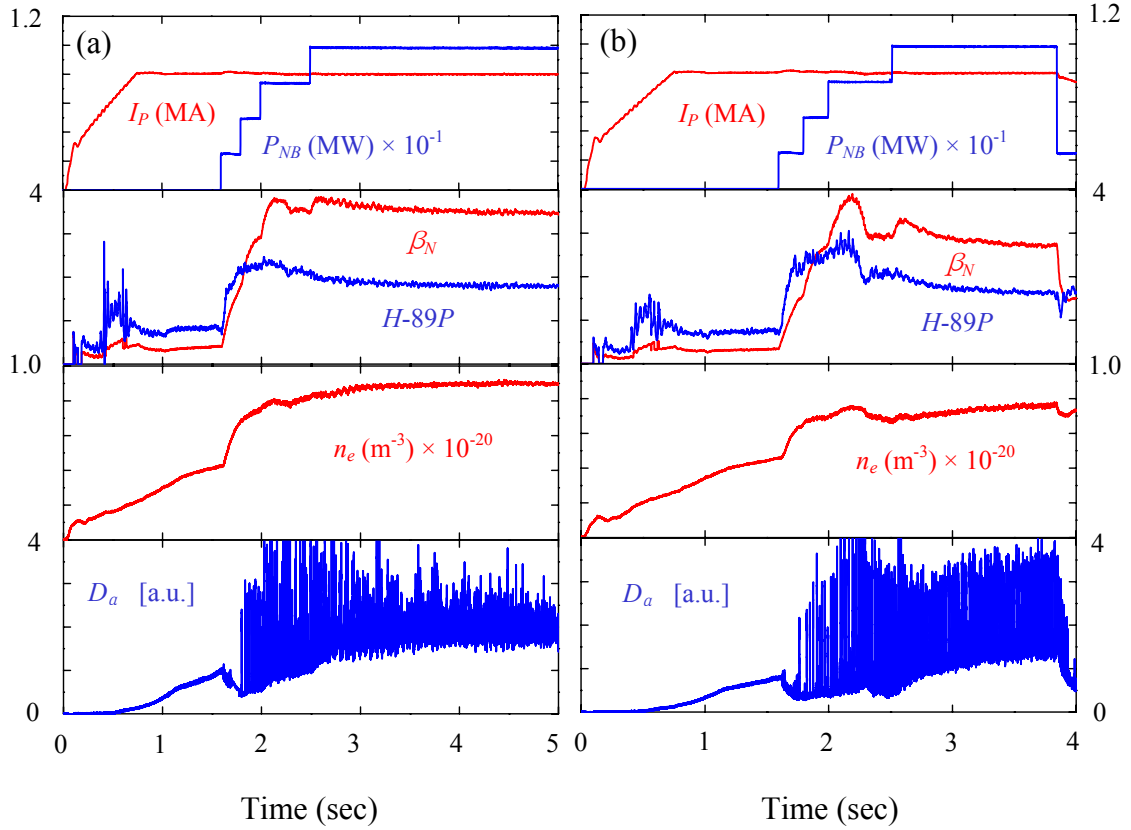

Figure 2.1. Time traces of plasma current, NB heating power, normalized beta, $H_{ITER89-P}$, line-averaged electron density, D alpha of high β_N discharges in ASDEX Upgrade; (a) pulse 14521, (b) pulse 14517.

For these experiments the plasma configuration has maximum shaping for ASDEX Upgrade, with triangularity $\delta = 0.42$ and elongation $\kappa = 1.65$ at the separatrix (figure 2.2). Due to the high triangularity the plasma can be made near double null, with a separation between the two flux surfaces that define the two X-points (dRXP) of 0.009m at the outer midplane. However, the lower X-point is still dominant with nearly all of the power flowing to the lower divertor target.

The highest β_N in conditions that approach steady state is observed in pulse 14521, presented in figure 2.1 (a). 10MW of NB is applied during the current flattop phase from four beam sources, two of these sources are tangential and deposit the power off-axis around $\rho_{tor} = 0.5$. During the NB heating phase, the ELM's reduce significantly in size as the density increases and the plasma configuration is moved up, closer to a double null configuration (figure 2.2). This movement to a double null configuration is made deliberately and is completed at 3.2 seconds. The electron density slowly increases to 88% of the Greenwald density limit due to a combination of NB injection and gas fuelling leading to a slow decrease in the stored energy. This decrease is a combination of the loss of confinement generally observed for discharges approaching the Greenwald density limit and the slow reduction of the plasma inductance during the first part of the NB heating phase. However, the confinement factor ($H_{ITER89-P}$) over the ITER89, L-mode scaling remains at or above 2. During the phase with 10MW NB heating, strong fishbone activity is observed. As a result the density and temperature profiles are moderately peaked.
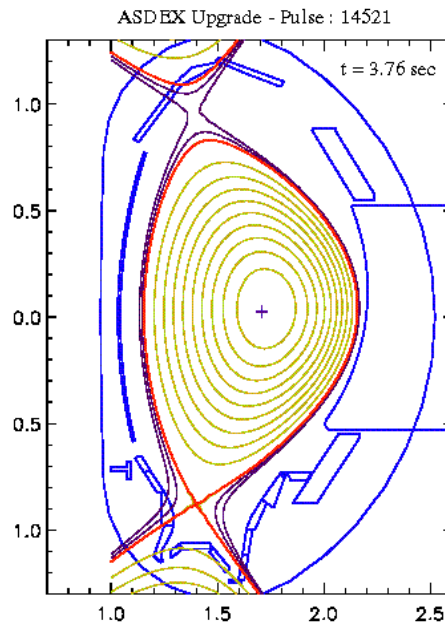

Figure 2.2. Plasma cross section for pulse 14521 at 3.76sec.

In addition, the lack of sawteeth activity eliminates one of the candidates for the triggering of a Neoclassical Tearing Mode (NTM; occurring at low-order rational surfaces (e.g. $q = 3/2$), driven unstable by the local gradient of the equilibrium current density, giving a loss (10%-30% of plasma stored energy) in these discharges.

Using the same plasma shape and heating waveforms, higher values for β_N have been achieved in pulse 14517 (figure 2.1 (b)) with $\beta_N = 3.8$ and $H_{ITER89-P} = 3$ at somewhat lower plasma density compared to pulse 14521. Under these conditions an NTM is triggered by a sawtooth collapse at the start of the high power phase, compared to pulse 14521 this is just before the time fishbone activity starts. The confinement drop during the NTM activity in pulse 14517 is modest and $\beta_N = 2.9$ is observed during the mode. The central temperature drops by 20%. At this beta, the width of the magnetic island at the (m=3, n=2) q-surface in the plasma is expected to saturate to 20-25 % of the minor radius [44], which would give a much larger drop in stored energy or central ion temperature. In this respect, the NTM is of the frequently interrupted ('FIR') type [44], where the growth of the mode is limited by other MHD modes.

Simulation of High β_N Discharges

As described in §2.1, all simulations are performed with the ASTRA code and two types of simulations are performed with ASTRA for the high β_N discharges presented in figure 2.1. First, simulations of the current density profile are carried out using experimental profiles assuming neoclassical electrical conductivity. Ion temperature (T_i) profiles are taken from the CXRS diagnostic and electron temperature (T_e) profiles are from TS. Density (n_e) profiles are taken from interferometry data. Radiation (P_{rad}) profiles are taken from bolometry measurements. Second, simulations of the current density profile and the energy transport are carried out with the Weiland transport model. For simulations using the Weiland transport model, experimental density and P_{rad} profiles are used. The effective ion charge (Z_{eff}) profiles are taken from an improved H-mode (pulse number 13679). For the high β_N discharges, only an estimate for the line-averaged Z_{eff} is available. Since the ITG instability is not expected to dominate transport in the H-mode edge barrier region, the boundary conditions are given in such way that $T^{sim}(\rho_{tor}=0.8) = T^{exp}(\rho_{tor}=0.8)$ for ion and electron temperatures. In ASTRA, the momentum equations are not solved, however the Weiland model uses the velocity shear in the computation of the transport coefficients. Hence for the toroidal velocity v_{tor}^{sim}, $v_{tor}^{sim} = cT_i^{sim}$ is used (as also has been found in [45]). The constant c is

determined from experimental data. The heat diffusivities are defined as the sum of the neoclassical and turbulent contributions, the poloidal rotation is assumed to be neoclassical [46]. The simulations are started using initial current density profiles in agreement with experimental data assuming neoclassical electrical conductivity.

For the simulation of pulse 14521 (figure 2.1 (a)) with experimental data, the initial current profile for the simulation is taken at 1.7sec, between the first (1.6sec) and the second (1.8sec) increase of the NB injection.
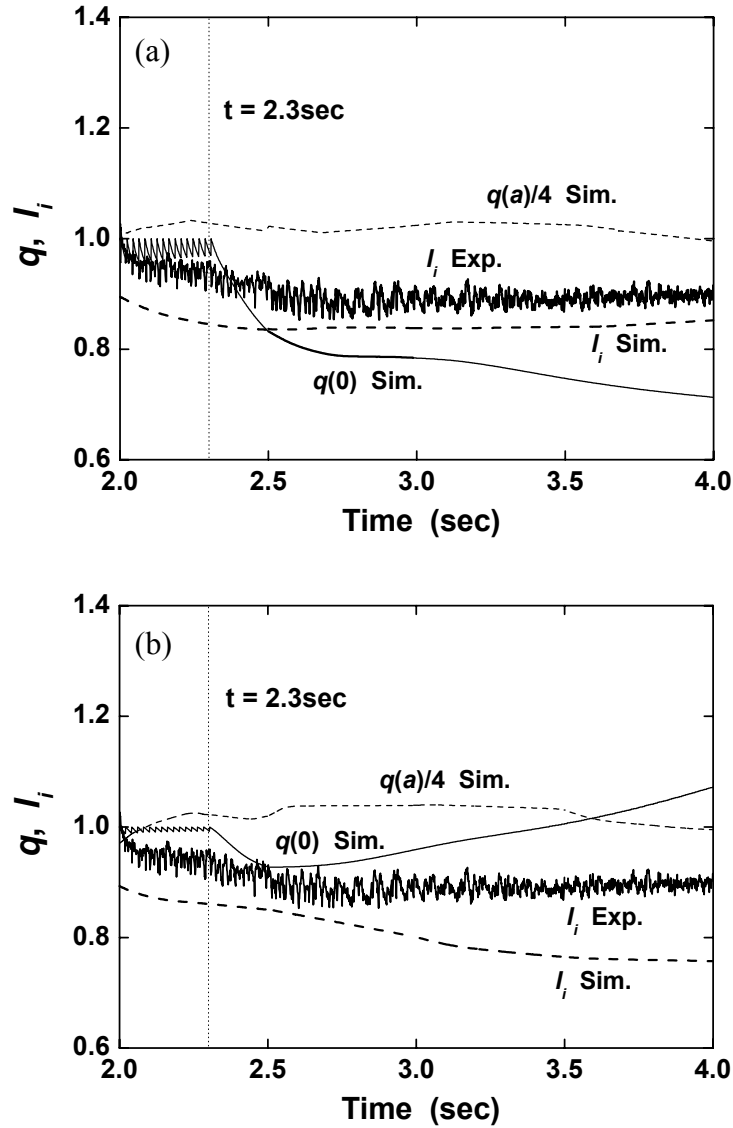

Figure 2.3. The time evolution of internal inductance (l_i), q-values at the centre (q_0) and at the edge (q_a) in the simulation using experimental temperature profiles (a) and using the Weiland model (b) for the high β_N discharge (pulse 14521).

For more realistic simulations, the sawteeth effects are taken into account with a Kadomtsev full reconnection model [47]. It is applied to the simulation until 2.3sec, since in the experiment from 2.3sec onwards, central MHD activity is dominated by fishbones. The simulated q-values at the centre (q_0) and at the edge (q_a) are presented in figure 2.3 (a). q_0 cannot be compared to the experimental data because no MSE measurements are available for this discharge. Accordingly, the internal inductance l_i is compared to the experimental measurements. As seen in figure 2.3 (a), the simulated l_i agrees well with the experimental observation. The result of the simulation reproduces the time trace of the l_i correctly and the difference is well in the range of the measurements errors: In this discharge, l_i is lower than β_p and the error for the identification of l_i from magnetic equilibrium reconstruction is therefore amplified. The time evolution of the q-values are compared to the simulation using the Weiland model in figure 2.3 (b). For the simulation using the Weiland model, the initial current profile is taken at 1.8sec at the start phase of the second NB injection. Figure 2.3 (b) shows different trends compared to figure 2.3 (a). In the simulation using experimental data, q_0 decreases continuously. In contrast, in the simulation using the Weiland model, q_0 decreases after the sawtooth collapse and then starts to increase from around $t = 2.5$sec. This difference is discussed in §2.4. Accordingly, l_i tends to decrease in the simulation using the Weiland model. Both simulated q-profiles are compared at 4sec in figure 2.4 (a). The shapes of the simulated q-profile agree well, however some difference in q-values near the centre is seen. This can be explained by the different temperature profiles between experimental and simulated by the Weiland model profiles. As shown in figure 2.4 (b), the ion temperature profiles are well reproduced by the Weiland model, however differences are observed in electron temperature profiles. This difference is most pronounced in the region $0.3 < \rho_{tor} < 0.6$. However, this difference is just within the range of a typical error bar on temperature measurements at this high density. The higher simulated electron temperature gives rise to lower resistivity. Subsequently, higher central q-values are reached as less plasma current flows in the centre. The contributions to current density profile from the ohmic, NB driven and bootstrap current are compared at 4sec for pulse 14521 in figure 2.4 (c), here the results are from simulations with experimental data. Due to the high plasma density and use of off-axis NB sources, the current density profile from the NB has a maximum at $\rho_{tor} = 0.45$. The shapes of the ohmic, bootstrap and NB current density profiles are similar when the Weiland model is used in the simulation. However, the fractions of the plasma current are slightly different.
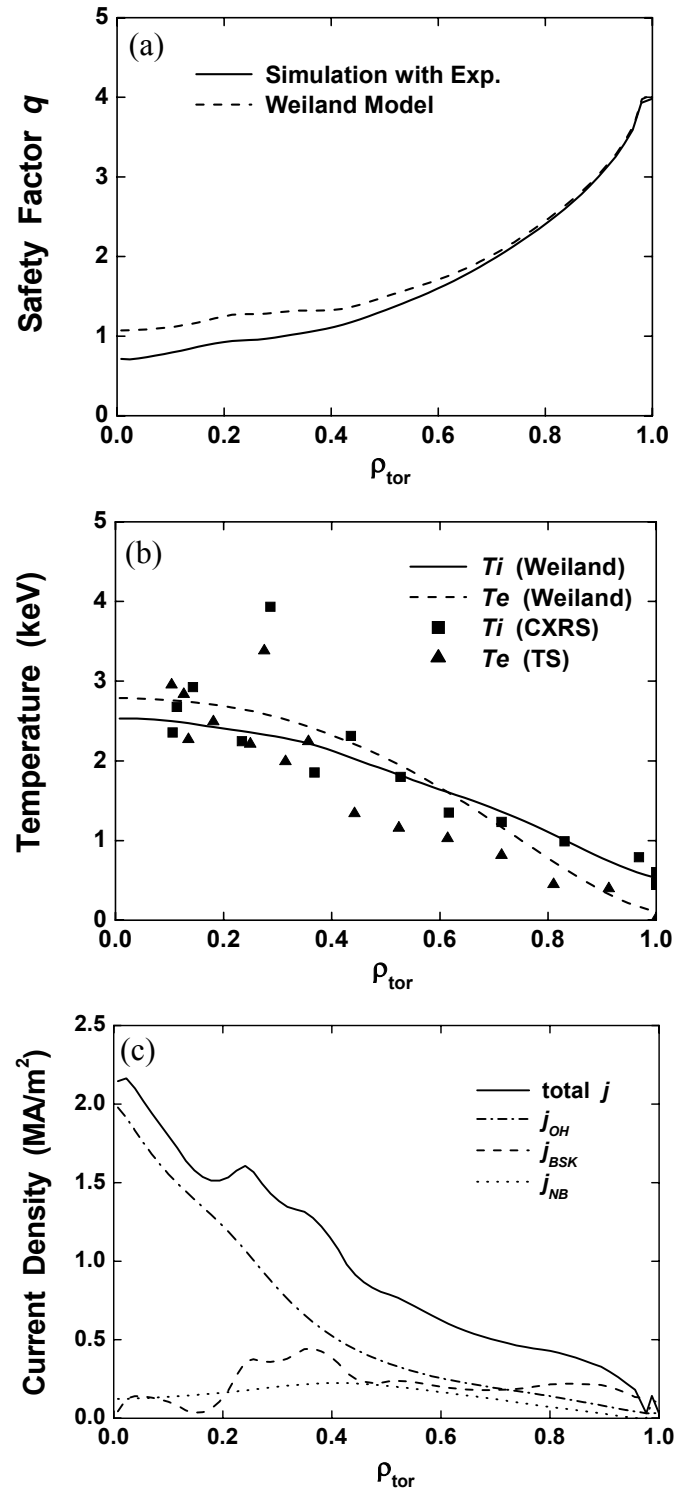
Figure 2.4. q-profiles (a), temperature profiles (b) and current density profiles (c) in the high β_N discharge (pulse 14521) at 4sec. Note that the T_i and T_e measurements around $\rho_{tor} \approx 0.3$ lie well above the other values of the measurements. The reason for this behaviour is not known but the values are given here for completeness.

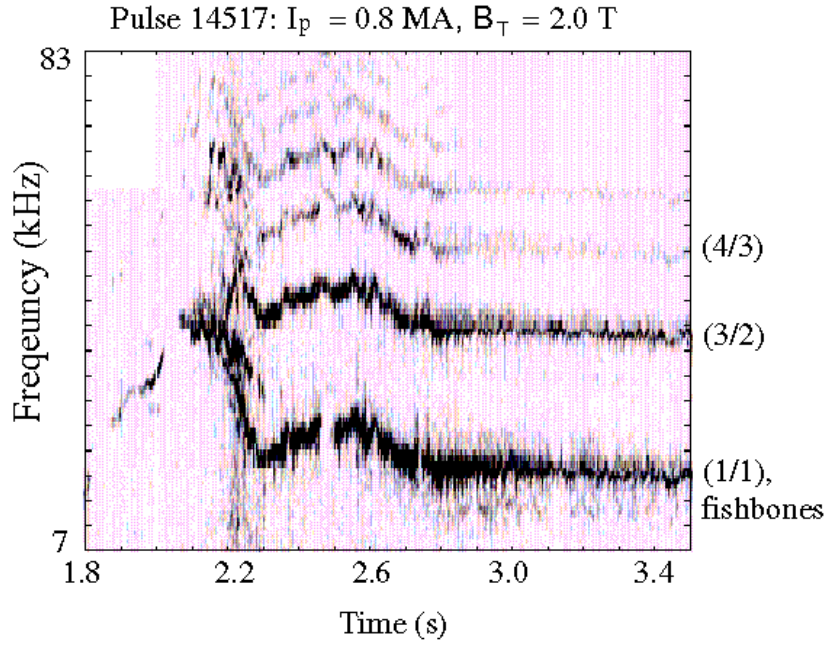|	High β_N discharge Pulse 14521		High β_N discharge Pulse 14517		Improved H-mode Pulse 13679	
	Experimental	Weiland	Experimental	Weiland	Experimental	Weiland
I_{NB}	0.15	0.13	0.16	0.15	0.12	0.08
I_{boot}	0.26	0.32	0.26	0.30	0.21	0.31
$I_{CD\text{-}tot}$	0.41	0.45	0.42	0.45	0.33	0.39
$T_e(0)$	2.9	2.8	2.9	3.3	5.1	5.8
$T_i(0)$	2.4	2.5	2.8	3.3	11.2	12.0
$q(0)$	0.71	1.07	0.79	1.09	0.97	1.00

Table 2.1. Current fractions, central temperatures and central q-values from experimental observations, ASTRA code simulations with experimental data and ASTRA code simulations using the Weiland transport model of high β_N discharges and an improved H-mode.
Currents are in MA and temperatures are in keV.

The non-inductive currents are given in table 2.1 for both simulations. Depending on the simulation used, 50% to 57% of non-inductive current fractions are obtained in this regime. The main difference between two simulations is the bootstrap current fraction. This is caused by the different local gradients of the temperature profiles obtained in the simulations.

In these simulations, at this high density the electron-ion energy exchange terms can be large. However, in the Weiland model, or any model based on drift wave turbulence, the temperature profile shape is fixed and the values in the centre are set by the edge temperatures. In the simulation with the Weiland model, the edge temperatures are taken from the experiment. Any change of the energy transfer to the ions from a difference in T_e compared to T_i will give little change to ion temperatures in the centre: The transport in an ITG based model adjusts itself to the heating profiles. Therefore, varying the energy transfer would only change the ion conductivity so that the profile keeps close to the critical gradient.

In order to investigate the influence of NTM's on the plasma performance and profile shapes, simulations with the experimental data and the Weiland model are performed in a high β_N discharge restricted by NTM's, pulse number 14517. As shown in figure 2.5, strong NTM ($m=3$, $n=2$) activity occurs around 2.2 seconds in this discharge. The MHD activity limits the confinement and achievable β_N. For the simulations, the same experimental conditions are used as in pulse number 14521. The evolution of the discharge is simulated until 3.6 seconds and the q-profile and temperature profiles are

compared to the experimental profiles in figure 2.6. Due to the NTM activity, the experimental temperatures are lower compared to the temperatures obtained by using the Weiland model as presented in figure 2.6 (b), because effects of NTM's are not included in the simulation.

Figure 2.5. Experimentally observed MHD activities in magnetic probe signals in the high β_N discharge (pulse 14517).

The experimental q-profile is reconstructed by the equilibrium code CLISTE using magnetic data and fixing the $q = 3/2$ surface at $\rho_{tor} = 0.34$, as has been measured with Soft X-ray diagnostics from the NTM activity. The agreement between the experimental q-profile and the two types of simulation with the ASTRA code is good, although the experimental profile lies in between the simulation using the Weiland model and the simulation with experimental data (figure 2.6 (a)). The q-profile from the simulation using the Weiland model is too high in the centre and has lower shear, on the other hand the simulation using experimental data has lower q-values in the centre compared to the CLISTE q-profile. The differences are small, however these could be explained by the MHD activity (not included in ASTRA) in this pulse, which may lead to a partial reconnection of the q-profiles around the $q = 3/2$ surface (magnetic island).
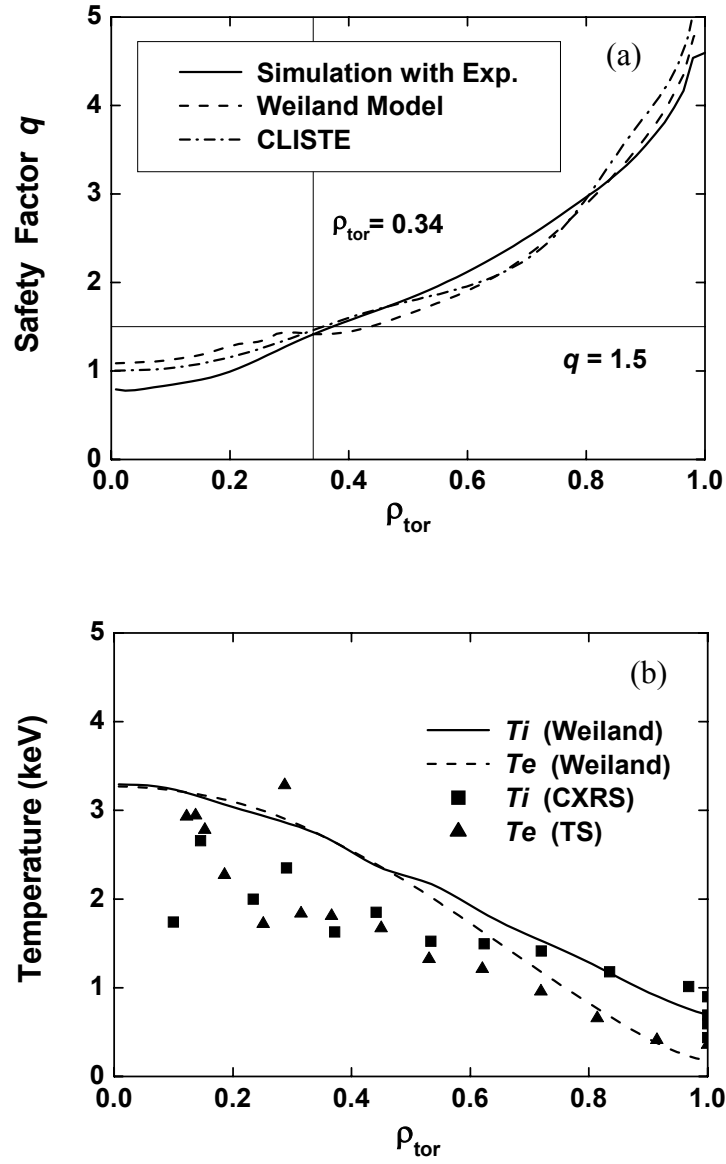
Figure 2.6. q-profiles (a) and temperature profiles (b) in the high β_N discharge with NTM's (pulse 14517) at 3.6sec.

2.3 Simulations for Improved H-mode and Comparison to JET

The approach used in previous section is applied to another improved H-mode in ASDEX Upgrade (pulse 17870) and that in JET (pulse 58323) for comparison. In these two discharges, ρ^* (normalised Lamor radius, defined as $\rho^* = (2eT/M)^{0.5}M/eBa$) and the plasma shape are matched for both devices. Therefore, ASTRA simulations can be performed for these two discharges in order to test the non-inductive current drive calculations in ASTRA using different beam geometry and different input diagnostics, thus the applicability of ASTRA simulations to other tokamak devices can be validated. Time traces of the main plasma parameters of these two discharges are shown in figure 2.7 and magnetic configurations are presented in figure 2.8.
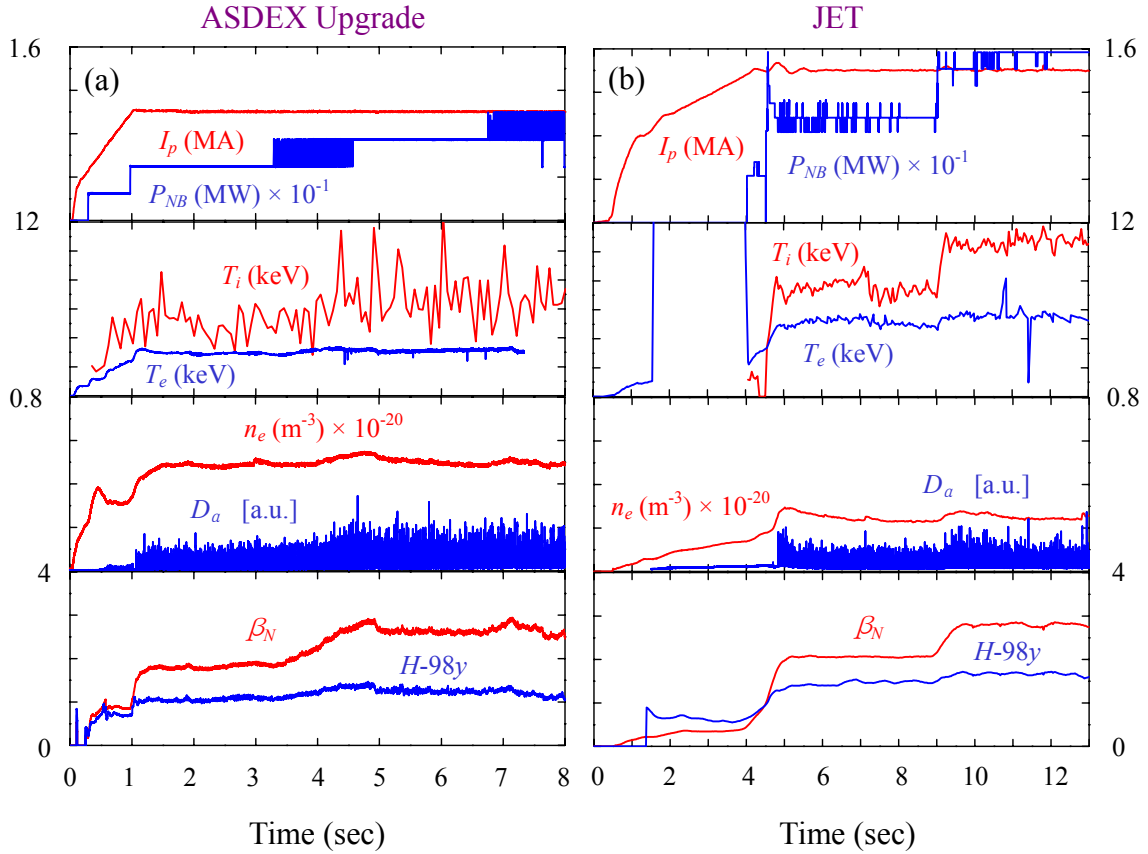

Figure 2.7. Time traces of plasma current, NB heating power, central ion temperature and averaged (maximum in (b)) electron temperature, line-averaged electron density, D alpha, normalised beta, $H_{98}(y,2)$ of pulse 17870 in ASDEX Upgrade (a) and 58323 in JET (b).
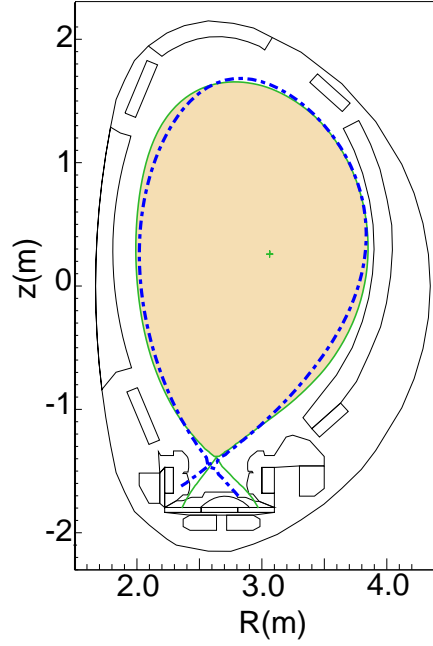
*Figure 2.8. Plasma cross sections matched for improved H-mode discharges
at ASDEX Upgrade (in blue dashed line) and JET (in green solid line).*

First, simulations of the current density profile are carried out using experimental profiles assuming neoclassical electrical conductivity as in §2.2. Ion temperature (T_i) profiles are taken from the CXRS diagnostic for both discharges and electron temperature (T_e) profiles are from ECE diagnostic and TS data for pulse 17870 in ASDEX Upgrade and pulse 58323 in JET, respectively. Density (n_e) profiles are taken from interferometry data with Li beam diagnostic and TS data for pulse 17870 and pulse 58323, respectively. Radiation (P_{rad}) profiles are taken from bolometry measurements for both discharges. Second, simulations of the current density profile are carried out with the Weiland transport model. For simulations using the Weiland transport model, experimental density and P_{rad} profiles are used. The effective ion charge (Z_{eff}) profiles for pulse 17870 are taken from an improved H-mode (pulse 13679 presented in previous section). The initial and boundary conditions, the toroidal velocity and the poloidal rotation are given in the similar way presented in §2.2. Here, the sawteeth effects are not taken into account.

The results of the ASTRA simulation are shown in figure 2.9, where the current density profiles for the two experiments are compared. The contributions of NB driven current and bootstrap current are presented in table 2.2.
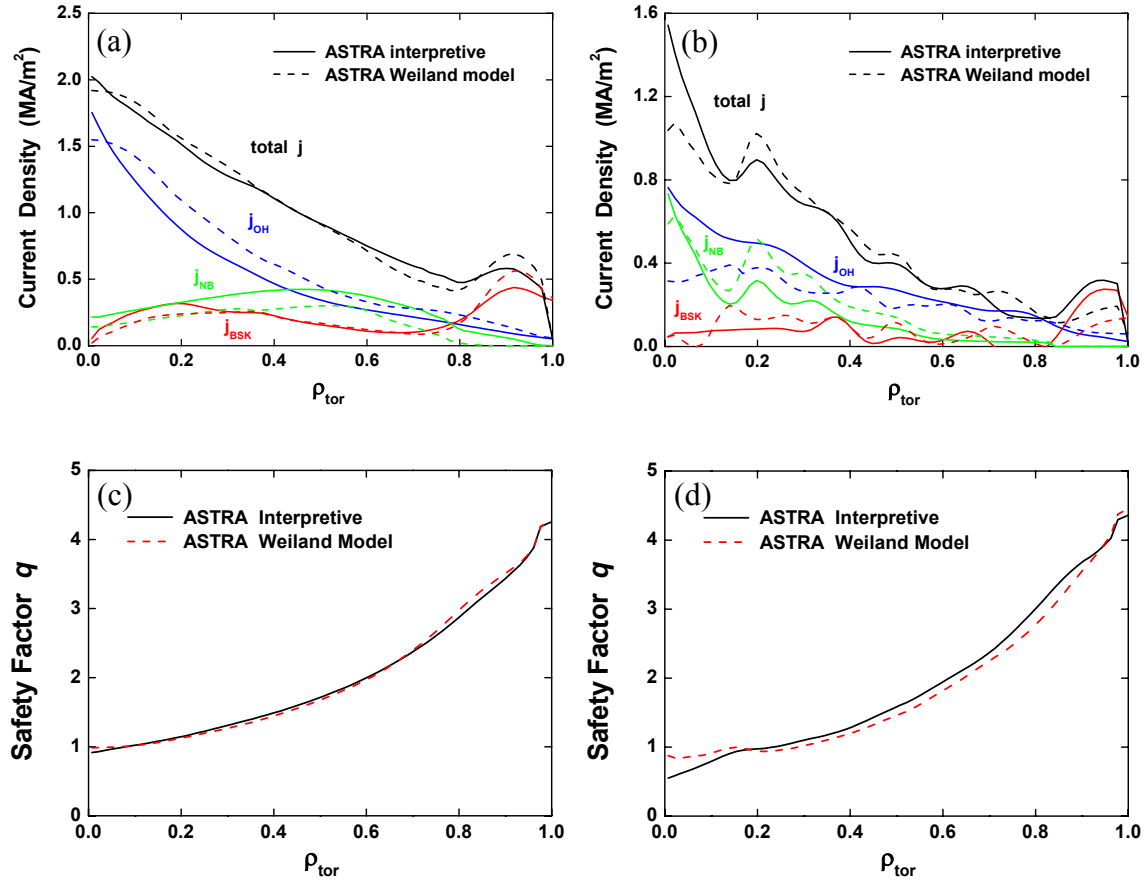
Figure 2.9. Current density profiles of pulse 17870 in ASDEX Upgrade (a) and pulse 58323 in JET (b) at 6.3sec and 12sec, respectively. q-profiles of pulse 17870 in ASDEX Upgrade (c) and pulse 58323 in JET (d) at 6.3sec and 12sec, respectively. Profiles are calculated using experimental profiles (ASTRA in interpretive mode) or the Weiland transport model.

As shown in figure 2.9, similar current density profiles and *q*-profiles are achieved for those discharges due to the similar experimental set-up for both devices. Fraction of the non-inductive current is about 40%-60% of total plasma current for both experiments as shown in table 2.2. Difference in the contributions of NB driven current (I_{NB}) and bootstrap current (I_{boot}) to total plasma current can be explained by the different NB geometry (more central heating in JET) between the two experiments.

	ASDEX Upgrade Pulse 17870 at 6.3sec		JET Pulse 58323 at 12sec	
	ASTRA Interpretive	ASTRA Weiland	ASTRA Interpretive	ASTRA Weiland
I_{NB}	31.9%	18.8%	18.7%	29.9%
I_{boot}	29.1%	31.0%	22.1%	20.4%
$I_{CD\text{-}tot}$	61.0%	49.8%	40.8%	50.3%

*Table 2.2. Current fractions (in %) from ASTRA code simulations with experimental profiles
(interpretive) and ASTRA code simulations using the Weiland transport model
of pulse 17870 at 6.3sec in ASDEX Upgrade and pulse 58323 at 12sec in JET.*

One interesting feature shown in figure 2.9 is that the ASTRA simulations of JET using experimental profiles (ASTRA in interpretive mode) show a peaked central current density for the NB current drive. It causes centrally peaked total current density profile and lower central *q*-value.

To verify a model implemented in ASTRA, which calculates the beam driven current, beam driven current density profile calculated is compared to beam driven current density profile calculated by PENCIL code [48]. So two types of ASTRA simulations are performed with experimental profiles; (i) using beam driven current profile calculated by the model implemented in ASTRA, (ii) using beam driven current profile calculated by PENCIL code. They are also compared to more sophisticated transport interpretation code (TRANSP [49]) (see figure 2.10). A comparison between the calculated non-inductive current drive fractions is also given in table 2.3.

As shown in figure 2.10, the model implemented in ASTRA gives most centrally peaked beam driven current density profile, on the other hand, TRANSP gives most broad profile. Particularly in the central region, TRANSP calculation returns nearly zero beam driven current while the model implemented in ASTRA returns the highest value. PENCIL shows centrally peaked NB driven current profile similar to the model implemented in ASTRA but with high NB current drive in the edge region similar to TRANSP. Thus, calculations using the PENCIL code results give the highest contribution of non-inductively driven currents to total plasma current. Total current density profile and *q*-profile calculated by the model implemented in ASTRA is very similar to that calculated by PENCIL.
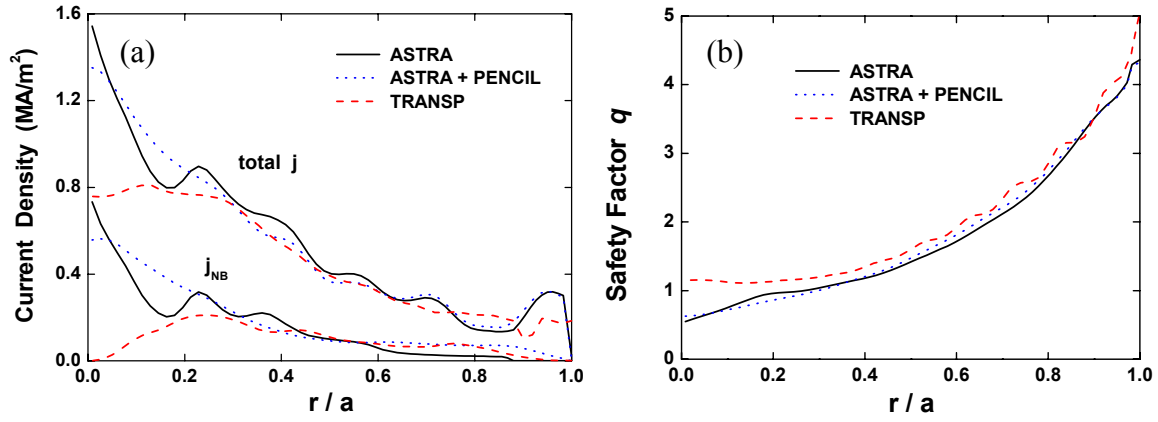
Figure 2.10. Total, NB driven current density profiles (a) and q-profile (b) of pulse 58323 in JET at 12sec. Profiles are calculated by ASTRA using experimental profiles (represented as ASTRA), by ASTRA using experimental profiles and beam driven current density profile calculated by PENCIL (represented as ASTRA+PENCIL), and by TRANSP using experimental profiles (represented as TRANSP).

	JET Pulse 58323 (ASTRA)	JET Pulse 58323 (ASTRA+PENCIL)	JET Pulse 58323 (TRANSP)
I_{NB}	18.7%	27.6%	23.2%
I_{boot}	22.1%	22.1%	21.8%
$I_{CD\text{-}tot}$	40.8%	49.7%	45.0%

Table 2.3. Current fractions (in %) from ASTRA code simulations with experimental profiles (represented as ASTRA), ASTRA code simulations with experimental profiles and beam driven current density profile calculated by PENCIL (represented as ASTRA+PENCIL) and TRANSP code simulations with experimental profiles (represented as TRANSP) of pulse 58323 at 12sec in JET.

The contradictory results between simulations, especially in the central region, are still under investigation in JET. Similar checks of the current density profile calculations of ASTRA simulations are not possible for ASDEX Upgrade as TRANSP is not available at ASDEX Upgrade.

2.4 Summary of the Results and Discussion

Transport in advanced scenarios is analysed with a transport code, ASTRA, particularly for discharges with low magnetic shear in the centre (described in §1.4) in ASDEX Upgrade. In order to analyse the transport in these scenarios with the ASTRA code, a transport model, the Weiland model, is employed to calculate energy transport in the plasma. Two types of simulations are performed with the ASTRA code: Simulation of the current density profile with measured experimental profiles assuming neoclassical electrical conductivity (ASTRA in interpretive mode), secondly simulation of the energy transport as well as the current density profile using the Weiland transport model (ASTRA in predictive mode).

In order to check the ASTRA simulations of advanced scenarios with zero magnetic shear in ASDEX Upgrade (high β_N discharges), time evolutions of the q-profiles and internal inductance (l_i) are simulated and compared to the experimental observations. The time evolution of l_i agrees well with the experimental one in the ASTRA simulation using the experimental profiles. However, in the case of the simulation with the Weiland transport model, the link between the current density and the energy transport can lead to a progressive deviation of q_0 from a simulation with experimental data. However, since the experiment the measure q_0 is not available (no MSE measurements in this experiment), it is difficult to say which simulation (if any) represents the correct behaviour. On top of this comes the influence of the MHD activity (fishbones) in the plasma, which is implicitly included in the measured temperature profiles. However, only a simple sawtooth model is included in ASTRA. Therefore, starting from the same initial conditions the simulation with the experimental profiles and the simulation with the Weiland model can diverge for the value of q_0. Clearly the inclusion of more sophisticated MHD models (fishbones, NTM's) in ASTRA could improve this situation. The contribution to the current density profile of the ohmic, bootstrap and NB driven current are calculated in both type of simulations. Similar results are obtained for the two simulations; the sum of the non-inductively driven plasma current fractions is above 50% of the total plasma current. The simulations of temperature profiles with the Weiland model are generally in agreement with experimental observations within the error bars of the measurements. However, any (small) difference in electron temperature profiles will affect the current diffusion to the plasma centre. This could lead to different behaviours of q_0 between two simulations as mentioned above. It emphasizes the difficulties a self-consistent simulation can have. In addition, the purity of the plasma also affects the current diffusion. For example, impurity accumulation in the central

region of the plasma is sometimes observed using off-axis (NB) heating, which would change resistivity of the plasma and the evolution of the current density profile. When this impurity accumulation is observed (not in the experiments described in this chapter), the effects have to be taken into account when doing ASTRA simulations.

Based on the observation that the Weiland model simulates the data well (within experimental errors) and that it simulates the data with the turbulence (ITG and TEM terms) 'still switched on' (not suppressed by strong $E{\times}B$ shear) is a clear indication that in these scenarios the temperature profiles are stiff (i.e. do not have ITB's). This is supported by previous publications ([35], [50] and [51]). The temperature profile stiffness is represented in figure 2.11 for the experimental measurements and for simulations using the Weiland model in some advanced scenarios with low magnetic shear in the centre at ASDEX Upgrade. The ion temperatures at $\rho_{tor} = 0.4$ are plotted against the ion temperatures at $\rho_{tor} = 0.8$ for several time points during the discharges analysed. In figure 2.11, so-called profile stiffness can be represented by a proportionality between these two temperatures, indicating a constant gradient length for the ion temperature in the region $\rho_{tor} = 0.4\text{-}0.8$. Consequently, it can be concluded that for these advanced scenarios, the data for the simulations as well as data from the experiments are in accordance with the profile stiffness.
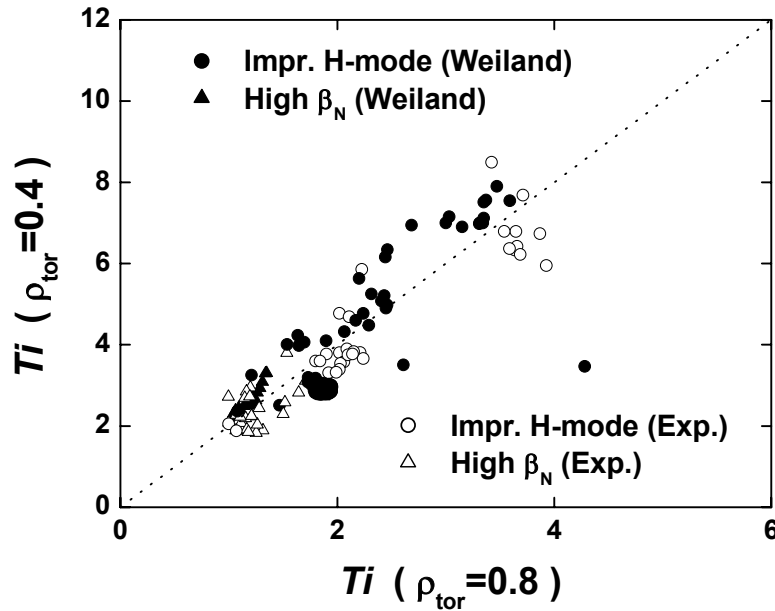

Figure 2.11. Experimental and simulated data of ion temperature profiles at $\rho_{tor} = 0.4$ against $\rho_{tor} = 0.8$ for improved H-modes and high β_N discharges

The maximum achievable β_N in high β_N discharges is limited by MHD instabilities, called NTM's. The effect of the NTM's on the temperature profiles is investigated by comparing ASTRA simulations using the Weiland model to the experimental data in a discharge with NTM activity. In the simulations using the Weiland model, no magnetic reconnection effects are included in ASTRA code. As a result, the simulated temperatures are higher compared to the experimental measurements since loss of temperatures by NTM's is not realised by ASTRA simulations. However, the location of the $q = 3/2$ surface, determined from experimentally measured location of the ($m=3$, $n=2$) NTM, is reproduced in the simulation.

Similar transport simulations are performed with ASTRA for improved H-mode discharges in ASDEX Upgrade and in JET to validate the non-inductive current drive calculations in ASTRA when different beam geometry and different input diagnostics are used. The current density profiles and q-profiles for the two experiments are compared and the results show that they are very similar due to the similar experimental set-up for both devices. 40-60% of non-inductive current drive fractions are achieved for the two discharges. In ASTRA simulations with experimental profiles for JET, centrally very peaked NB current density profiles are observed (as a result, lower central q-value is obtained compared to that of ASDEX Upgrade). In order to investigate this in more detail, NB current density profiles are calculated by other codes, PENCIL and TRANSP and compared to those calculated by the model implemented in ASTRA code. PENCIL gives centrally peaked NB driven current profile similar to the model implemented in ASTRA but with higher NB current drive in the edge region. Whereas, TRANSP gives very broad profile with high NB driven current in the edge region but with nearly zero central NB driven current. The different results between simulations, especially in the central region, are still under investigation in JET.

For simulations with the ASTRA code, there are several sensitive variables, in particular for simulations using the Weiland transport model. The boundary conditions and the model for toroidal rotation play an important role. A particle transport model is not used for simulations in this thesis and would be required to simulate the evolution of density profiles in advanced scenarios for more realistic analysis.

In this chapter, transport simulations of advanced scenarios using the ASTRA code with the Weiland transport model are validated. The current profile evolution and energy transport in advanced scenarios on ASDEX Upgrade are well described by these simulations (with the exceptions presented here). In addition, the applicability of ASTRA simulations in other tokamak devices is checked.

Chapter 3

Modelling of Current Profile Control

In the previous chapter, transport in advanced scenarios with zero magnetic shear in the centre is analysed using the ASTRA code with the Weiland transport model. The satisfactory results of this analysis are used as a basis for this chapter. Starting with a specific plasma discharge (§3.1), the ASTRA code is employed to model the evolution of the current density profile when different NB sources are used (§3.2). Here the ASTRA code is used in a predictive mode using the Weiland transport model to calculate the temperature profiles, and various models for the current diffusion, to simulate the response of the current density profile to the different NB sources at ASDEX Upgrade. The ASTRA simulations are used to obtain a transfer function between current density profile and NB sources. System modelling is described generally in §3.3. This can be used as basis for obtaining a control matrix of a real-time control system with the NB sources as actuators trying to match the demand waveforms for the current density at several radial positions of the plasma, while keeping the poloidal beta of the plasma at a specified value. The best choice of radial positions for output parameters is described in §3.4. To find a model, relationship between NB power and current density, poloidal beta, the ASTRA code is used to predict the response of current density and poloidal beta against NB power. The calculated models are given in §3.4. The results of this chapter are summarized and discussed in §3.5.

3.1 Discharge for Modelling

The effect of the NB current drive and changing beam sources is more pronounced in low plasma current phases. In high poloidal beta discharges the plasma current is driven almost fully non-inductively, consisting of 51% bootstrap and 43% NB driven current [52]. Therefore, a high poloidal beta discharge (pulse 13686) with low plasma current (400kA) is selected for modelling. Time traces of the main plasma parameters of this

discharge are shown in figure 3.1. Here, central ion temperature (T_i) is obtained from CXRS diagnostics and averaged electron temperature (T_e) from ECE diagnostics. Line-averaged electron density (n_e) is taken from interferometry data. A NB power of P_{NB}=7.5MW was injected into a plasma, where beam source 3 is fixed for MSE measurements during the discharge. As shown in figure 3.1, poloidal beta (β_p) and a confinement improvement factor above L-mode ($H_{98}(y,2)$) increase with every step of the NBI power. In the D_α emission the ELM activity can be seen from the first heating step onwards, indicating the H-mode transition.
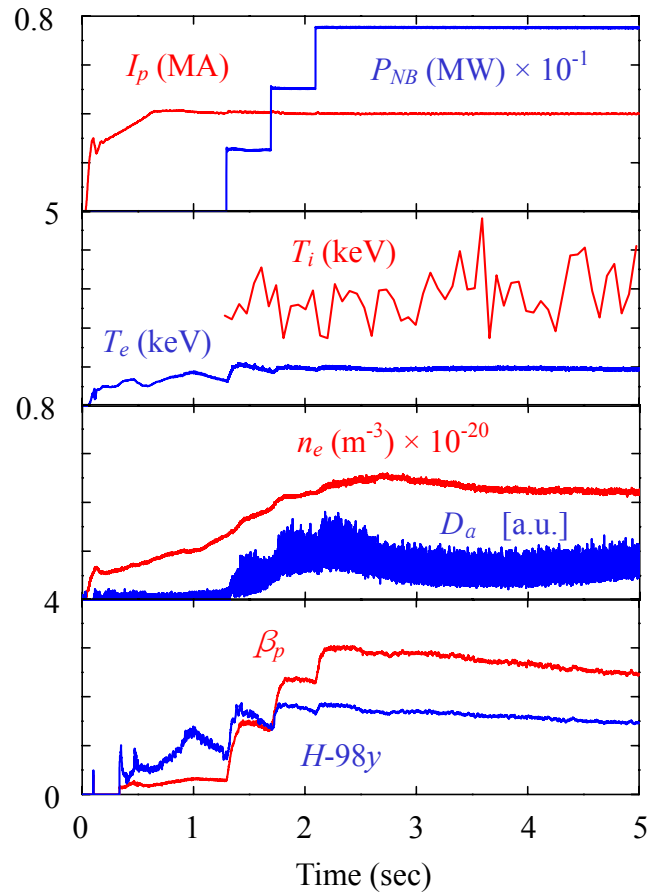
Figure 3.1. Time traces of plasma current, NB heating power (beam sources 3, 7, 6 are used), central ion temperature and averaged electron temperature, line-averaged electron density, D alpha, poloidal beta, $H_{98}(y,2)$ of pulse 13686 in ASDEX Upgrade.

3.2 The Effect of Changing Beam Sources

Simulations are made of the discharge presented in §3.1. First, the simulations of the discharge are given then, the NB sources are varied to document the changes to the current density profile. As for the ASTRA simulations presented in Chapter 2, the energy transport is calculated by applying the Weiland transport model for the simulations, while electron density (n_e), radiation (P_{rad}) and the effective ion charge (Z_{eff}) profiles are taken from experimental measurements; interferometry data with Lithium beam diagnostic, bolometry measurements and CXRS diagnostics for Carbon only, respectively. The boundary conditions are given in such way that $T^{sim}(\rho_{tor}=0.7)=T^{exp}(\rho_{tor}=0.7)$ for ion and electron temperatures. For the toroidal velocity, the assumption used in Chapter 2, $v_{tor}{}^{sim} = cT_i{}^{sim}$ is applied as well. The heat diffusivities are defined as the sum of the neoclassical and turbulent contributions, the poloidal rotation is assumed to be neoclassical. The simulations are started using initial current density profiles in agreement with experimental data, assuming neoclassical electrical conductivity.

A simulation is performed for pulse 13686 with original experimental conditions (using the same beam sources as used in the experiment) to validate the ASTRA simulation for this discharge. Time traces of central ion, electron temperatures and stored energy from the ASTRA simulation results are compared to those from experimental observations in figure 3.2.
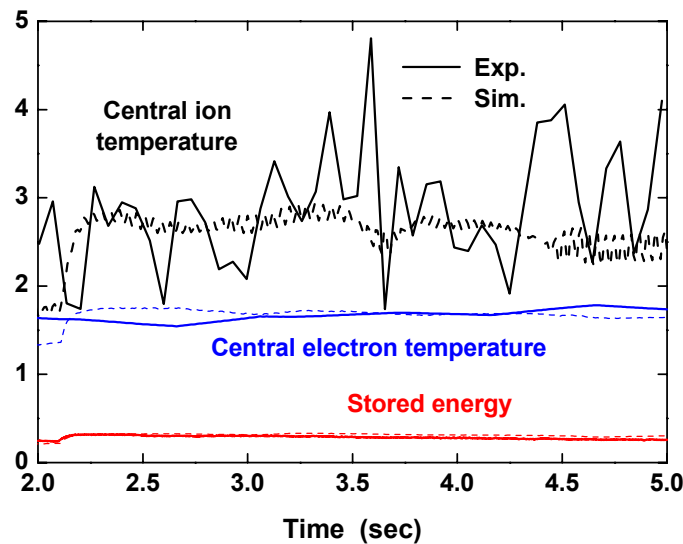

Figure 3.2. Time traces of central ion, electron temperatures and stored energy
from ASTRA simulations and experimental observations.

As shown in figure 3.2, The ASTRA simulation reproduces the measurements for this discharge, well within the measurement error bars. From this result, it is concluded that ASTRA simulations are appropriate to analyse transport in this discharge.

For investigation of the effect of changing beam sources, ASTRA simulations are performed for the same discharge (pulse 13686) but with different NB sources. They use two nearly perpendicular beam sources including source 3 for MSE measurements while for the third beam source, one of the four sources at 93kV is chosen, hence four different simulations are required. The beam trajectories of this discharge are shown in figure 3.3.
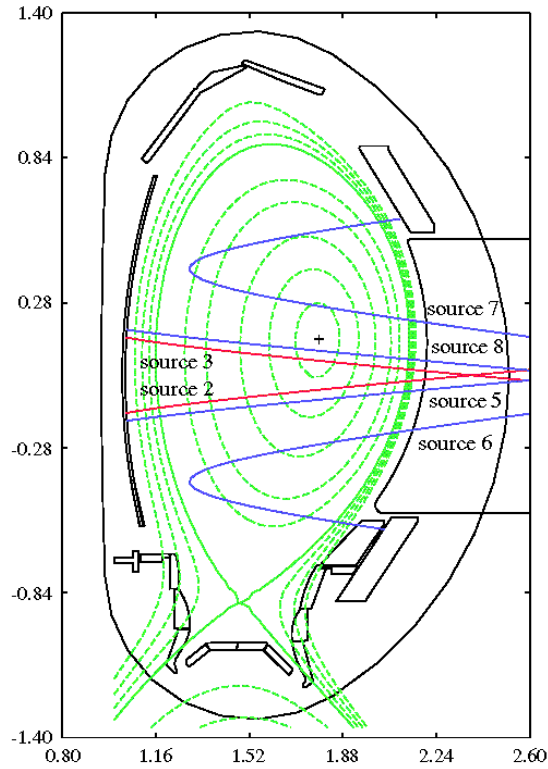
Figure 3.3. Beam injection trajectory of discharge 13686 at 2.5sec.
Vertical position of the magnetic axis is about 0.14m.

It is expected that for the plasma configuration used (Z_{axis} = 0.14m) from 2.5sec onwards, beam source 6 gives the most off-axis and beam source 8 gives the most on-axis current drive for this discharge (see figure 3.3).

The calculated current density profiles and corresponding q-profiles are shown in figure 3.4 and 3.5, respectively. In the simulation, a clear difference is observed in the current density profiles when different beam sources are used as the third beam source during stationary conditions as expected. Figure 3.4 (a) shows that beam source 6 gives the most broad current density profile, on the other hand beam source 8 gives the most centrally peaked current density profile. As a consequence, the highest central q-value and the lowest internal inductance are acquired by beam source 6 and the lowest central q-value and the highest internal inductance are obtained by source 8 as shown in figure 3.5. The non-inductive current drive fractions are compared for beam sources in table 3.1. It is observed that for the more off-axis the beam source, less NB and bootstrap current are observed. The simulated ion and electron temperature profiles using the Weiland transport model are shown in figure 3.6 for each beam source. As shown in figure 3.6, when beam source 8 is applied the highest temperature is observed for both ion and electron temperature profiles. Contrarily, when source 6 is applied the lowest temperatures are observed. This effect is dominant at the central region of the plasma. From these simulations, it is demonstrated that it is possible to change the current density profile by changing beam sources. This forms the basis to propose NBI as tool to control current profile at ASDEX Upgrade.

	NBI5	NBI6	NBI7	NBI8
$q(0)$	1.56	1.66	1.40	1.20
l_i	.879	.813	.912	.932
I_{NB}	.094 (23.5%)	.079 (19.8%)	.096 (24%)	.097 (24.3%)
I_{boot}	.201 (50.3%)	.188 (47%)	.204 (51%)	.204 (51%)

Table 3.1. Central q-value, internal inductance and contribution of the non-inductive current drive to total plasma current 400kA for each beam source. Currents are in MA.
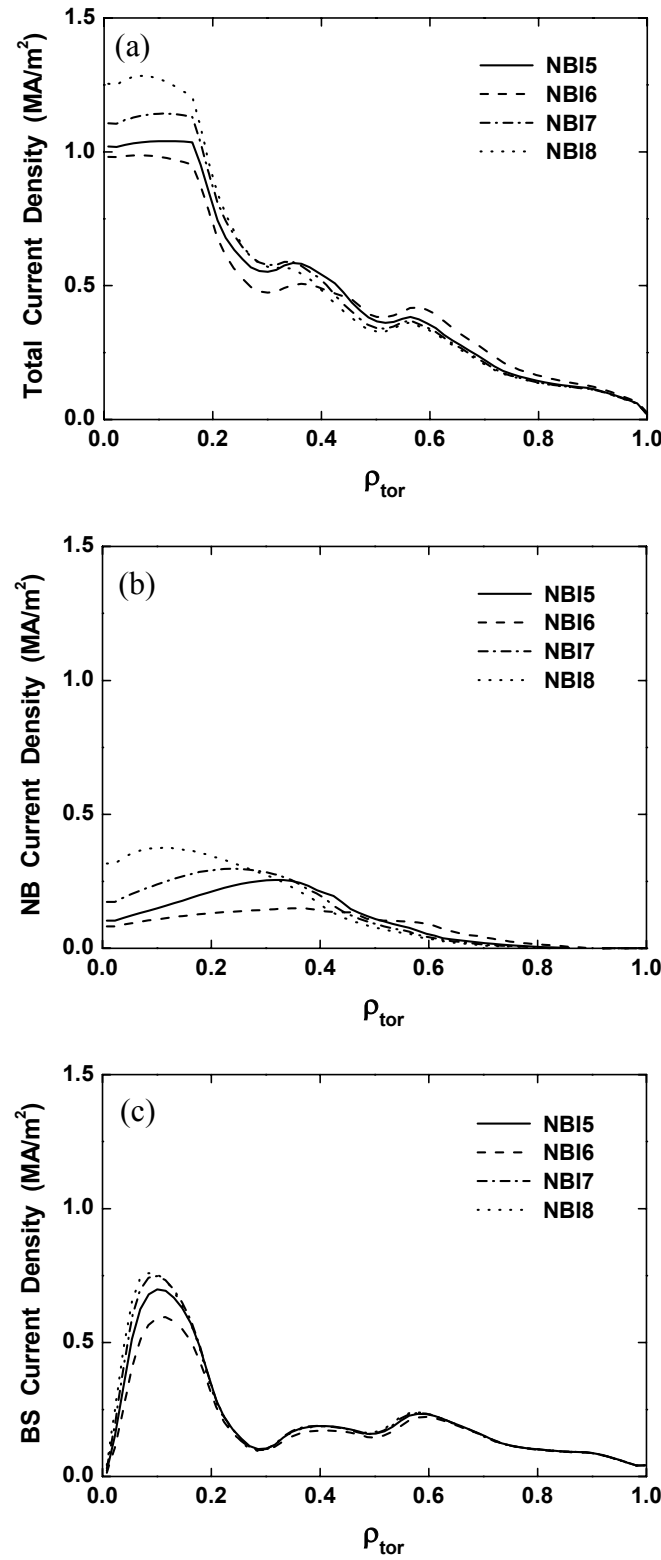
Figure 3.4. Total (a), NB driven (b), and bootstrap (c) current density profile for different beam sources at 6.5sec of pulse 13686. Here, bootstrap current is calculated by Kim's model.
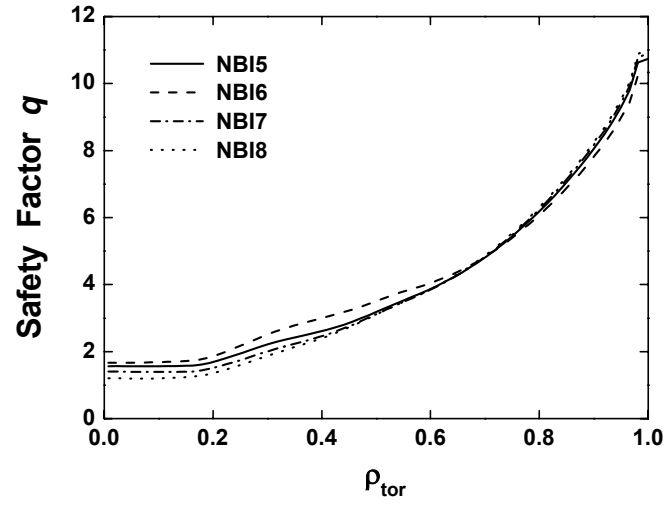
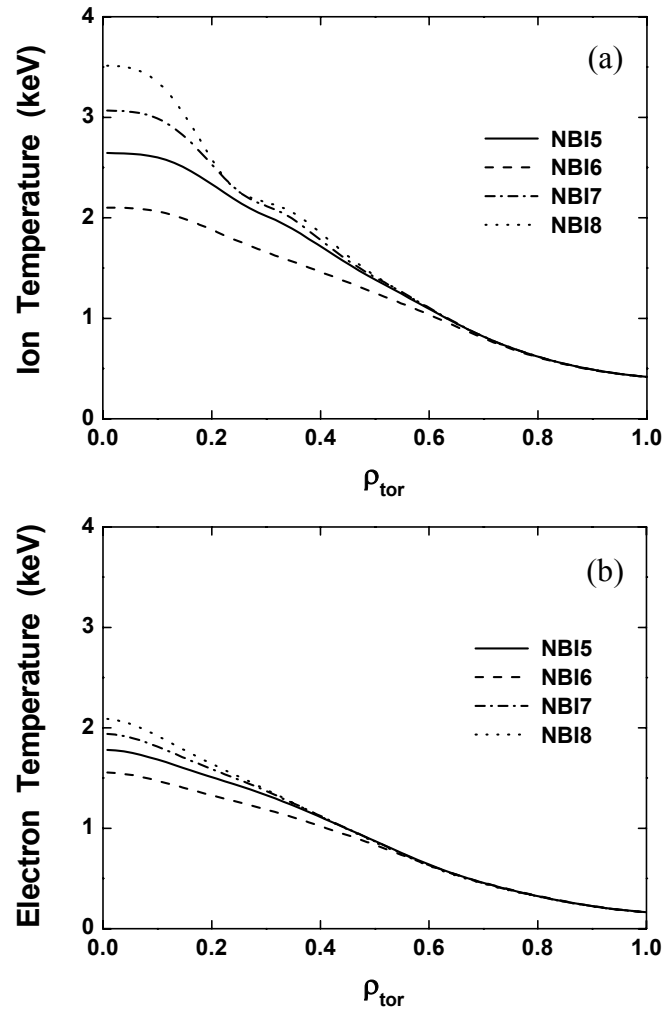*Figure 3.5. q-profiles for different beam sources at 6.5sec of pulse 13686.*

Figure 3.6. Ion (a) and electron (b) temperature profiles for different beam sources
at 6.5sec of pulse 13686.

3.3 System Modelling

In this section, system modelling is described generally. Firstly, signals, which compose a system, are described and basic dynamic models are given. Then, several models are expressed in polynomial forms and the state-space model, employed in this thesis is described in detail. System considered here is so-called a multivariable system which consists of several inputs and outputs. Treatment of this multivariable system and the basic steps of system modelling are presented.

The Signals

System modelling is to build mathematical models of a dynamic system based on measured data. Models describe relationships between measured signals, so-called input signals and output signals. The outputs are partly determined by the inputs. However, in most cases, the outputs are also affected by more signals than the measured inputs. Such unmeasured inputs are called disturbance signals or noise. If inputs, outputs, and disturbances are denoted by u, y and e, respectively, the relationship can be depicted in the following figure.
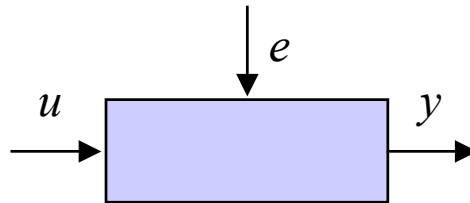

Figure 3.7. Input signals u, output signals y, and disturbances e.

All these signals are functions of time in a dynamic systems, and the value of the input at time t is denoted by $u(t)$. In many cases, only discrete-time points are considered, since the measurement equipment typically records the signals just at discrete-time instants, often equally spread in time with a sampling interval of T time units.
The modelling is to describe how the three signals relate to each other.

The Basic Dynamic Model

The basic input-output configuration is presented in the figure above. Assuming unit-sampling interval, there is an input signal

$$u(t); \quad t = 1, 2, \ldots, N$$

and an output signal

$$y(t); \quad t = 1, 2, \ldots, N$$

Assuming the signals are related by a linear system, general linear models, which describe the relationship between input and output signals can be written

$$y(t) = G(q)u(t) + v(t) \tag{3.1}$$

where $v(t)$ is an additional, immeasurable disturbance (noise). Alternatively, it can be described as filtered white noise:

$$v(t) = H(q)e(t) \tag{3.2}$$

Where $e(t)$ is white noise. Equations (3.1) and (3.2) together give a time domain description of the system:

$$y(t) = G(q)u(t) + H(q)e(t) \tag{3.3}$$

Which says that the measured output $y(t)$ is a sum of one contribution that comes from the measured input $u(t)$ and one contribution that comes from the noise $H(q)e(t)$. The symbol $G(q)$ then denotes the dynamic properties of the system, that is, how the output is formed from the input. For linear systems it is called the transfer function from input to output. The symbol $H(q)$ refers to the noise properties, and is called the noise model. It describes how the disturbances at the output are formed from some standardized noise source $e(t)$.

In equation (3.1), q is the shift operator and $G(q)u(t)$ is short for

$$G(q)u(t) = \sum_{k=1}^{\infty} g(k)u(t-k) \tag{3.4}$$

and

$$G(q) = \sum_{k=1}^{\infty} g(k)q^{-k} ; \qquad q^{-1}u(t) = u(t\text{-}1) \tag{3.5}$$

The numbers $\{g(k)\}$ are called the impulse response of the system. Clearly, $g(k)$ is the output of the system at time k if the input is a single (im)pulse at time zero.

The basic description (3.3) also applies to the multivariable case; systems with several input signals (nu) and several output signals (ny), which will be described in detail later on. In that case $G(q)$ is an ny by nu matrix while $H(q)$ is ny by ny matrix.

Polynomial Representation of Transfer Functions

The functions G and H in (3.3) can be specified in terms of functions of q^{-1} and the numerator and denominator coefficients in some way.

A commonly used parametric model is the ARX model that corresponds to

$$G(q) = q^{-nk} B(q) / A(q) ; \qquad H(q) = 1/A(q) \tag{3.6}$$

Where B and A are polynomials in the delay operator q^{-1}:

$$A(q) = 1 + a_1 q^{-1} + \ldots + a_{na}q^{-na} \tag{3.7}$$
$$B(q) = b_1 + b_2 q^{-1} + \ldots + b_{nb}q^{-nb+1} \tag{3.8}$$

Here, the numbers na and nb are the orders of the respective polynomials. The number nk is the number of delays from input to output. The model is usually written

$$A(q)y(t) = B(q)u(t\text{-}nk) + e(t) \tag{3.9}$$

or explicitly

$$y(t) + a_1 y(t\text{-}1) + \ldots + a_{na}y(t\text{-}na) =$$
$$b_1 u(t\text{-}nk) + b_2 u(t\text{-}nk\text{-}1) + \ldots + b_{nb}u(t\text{-}nk\text{-}nb+1) + e(t) \tag{3.10}$$

Note that (3.9)-(3.10) apply also to the multivariable case, where $A(q)$ and the coefficient a_i become ny by ny matrices, $B(q)$ and the coefficients b_i become ny by nu matrices.

Another very common, and more general, model structure is the ARMAX structure.

$$A(q)y(t) = B(q)u(t-nk) + C(q)e(t) \qquad (3.11)$$

Here, $A(q)$ and $B(q)$ are as in (3.7)-(3.8), while

$$C(q) = 1 + c_1q^{-1} + \ldots + c_{nc}q^{-nc} \qquad (3.12)$$

An Output-Error (OE) structure is obtained as

$$y(t) = B(q)u(t-nk)/F(q) + e(t) \qquad (3.13)$$

with

$$F(q) = 1 + f_1q^{-1} + \ldots + f_{nf}q^{-nf} \qquad (3.14)$$

The so-called Box-Jenkins (BJ) model structure is given by

$$y(t) = B(q)u(t-nk)/F(q) + C(q)e(t)/D(q) \qquad (3.15)$$

with

$$D(q) = 1 + d_1q^{-1} + \ldots + d_{nd}q^{-nd} \qquad (3.16)$$

All these models are special cases of the general parametric model structure:

$$A(q)y(t) = B(q)u(t-nk)/F(q) + C(q)e(t)/D(q) \qquad (3.17)$$

Within the structure (3.17), virtually all of the usual linear black-box model structures are obtained as special cases. The ARX structure is obtained for $nc = nd = nf = 0$. The ARMAX structure corresponds to $nf = nd = 0$. The ARARX structure (generalized least-squares model) is obtained for $nc = nf = 0$, while the ARARMAX structure

(extended matrix model) corresponds to $nf = 0$. The OE model is obtained with $na = nc = nd = 0$, while the BJ model corresponds to $na = 0$.

The same type of models can be defined for systems with an arbitrary number of inputs. They have the form

$$A(q)y(t) = B_1(q)u_1 (t\text{-}nk_1)/F_1 (q) + \ldots + B_{nu}(q)u_{nu} (t\text{-}nk_{nu})/F_{nu} (q) + C(q)e(t)/D(q)$$

State-Space Model

State-space models are common representations of dynamical models. They describe the same type of linear difference relationship between the inputs and the outputs as in the ARX model, but they are rearranged so that only one delay is used in the expressions. To achieve this, some extra variables, the state variables, are introduced. They are not measured, but can be reconstructed from the measured input-output data. This is especially useful when there are several output signals, i.e., when $y(t)$ is a vector. The order of the state-space model relates to the number of delayed inputs and outputs used in the corresponding linear difference equation. The state-space representation looks like

$$x(t+1) = Ax(t) + Bu(t) \tag{3.18a}$$
$$y(t) = Cx(t) + Du(t) + v(t) \tag{3.18b}$$

Here the relationship between the input $u(t)$ and the output $y(t)$ is defined via the nx-dimensional state vector $x(t)$. In transfer function form (3.18) corresponds to (3.1) with

$$G(q) = C(qI_{nx}\text{-}A)^{-1}B + D \tag{3.19}$$

Here I_{nx} is the nx by nx identity matrix. (3.18) can be viewed as one way of parameterising the transfer function: Via (3.19) $G(q)$ becomes a function of the elements of the matrices A, B, C, and D.

To further describe the character of the noise term $v(t)$ in (3.18), a more flexible innovations form of the state-space model can be used:

$$x(t+1) = Ax(t) + Bu(t) + Ke(t) \tag{3.20a}$$
$$y(t) = Cx(t) + Du(t) + e(t) \tag{3.20b}$$

This is equivalent to (3.3) with $G(q)$ given by (3.19) and $H(q)$ by

$$H(q) = C(qI_{nx}-A)^{-1}K + I_{ny} \qquad (3.21)$$

Here ny is the dimension of $y(t)$ and $e(t)$. The matrix K determines the noise properties. If $K = 0$, then the noise source $e(t)$ affects only the output, and no specific model of the noise properties is built. This corresponds to $H = 1$ in the general description above, and is usually referred to as an OE model. Also $D = 0$ means that there is no direct influence from $u(t)$ to $y(t)$. Thus the effect of the input on the output all passes via $x(t)$ and will be delayed at least one sample. The first value of the state variable vector $x(0)$ reflects the initial conditions for the system at the beginning of the data record. When dealing with models in state-space form, a typical option is whether to estimate D, K, and $x(0)$ or to let them be zero.

Multivariable Systems

Systems with many input signals and/or many output signals called multivariable. Such systems are hard to model. In particular, systems with several outputs could be difficult. A basic reason for the difficulties is that the couplings between several inputs and outputs lead to more complex models. The structures involved are richer and more parameters will be required to obtain a good fit. Generally, the fit gets better when more inputs are included and worse when more outputs are included. Models mentioned above are supported in the single output, multiple input cases. For multiple outputs, ARX models and state-space models are covered. Multi-output ARMAX and OE models are covered via state-space representations: ARMAX corresponds to estimating the K-matrix, while OE corresponds to fixing K to zero.

Generally, it is regarded that it is preferable to work with state-space models in the multivariable case, since the model structure complexity is easier to deal with [53]. Then, only choosing the model order is a task, which remains.

The Basic Steps of System Modelling

The system modelling is to estimate a model of a system based on observed input-output data. The system modelling process can be itemized as follows:

1. Design an experiment
2. Define input-output signals
3. Collect input-output signals from the process to be identified
4. Select and define a model structure (a set of candidate system descriptions) within which a model is to be found
5. Compute the best model in the model structure according to the input-output data
6. Examine the obtained model's properties (validation of the model)

Points 1 and 2 have been presented in §3.1 and §3.2, respectively. In the next section, the collection of input-output signals (point 3), the model will be defined (point 4), and the best models will be presented and discussed (point 5). A thorough validation of the models is given in chapter 4 (point 6).

3.4 Modelling of the Current Profile Control at ASDEX Upgrade

Modelling of the current profile control at ASDEX Upgrade will be described in this section following the system modelling process, which is described in §3.3. Results are given describing the best system model for the evolution of the current density and poloidal beta with the NB sources as input.

Design of an Experiment and Definition of input-output Signals

For the first step of system modelling, the design of an experiment is performed. The experiment is dynamic system of ASDEX Upgrade tokamak and the relationships between current profile and NB power and source are to be described by models. Variations of NB power from four tangential beam sources at 93kV (ΔP_{NB}) are defined as input signals. The number of output signals is matched to that of input signals because of the stability in controller design. Output signals are defined as variation of poloidal beta ($\Delta \beta_p$) and variation of current density values (Δj) at three radial positions.

Collection and Selection of Input-Output Signals

ASTRA simulations are carried out to produce a database; pairs of input-output signals. For the simulations, the discharge described in section 3.1 is taken as a basis. In the simulations, two beam sources (source 3 and 2, both at 60kV) are used to provide 5MW out of the 7.5MW used in the experiment of pulse 13686. In addition each of the four beam sources at 93kV is used, with modulated NB power for each beam source. The NB power from each beam sources is modulated with 10ms time scale for optimum response on current diffusion time scale. The waveform of the modulation is presented in figure 3.8.

Four different ASTRA simulations are performed for each of the four NB sources at 93kV (see figure 3.3 for the beam source alignment). The beam power in the simulations is modulated from 2.5sec to 10.11sec with an average power of 7.5MW. A total of 762 time points are saved as a database with a sampling time of 10ms. The modulation consists of two periods of 3.8seconds with the same modulation waveform. The second period from 6.31 to 10.11sec is chosen for the training dataset, that is to say, database for determination of the transfer functions, since the current density profile only reaches stationary conditions in the simulations in this period.
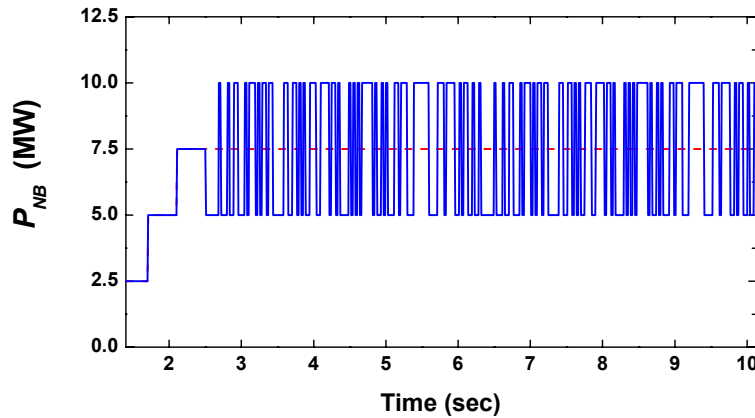

Figure 3.8. Waveform of the beam power modulation for each beam source.

The time variation of the current density profile during the modulation is compared that of without the modulation for source 6, the most off-axis current drive beam source, in figure 3.9. A clear difference is observed for r/a = 0.2-0.6, the region of off-axis beam

deposition as shown in figure 3.4 (b). The time variations of the current density profiles are computed for each beam source and stored as a training dataset.
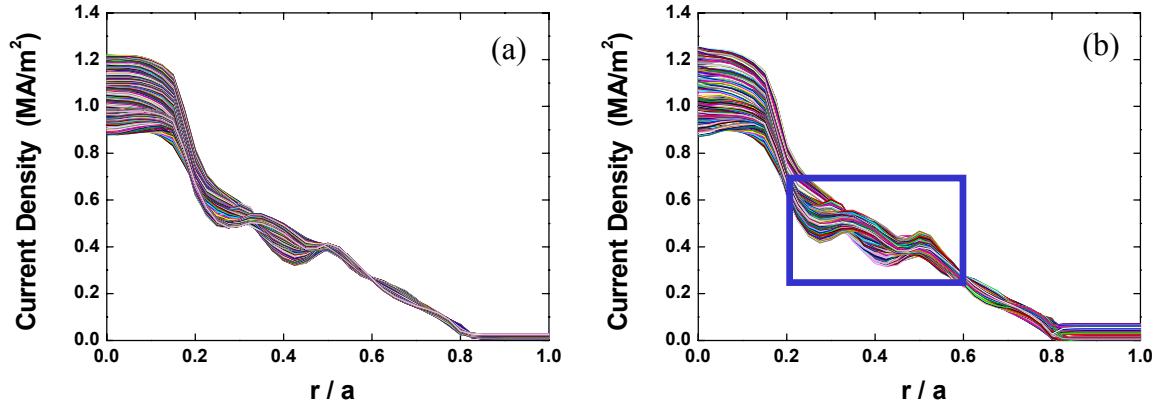

Figure 3.9. Time variation of the current density profile without (a), and with (b) the modulation for beam source 6 from 2.5 to 10.11sec, comprising two modulation time sequences as described in the text (the evolution includes the non-stationary first period, 2.5 to 6.3sec).

As mentioned in the beginning of this section, the output signals are defined as $\Delta\beta_p$ and Δj at three radial positions. Therefore, three radial positions, which are sensitive to the modulation of the beam power and change of the beam source, need to be selected among 41 positions at which time variation of current density values is stored during the ASTRA simulations. In figure 3.10, time variations of current density values at 41 radial positions are presented for each beam source. Each line represents the time variation of current density value at each radial position, where $j0$ is the current density calculated without the modulation of the beam power, total beam power is fixed to 7.5MW and $j1$ is one with the modulation.

Variance of $j1$-$j0$ is calculated from 2.5sec to 10.11sec for each radial position and compared for each beam source in figure 3.11. Numbers represented in abscissa indicate 41 radial positions for which corresponding radial positions are every 0.015m from r=0.00m to 0.600m; 0.000m, 0.015m, 0.030m, 0.045m, … , 0.585m, 0.600m.

In figures 3.10 and 3.11, beam source 8, the most on-axis source as shown in figure 3.3, shows the largest variation during the beam power modulation and gives centrally peaked profile for variance of $j1$-$j0$. On the other hand, beam source 6, the most off-axis current drive source as shown in figure 3.3, presents the smallest variation during the beam power modulation and gives broad profile for variance of $j1$-$j0$; current density is modulated over a wider region in the plasma, by the variation of the beam power.

Similarly, more or less on-axis beam source 7 and off-axis beam source 5, gives nearly centrally peaked profile and wide profile, respectively.

Three radial positions are selected, which are sensitive to change of the beam source and the variation of the beam power from figure 3.10, 3.11. One position is chosen in the central region, another in the off-axis region and the third in the edge region. In principle, it is desirable to choose the most central and the most edge positions because they are the most sensitive positions. However, present MSE diagnostic cannot cover the most central and edge regions. As a result, three positions at $r = 0.09$m, 0.225m, 0.435m are selected and which are indicated with arrows in figure 3.11.
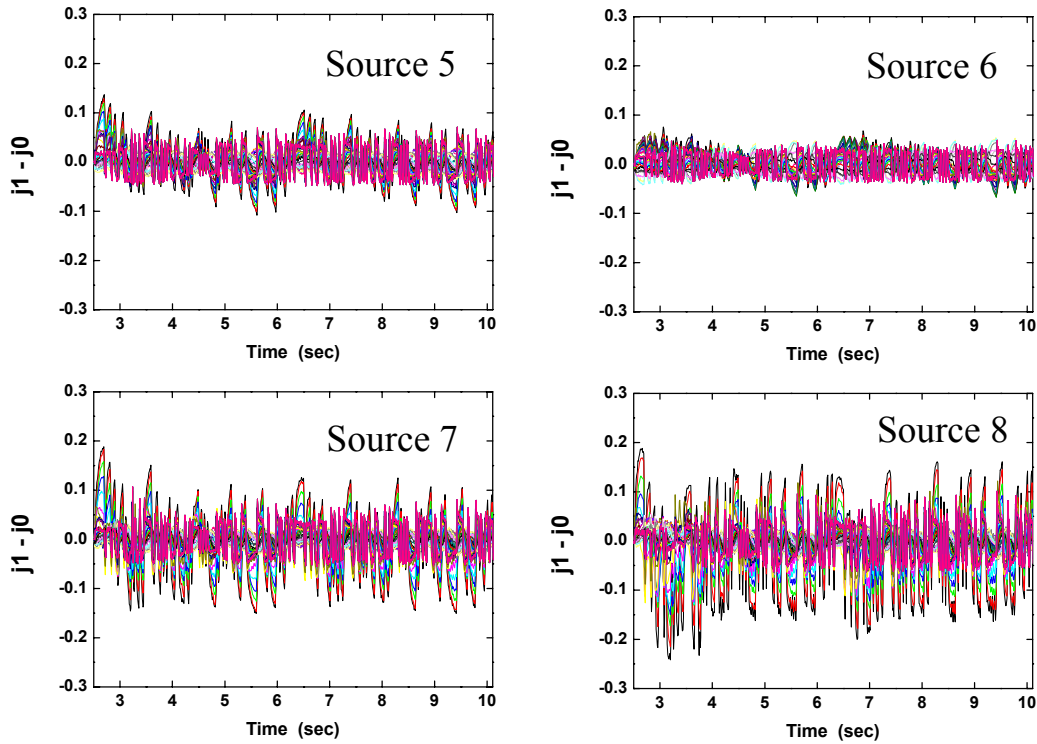
Figure 3.10. Time variation of current density values at 41 radial positions from 2.5 to 10.11sec.
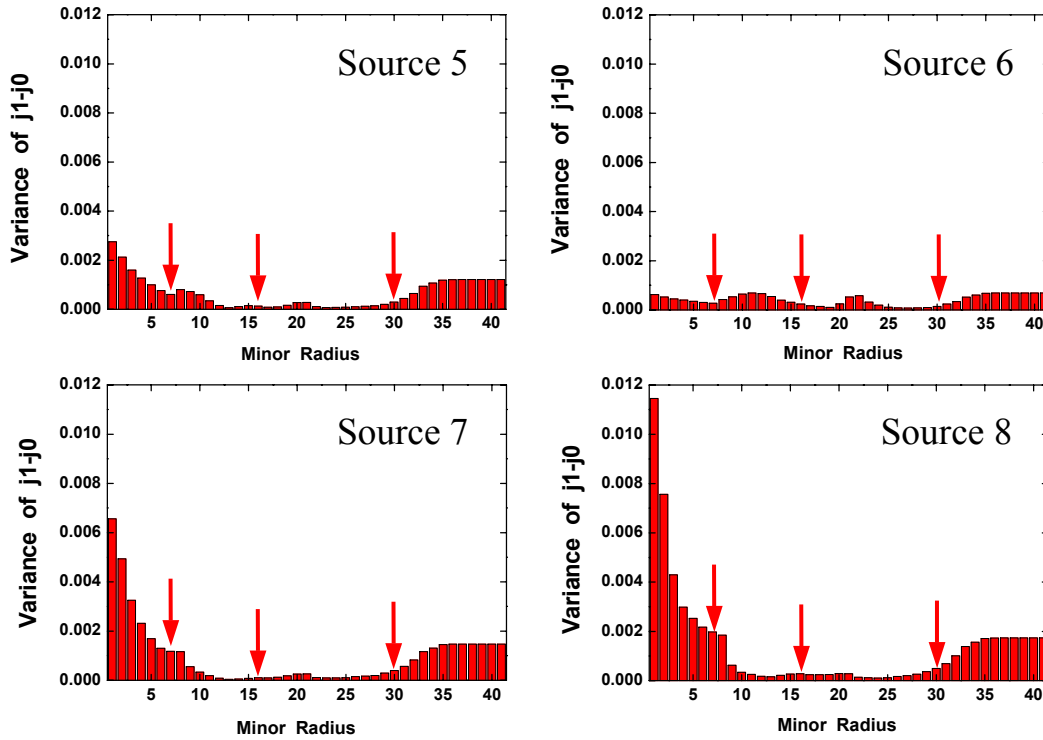
Figure 3.11. Variance of j1-j0 for 41 radial positions from 2.5 to 10.11sec.
3 selected positions are indicated with arrows.

Selection and Definition of Model Structures

The system for current profile control is multivariable system, multi-input multi-output (MIMO). Therefore, a state-space model is employed for system modelling since it is well suited for MIMO systems as described in Multivariable Systems in §3.3.

Once a model, state-space model, is selected, then it is necessary to define a model structure. For state-space model, the model structure is determined by the order. The nth order of state-space model, which can be applied for this system, is given from (3.20)

$$x(t+1) = Ax(t) + Bu(t) + Ke(t) \qquad (3.20a)$$
$$y(t) = Cx(t) + Du(t) + e(t) \qquad (3.20b)$$

where *A* is *n* by *n* matrix, *B* is *n* by 4 matrix, *C* is 4 by *n* matrix, *D* is 4 by 4 matrix, *K* is *n* by 4 matrix and *u* is four input signals, *y* is four output signals (details are in §3.3).

Optimisation of the Model According to the Training Dataset

In general, the accuracy of the system model can be improved by increasing the order of state-space model, provided enough data are available to obtain the model. However, it is required to trade-off between accuracy of the model and complexity of the model structure, directly associated with the computational time, which is important for real-time control.

Determination of the transfer functions for a given model structure is performed using "System Identification tool box" in MATLAB (MATrix LABoratory) program [53]. It regards the current profile control system as a black box and calculates the transfer functions with the training dataset for given model structure. Therefore, in effect the model replaces the ASTRA simulations.

A variety of state-space models with different orders are tried to find an optimal model for the given system. Among them, the 8th and 15th order of state-space models, which give globally good results, are chosen for comparison. They are shown in figure 3.12.

Shown is the fit accuracy of the computed models for four output signals (variation of poloidal beta and current density values at r = 0.09m, 0.225m, 0.435m) for four different input signals (variation of NB powers from four tangential beam sources at 93kV). The results are presented as open and closed symbols for 8th and 15th state-space models, respectively.
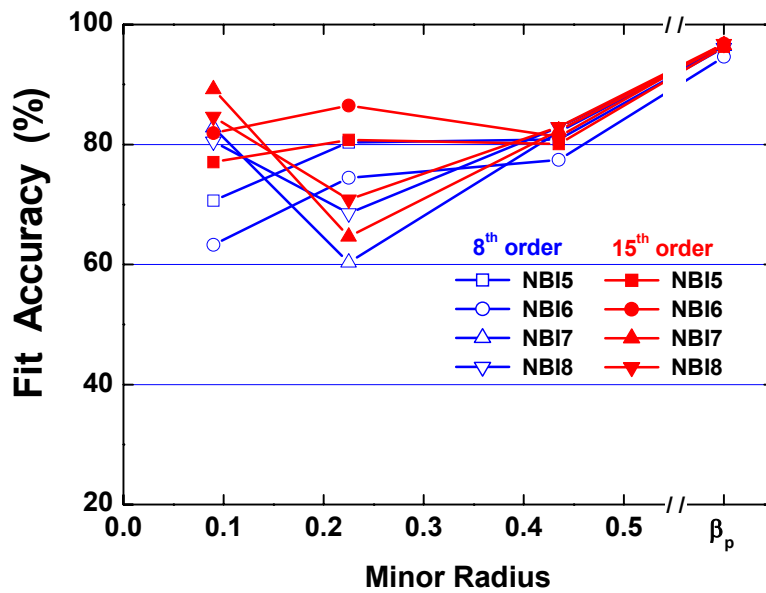

Figure 3.12. Model fit accuracy for 8th and 15th order of state-space model for training dataset.

The fit accuracy is defined as

$$\text{Fit accuracy (\%)} = \{1 - norm(y\text{-}y_{sim})/norm(y\text{-}mean(y))\} \times 100$$

Where y is the measured/reference output from ASTRA simulations and y_{sim} is the simulated/predicted output from the model. The function, $mean(x)$ is the mean value of x and $norm(x)$ is the Euclidean length of a vector x.

As shown in figure 3.12, both state-space models show fit accuracies above 60% for every case. Particularly for poloidal beta, very high fit accuracy above 96% is achieved for every beam source. However, for current density at $r = 0.225$m, the worst result is observed among four output signals. For this radius, the ASTRA simulations show the smallest response ($j1$-$j0$) for modulation of the NB sources (see figure 3.11), hence more prone to system noise.

3.5 Application to JET

For real-time control of current density profile, model-based control method for current profile has been proposed in JET [54] and current profile control experiments have been performed with LHCD during the initial phase of the discharge (plasma current rise phase) [55] and with combined LHCD/ICRH/NBI in an ITB scenario with a significant bootstrap current fraction [56]. In JET, MSE and Faraday rotation diagnostics are used for identifying the current density profile.

As ASDEX Upgrade, NB sources are available to drive a current in the plasma at JET (see figure 1.4). Thus, the similar approach in ASDEX Upgrade can be applied to current profile control in JET using the individual NB sources as actuators. Using similar methods introduced in §3.4, modelling of current profile control is performed for JET.

As input signals for the current profile control system at JET, variations of NB power (ΔP_{NB}) from six beam sources (PINIs 3 to 8) at octant 4 (80kV) are selected. Other two sources (PINIs 1 and 2) at octant 4 are excluded due to the MSE measurements (they are applied independently to allow discrimination of the MSE spectrum obtained from PINI 1). As output signals variation of poloidal beta ($\Delta \beta_p$) and variation of current density values (Δj) at (maximum) five radial positions are selected. To perform the ASTRA simulations for JET, a discharge (pulse 55425) in H-mode at low plasma current at JET

(1.2MA, 1.2T) with up to 6.9MW beam power is chosen, as this discharge is similar to the ASDEX Upgrade used in this chapter (introduced in §3.1).

As for ASDEX Upgrade, a training dataset is produced from ASTRA simulations applying beam power modulation for each beam source. A different time scale is used for the beam modulation in JET. Initial modulation tests were performed using the same modulation frequency as used for ASDEX Upgrade, however this resulted in non-satisfactory system identification. The optimum modulation frequency is 10-15 times lower than that of ASDEX Upgrade in agreement with a slower current diffusion time scale at JET compared to ASDEX Upgrade.

From the simulation results, five radial positions, sensitive to the modulation of the beam power and change of beam sources, are selected for output signals; $r = 0.083$m, 0.138m, 0.192m, 0.248m, 0.88m. The 15th order of state-space model shown in §3.4 is employed for modelling. The modelling results are shown in figure 3.13 with fit accuracies. They are similar to results observed for ASDEX Upgrade; for poloidal beta, the best result (fit accuracies above 90%) is achieved for every beam source. However for current density at $r = 0.248$m, the worst result is observed among six output signals as for this radius, the ASTRA simulations show the smallest response ($j1$-$j0$) for modulation of the NB sources and change of beam sources.
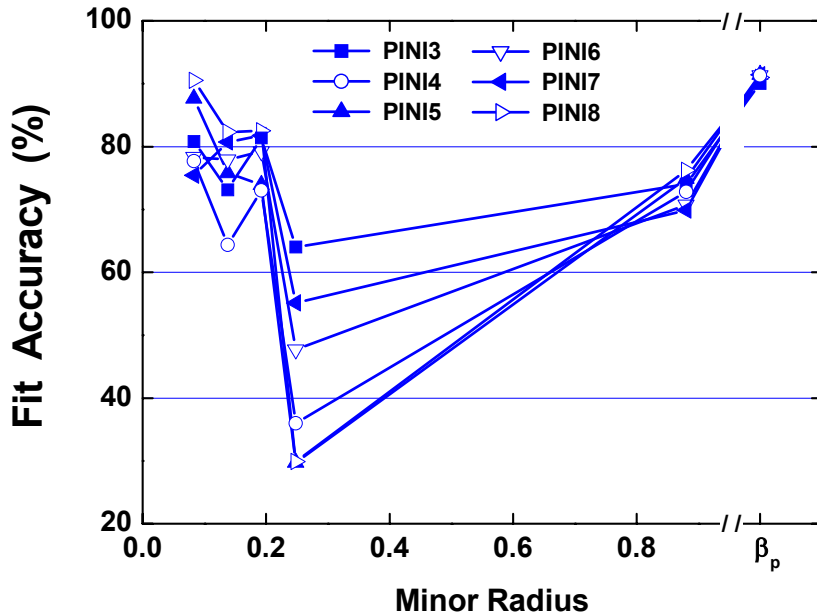

Figure 3.13. Model fit accuracy for 15th order of state-space model for training dataset in JET.

Seeing these results for JET, the method developed at ASDEX Upgrade can be used directly for current profile control in other devices like JET provided, the modulation time is adjusted to typical current diffusion time scale of the experiment. This is the main reason that results have been presented here. However, using the model obtained for JET control purposes is not possible yet. The ASTRA simulations of the NB current drive overestimates the central current density as given in chapter 2, where the current densities from different transport codes are compared for JET. This problem is not solved yet. Therefore, the region inside $r < 0.083$m has been excluded from the modelling results. Moreover, the six NB sources in JET mainly drive current in the central region. This makes control of the current profile shape difficult, as there is redundancy in the actuators. One can see from figure 3.13 that only for the central and edge regions of the plasma satisfactory modelling results are obtained.

3.6 Summary of the Results and Discussion

The possibility of changing current density profile at ASDEX Upgrade by changing NB sources is checked by ASTRA code simulations. A high poloidal beta discharge with low plasma current is chosen for the simulations in which the effect of NB current drive is more pronounced. It is observed that different current density profiles are achieved in stationary conditions when different beam sources are applied. The different NBI sources change the ohmic, the bootstrap and the directly beam driven current density profiles due to changes in the temperature profiles, density profiles and tangential injection angle of the neutral beams.

Based on these results, modelling of the current density profile control at ASDEX Upgrade is carried out. Input signals for the system are variations of NB power from four tangential NB sources at 93kV (ΔP_{NB}) and output signals are variation of poloidal beta and variation of current density values at three radial positions ($\Delta \beta_p$ and Δj). State-space models are chosen for modelling of this system since they are well suited for multivariable systems. A training dataset is produced by the ASTRA code to determine transfer functions of state-space models. NB power is modulated during the simulations for each beam source and corresponding variation of current density profile is recorded in the training dataset. Three radial positions in range of diagnostic measurements (MSE diagnostic) and sensitive to change of the beam source, the modulation of the beam power are selected as output signals.

To obtain an optimal state-space model for the given system, a variety of orders of state-space model are applied for modelling. Their average fit accuracies are compared in figure 3.14, where fit accuracy represents accuracy of the model in terms of ASTRA results. As shown, average fit accuracy roughly increases with order. It rises to 8th order clearly and then stays around 80% to 13th order. It starts to increase again for higher orders. The 8th order, model that has average fit accuracy higher than 80% and the 15th order, model that has the highest value (84.3%), are chosen for modelling. Higher than 15th order of state-space models are ruled out in this work since structural complexity of them will increase the computational time, when they are employed for real-time control. For 8th and 15th state-space models, over 60% of fit accuracies are obtained for all output signals. In case of poloidal beta, high fit accuracy above 96% is obtained for every beam source. For current density at $r = 0.225$m, however, the worst results are observed. It seems to be more difficult to find a good model for this compared to other output signals.
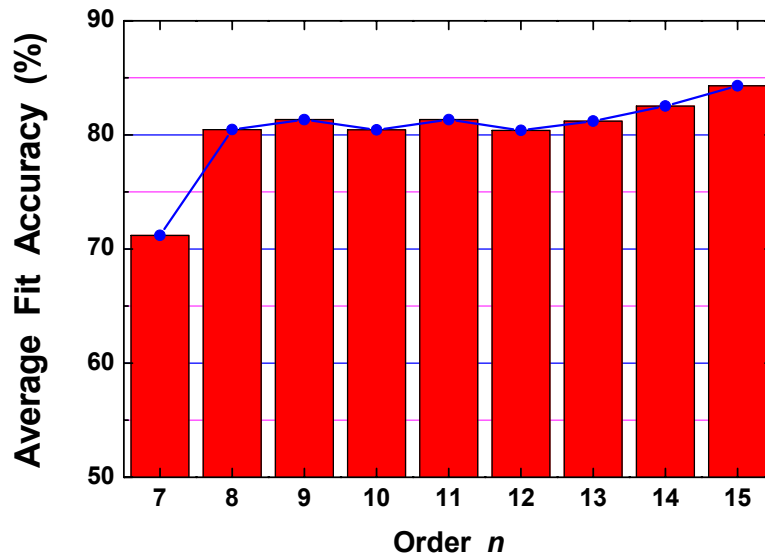

Figure 3.14. Average fit accuracies for 7th to 15th state-space models. Average is taken on fit accuracies of all output signals of a state-space model.

The output signal for the worst result is represented in figure 3.15, which observed for current density at 0.225m for beam source 7 by the 8th order state-space model (represented as an open triangular in figure 3.12). The fit accuracy for this case is 60.3%. The predicted signal follows the time trend of reference signal, though it shows an

overshoot sometimes. As shown in figure 3.15, it comes from the fact that the model cannot produce the spikes well from the ASTRA simulations at some time points. The model does not have the same frequency response as the ASTRA simulations.
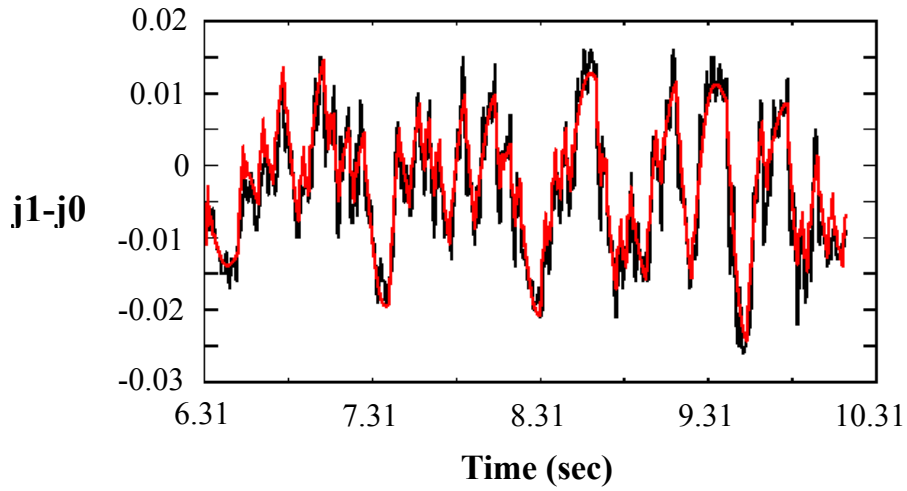

Figure 3.15. Time variation of current density (j1-j0) at r = 0.225m for modulation of beam source 7 (ΔP_{NB}). The dark line (in black) represents reference signal (y); computed by ASTRA code and the light line (in red) represents predicted output signal (y_{sim}); computed by the 8th order state-space model.

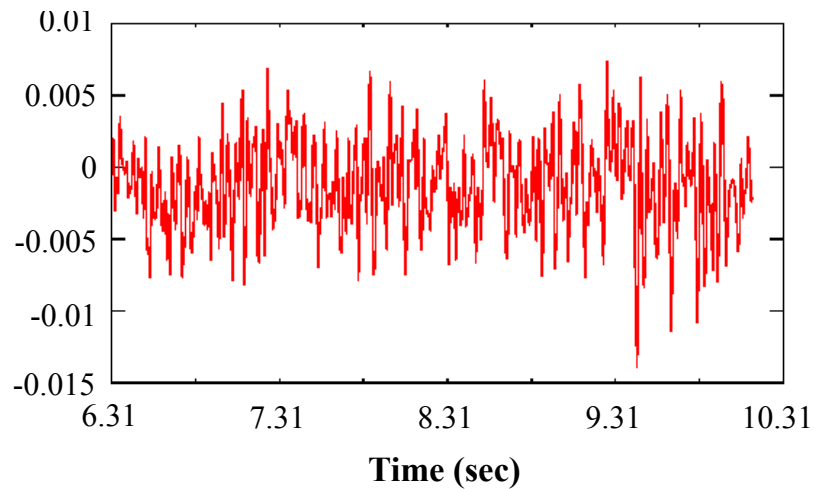The error plot of model versus simulation is given in figure 3.16, where error is defined as y- y_{sim}.

Figure 3.16. Error (y- y_{sim}) plot of the identified model for current density at r = 0.225m for source 7.

While in figures 3.15 and 3.16 an example is given for the worst case comparing the model and ASTRA simulation, the best results are shown in figure 3.17 and 3.18. These are achieved for the variation of poloidal beta with the modulation of beam source 6, represented as a closed circle in figure 3.12. The accuracy for this case is 96.8%.
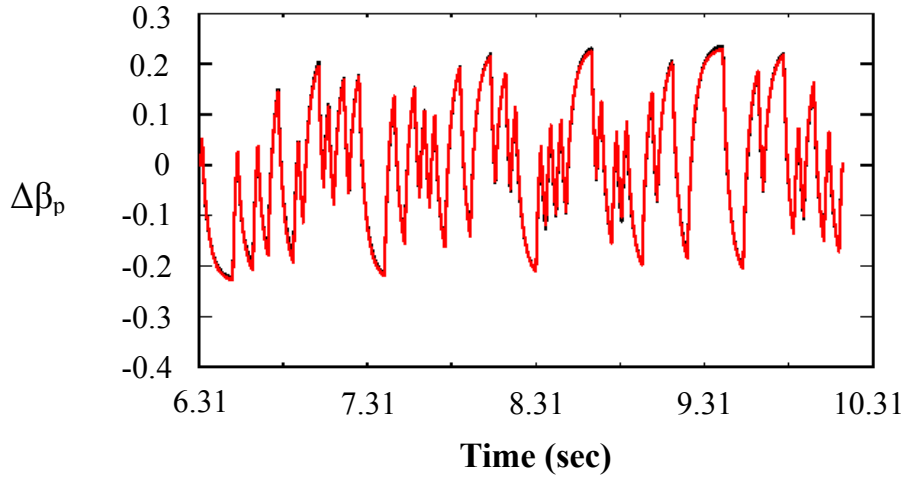

Figure 3.17. Time variation of poloidal beta ($\Delta\beta_p$) for modulation of beam source 6 (ΔP_{NB}).
The dark line (in black) represents reference signal (y); computed by ASTRA code and the light line (in red) represents predicted output signal (y_{sim}); computed by the 15th order state-space model.
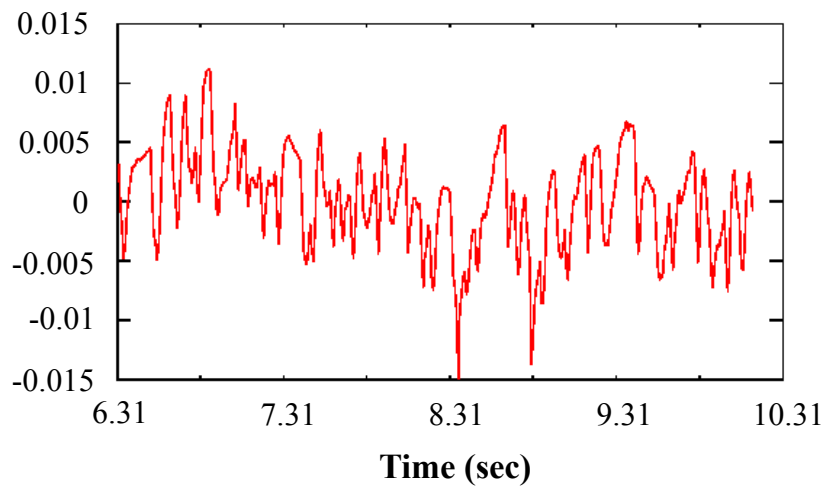

Figure 3.18. Error (y- y_{sim}) plot for the identified model for poloidal beta for source 6.

As shown in figure 3.14, the higher order of state-space models give globally better result than that of lower order of state-space models. Nevertheless, it cannot be concluded that the higher order model performs better compared to a lower order model. As shown in figure 3.12, better fit accuracies are observed for certain cases with 8th state-space model. Therefore, it is required to validate the calculated models by using a test dataset, which does not contain data used for calculation of the models. This type of model validation will be discussed in following chapter.

The method used at ASDEX Upgrade can be applied to modelling of current density profile control in JET with variations of NB power from six beam sources at 80kV (ΔP_{NB}) as input signals and variation of poloidal beta and variation of current density values at five radial positions ($\Delta \beta_p$ and Δj) as output signals. Owing to the different current diffusion time scale in JET, different frequencies of beam power modulation are used to ASTRA simulations preparing a training dataset.

Very similar results are obtained in JET compared to ASDEX Upgrade but with slightly lower fit accuracies. Moreover, from the ASTRA simulations and the modelling results, it is observed that it is more difficult to find a good model for off-axis regions compared to ASDEX Upgrade. For current density at $r = 0.248$m, the worst result (29.7% of fit accuracy for PINI 5) is observed out of six output signals. From the simulations with the beam power modulation, it is observed that off-axis regions show small response ($j1$-$j0$) for modulation of the NB sources and change of beam sources.

ASTRA results are presented in figure 3.19 to see the effect of changing beam sources in JET. In figure 3.19 (b), centrally peaked NB driven current density profiles are observed as discussed in §2.3. It is unclear at present why these ASTRA simulations give such a peaked NB driven current density profile on-axis and this will be investigated as a future work. As shown in the figure 3.19 (a), pronounced off-axis current drive is not observed at a stationary state even using the most off-axis beam source at JET. The bootstrap current density profiles are nearly the same for all beam sources due to the similar temperature profiles. However, grouping of the most off-axis beam sources or changing the alignment of the beam sources is believed to maximize the off-axis current drive in JET.

Seeing the results for JET, the method developed for ASDEX Upgrade can be used directly for current profile control in other tokamaks like JET, provided the modulation time is adjusted to typical current diffusion time scale of the experiment. This method can also be used for other current drive methods, for example RF heating methods, if models for these current drive actuators are available in ASTRA or other transport codes.
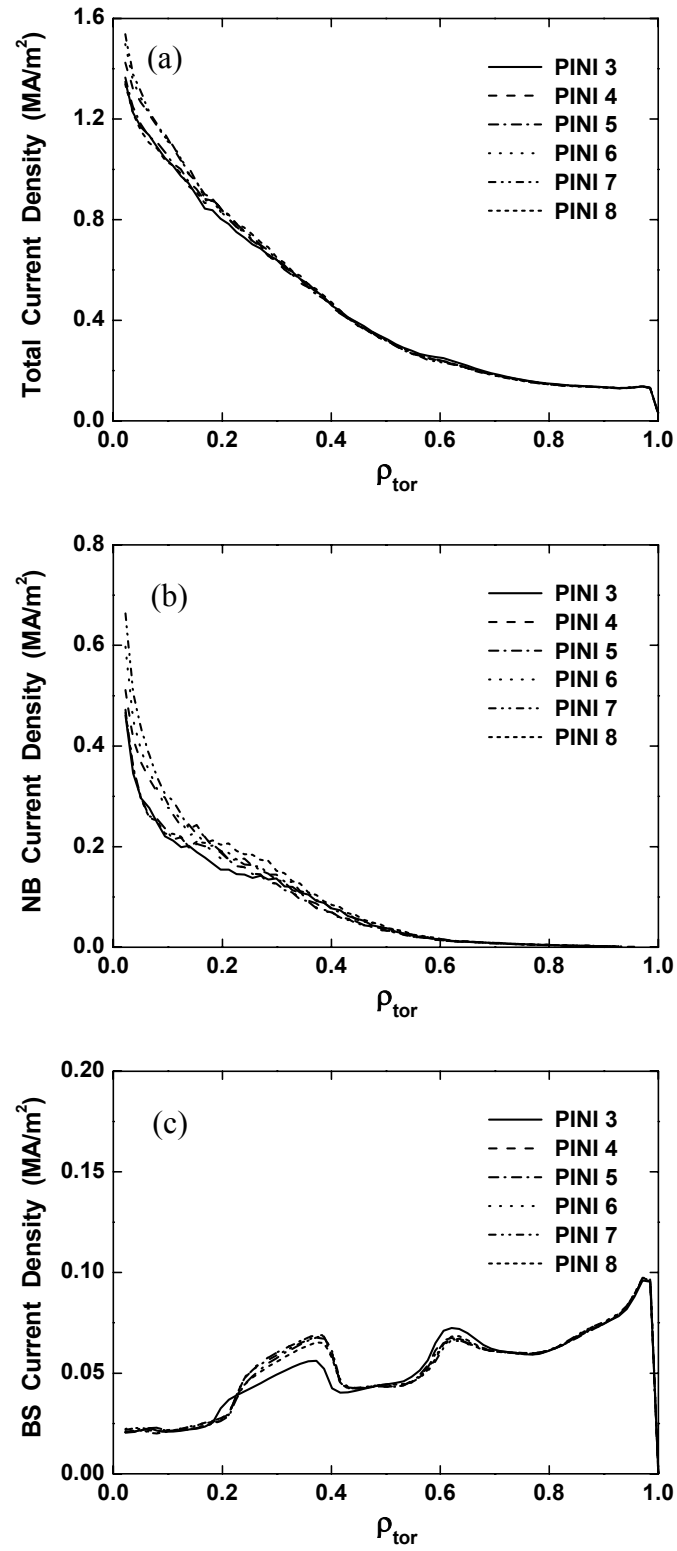
Figure 3.19. Total (a), NB driven (b), and bootstrap (c) current density profile in different scales for different beam sources at 12.5sec of pulse 55425. Here, bootstrap current is calculated by Kim's model.

Chapter 4

Model Validation and Comparison to Experimental Observations

In the previous chapter, possible models for current profile control have been calculated. These models are identified by determining transfer functions between input signals and output signals. The input signals are the variation of NB powers from four tangential beam sources at 93kV (ΔP_{NB}), the output signals are the variation of poloidal beta ($\Delta \beta_p$), current density values (Δj) at three radial positions. The results of the calculation in chapter 3 are based on a training dataset produced by the ASTRA code. In this chapter, validation of these identified models is performed with a step response to NB power (§4.1). Again the ASTRA code is used to produce a database for validation. Second, an experiment is designed changing beam sources keeping the total beam power constant in order to verify the calculation of current density profiles by the ASTRA code (§4.2). Here, measurements of the variation of the current density profile with the MSE diagnostic at ASDEX Upgrade are compared to ASTRA simulations and the model obtained from the training dataset (§4.3). For this discharge, more detailed ASTRA calculations are performed to verify the experimentally observed changes to the measured polarisation angles in §4.4. In addition, the effect of local NB current drive is discussed. The results of this chapter are summarised and discussed in §4.5

4.1 Model Validation

Model validation is the process of gaining confidence in a model obtained from a training dataset. It can be a test to take a close look at the model's output compared to the measured one on a dataset that wasn't used for the fit. Of particular importance is the model's ability to reproduce the behaviour of a test dataset, database for validation. A test dataset is produced by the ASTRA code. The same discharge (pulse 13686) is used as for producing the training dataset (described in §3.1). A step response of the NB

sources is used for test dataset shown in figure 4.1. The beam power is perturbed after 6.31sec where the current density profile reaches stationary conditions. This is in contrast to the modulated NB oscillation, which contained a range of frequencies used for the training dataset. The results of the ASTRA simulations are stored from 6.31sec to 10.11 as a test dataset. The models obtained in §3.4, 8th and 15th state-space models, are validated with this test dataset. First, output signals are calculated by transfer functions, determined by training dataset, using input signals given by test dataset. Second, calculated output signals are compared to reference output signals given by test dataset. Their fit accuracies are represented in figure 4.2.
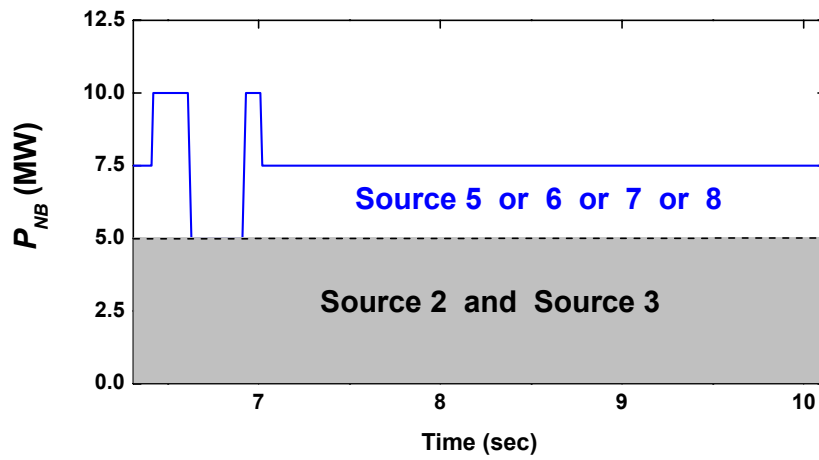

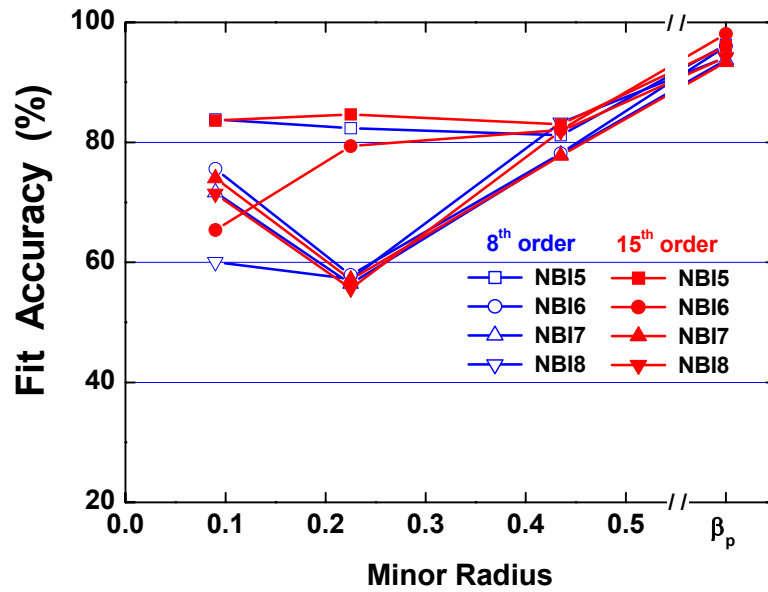*Figure 4.1. Waveform of a step response in beam power for each beam source.*

Figure 4.2. Model fit accuracy for 8th and 15th order of state-space model for test dataset.

As shown in figure 4.2, similar fit accuracies are observed for both models as those of the training case, presented in figure 3.12. This implies that both models can be used for the system, describing the relationship between ΔP_{NB} from four NB sources as input and $\Delta\beta_p$, Δj at three radial positions as output. For the current density at $r = 0.225$m, the test results confirm that the modelling for this output signal is not as good as for other output signals (see figure 3.12). The worst and the best results are presented in figures 4.3, 4.4 and 4.5, 4.6, respectively. The worst one is observed for the current density at r=0.225m for the step response of beam source 8 using a 15th state-space model. The fit accuracy of this is 55.7% and presented as a closed nabla in figure 4.2.
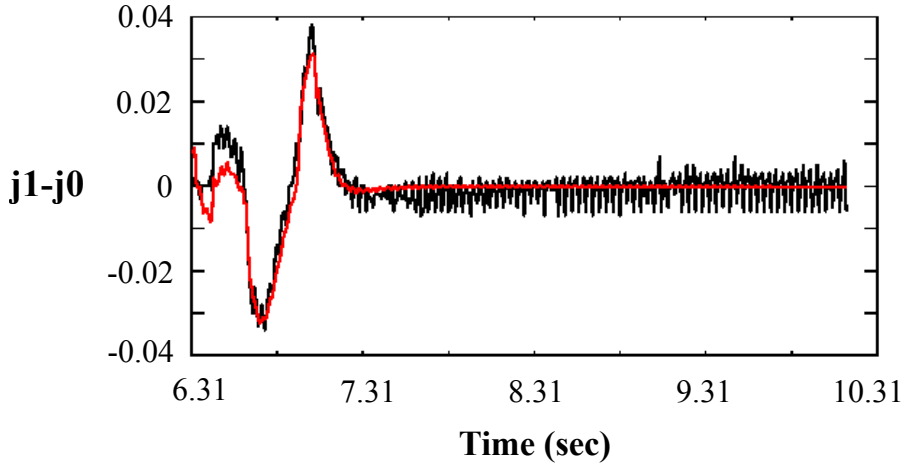

Figure 4.3. Time variation of current density (j1-j0) at r = 0.225m for the step response of beam source 8 (ΔP_{NB}). The dark line (in black) represents reference signal (y); computed by ASTRA code and the light line (in red) represents predicted output signal (y_{sim}); computed by the 15th state-space model.

The largest difference between reference and predicted signals comes out in the beginning of the step response as shown in figure 4.3. The model overshoots the value at the initial stage. It tries to recover this, however overshoots again but downward. Due to this overshot, it fails to match the reference signal till around 6.6sec. In spite of these overshoots, the predicted signal follows the trend of the reference signal well. This is essential to use a model for current profile control.

As shown in figure 4.3 and 4.4, oscillations are observed on the reference signal. They are regarded as a numerical noise. Although it gives rise to lower fit accuracy of the model, it does not disturb the model to predict the time trend well.
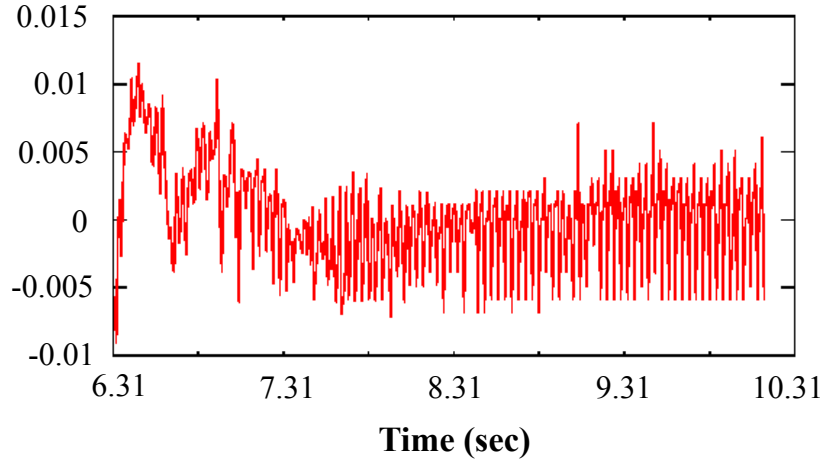
Figure 4.4. Error (y- y$_{sim}$) plot for the identified model for current density at r = 0.225m for source 8.

The best result is shown in figure 4.5 and 4.6 for comparison. It is achieved for the output of poloidal beta with beam source 6 using a 15th state-space model. The fit accuracy of this is 98.1%, presented as a closed circle in figure 4.2.
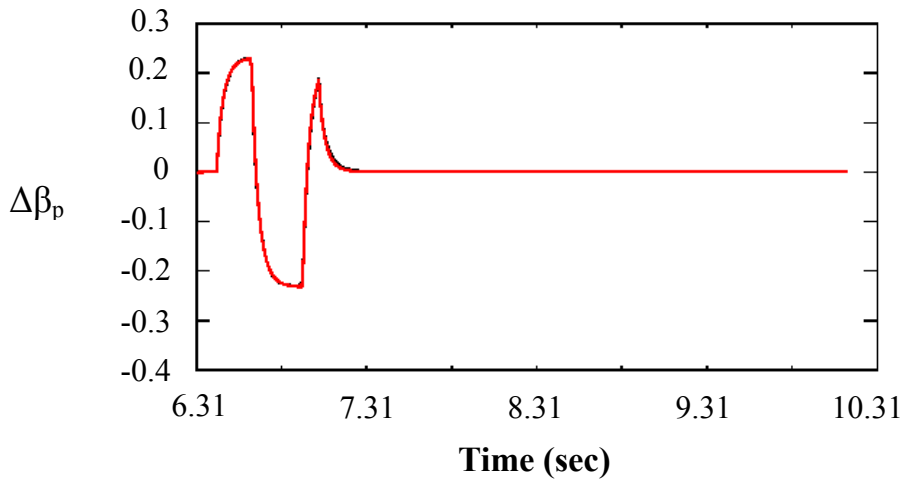

Figure 4.5. Time variation of poloidal beta (Δβ$_p$) for the step response of beam source 6 (ΔP$_{NB}$). The dark line (in black) represents reference signal (y); computed by ASTRA code and the light line (in red) represents predicted output signal (y$_{sim}$); computed by the 15th state-space model.
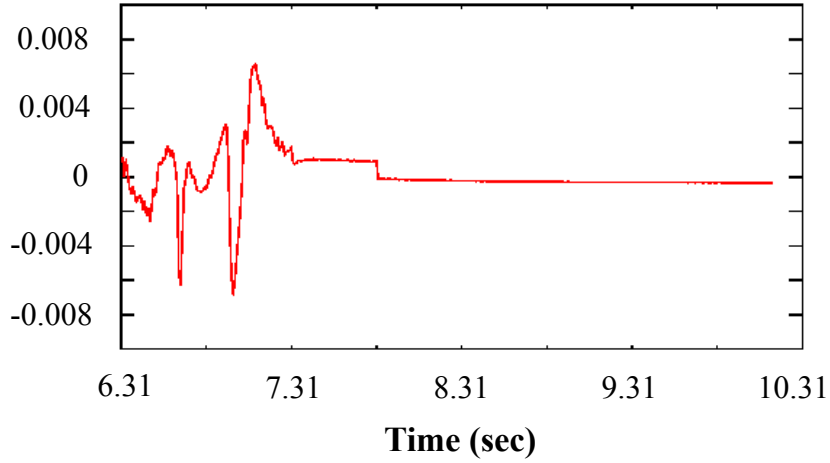
Figure 4.6. Error (y- y$_{sim}$) plot for the identified model for poloidal beta for source 6.

4.2 Experimental Set-up

A discharge (pulse 17530) is designed to validate the calculations of current density profile by ASTRA. It is based on the experimental set-up of a high poloidal beta discharge, pulse 13686 (figure 3.1), which is employed to produce a database for modelling. The time traces of experimental parameters for pulse 17530 are shown in figure 4.7.

Here, central ion temperature (T_i) is obtained from CXRS diagnostics and averaged electron temperatures (T_e) from ECE diagnostics. Line-averaged electron density (n_e) is taken from interferometry data. n_e is kept above 3.5×10^{19} in order to avoid shinethrough (the fraction of the injected power not absorbed by the plasma, which hits the inner walls) of the beams. Plasma current is 400kA and toroidal magnetic field is 2T. Total beam power is kept constant at 5MW with two beam sources. One of them, beam source 3, is fixed for MSE measurements during the discharge. For the second NB, source 8 is switched on until 3.5sec when current profile reaches stationary conditions. After this, source 8 is replaced by other three beam sources at 93kV in sequence. Each beam source lasts for 1sec; source 6, 5 and 7 is applied from 3.5 to 4.5sec, 4.5 to 5.5sec and 5.5 to 6.5sec, respectively. Source 8 is turned on again after 6.5sec. Here, two tangential

current drive beam sources (source 6 and 7) are not used in succession to avoid central impurity accumulation, sometimes observed with off-axis heating at ASDEX Upgrade [57].
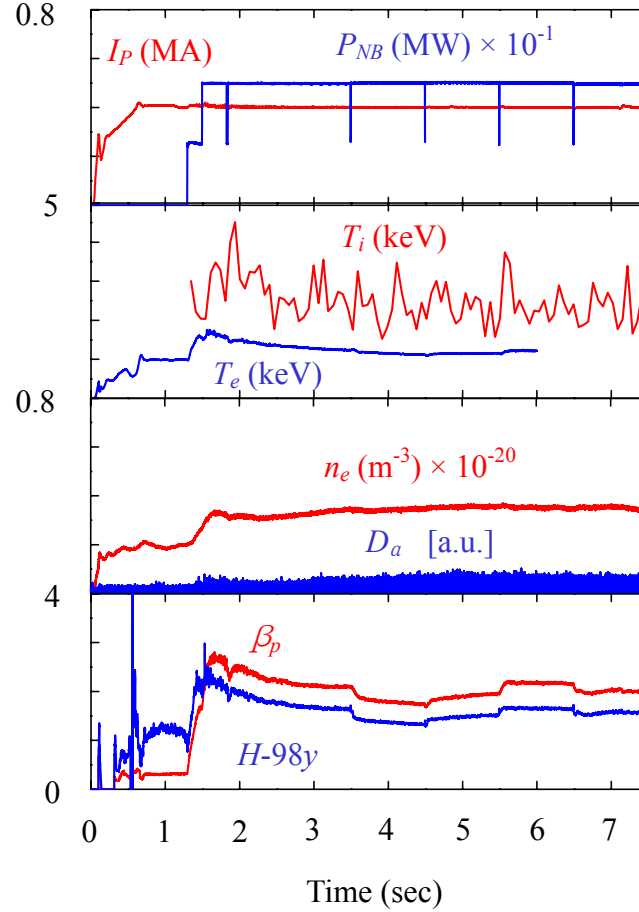

Figure 4.7. Time traces of plasma current, NB heating power (beam source 3 is fixed for MSE diagnostics), central ion temperature and averaged electron temperature, line-averaged electron density, D alpha, poloidal beta, $H_{98}(y,2)$ of pulse 17530 in ASDEX Upgrade

The beam injection trajectory for sources is depicted in figure 4.8. Similar to figure 3.3, source 8 is expected to give most on-axis and source 6 most off-axis current drive. As shown in figure 4.7, temperature, β_p and $H_{98}(y,2)$ are reduced most when most off-axis beam source 6 is applied.

Other discharges are also performed to check the effect of changing beam sources but with a similar experimental set-up to pulse 13686 (7.5MW beam power with three beam sources). Among three beam sources, source 3 is fixed for MSE measurements. For

other two sources, pair of on-axis beam sources or pair of off-axis beam sources are applied in order to amplify the on-axis or off-axis current drive effect. They are replaced by each other for 1sec when the plasma reaches stationary conditions. However, using two on-axis beam sources causes problems during the experiment due to overheating of the inner limiters.

In the following section, measured change of MSE polarisation angles is compared to the simulated one by the ASTRA code for pulse 17530.
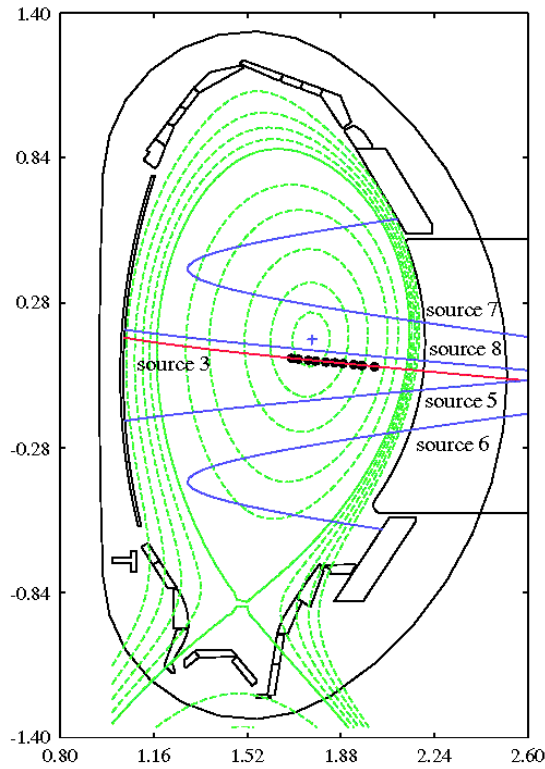
Figure 4.8. Beam injection trajectory of discharge 17530 at 2.5sec. Vertical position of the magnetic axis is 0.14m. The location of 10 MSE channels are presented as black closed circles

4.3 Comparison of the Simulated MSE Angles to the Measured MSE Angles

MSE angles can be calculated from simulated current density profiles in the ASTRA code. Therefore, the calculated MSE signals can be compared to those observed in the experiment in order to verify the calculation of current density profiles using ASTRA. As MSE measurements have not been calibrated in ASDEX Upgrade, the MSE angles, only the time variation of the 10 channels, are compared to those calculated by ASTRA. For ASTRA simulations, ion (T_i) and electron (T_e) temperature profiles are taken form CXRS diagnostics and ECE diagnostics, respectively. Electron density (n_e) profiles are acquired from TS data. Radiation (P_{rad}) profiles are obtained from bolometry measurements. The effective ion charge (Z_{eff}) is assumed to be constant during the discharge, Z_{eff}= 2.5. Total stored energy is matched to that from the experiment, since change of MSE angles are considerably influenced by change of the stored energy (see below).

The measured MSE signals are given in figure 4.9 (b) as a solid line with small oscillations, where they are compared to those calculated by the ASTRA code using experimental profiles. The lowest MSE signal is obtained from channel 1, which located in the most off-axis region and the highest one from channel 10, which located in the most on-axis region. The location of the 10 channels for MSE diagnostics is presented as black closed circle in figure 4.8. An offset to the measured MSE signals is given manually around 3sec where MSE angles reach stationary conditions, so a direct comparison of the time evolution of the MSE measurements and simulated MSE signals can be made.

As shown in figure 4.9 (b), variations in time of the modelled MSE angles do agree well with the measured polarization angles. The main contribution to the change of the MSE angles seems to be the change in the stored energy as shown in figure 4.9 (a). Clear changes are observed each time, the beam source is replaced. Particularly, when most off-axis current drive source (source 6) is applied, it is observed that angles from central channels decrease and angles from edge channels increase. Corresponding current density and *q*-profiles are shown in figure 4.10 at 3.45, 4.45, 5.45, 6.45sec, where 0.05sec before replacement of each source, and at 7.45sec. The current density, which reaches stationary conditions at 3.45sec is presented as a solid line and at 4.45sec at the end of the phase using source 6 is presented in dashed line. The current density profile at 5.45sec at the end of the phase using source 5 is presented in dashed dot line, at 6.45sec at the end of the phase using source 7 is presented in dot line and finally at

7.45sec at the end of the heating phase using source 8 again is presented in dashed dot dot line. When source 8 is replaced by source 6, the current density profile broadens. The broadest current density profile is observed at 6.45sec, at the end of the phase using source 7. As shown in figure 4.10 (b), it allows the highest central and minimum q-values. On the other hand, when it is replaced by source 8, then current density profile changes to a more peaked profile with lower central q.
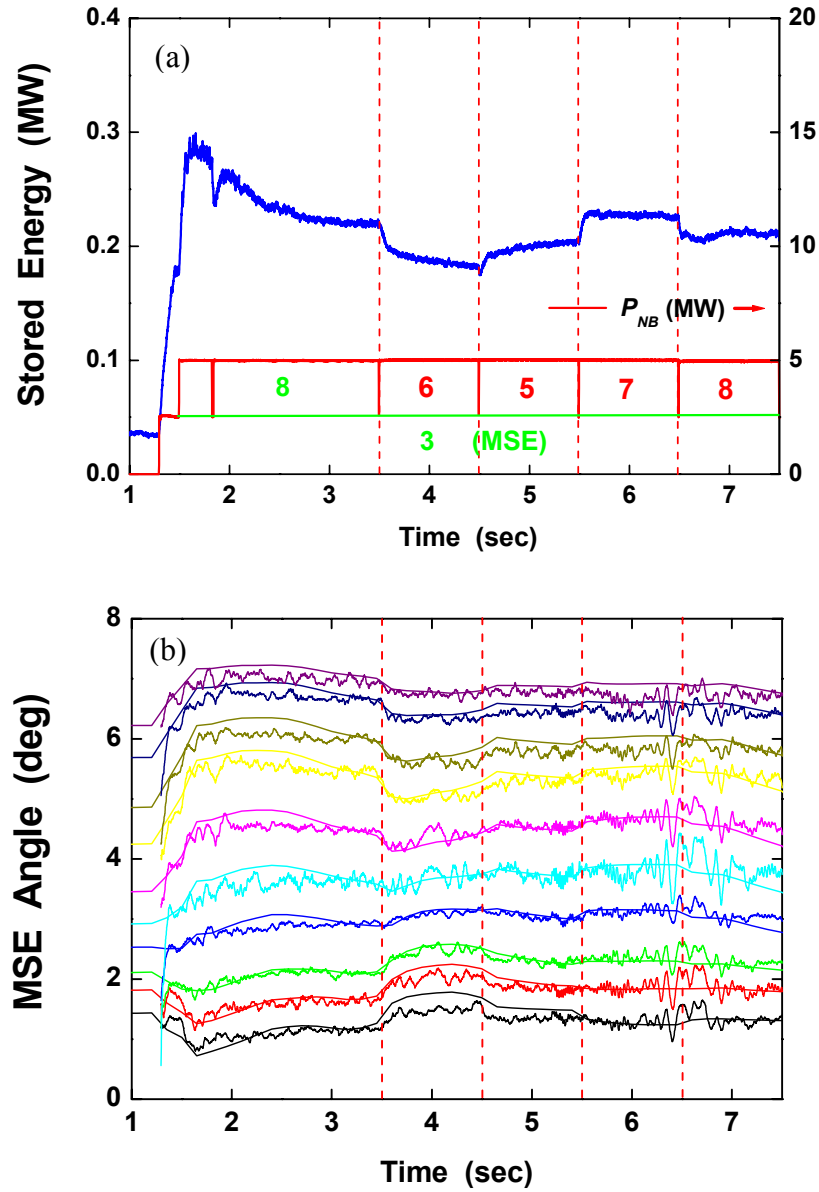

Figure 4.9. Pulse 17530 at ASDEX Upgrade; stored energy and beam power is presented in (a), beam source is changed at 3.5sec to source 6, at 4.5sec to source 5, at 5.5sec to source 7 and at 6.5sec to source 8. Time points where the beam source is changed are presented in vertical dashed lines. MSE angles from the experiment (with small oscillations) and the ASTRA simulation are presented in (b).
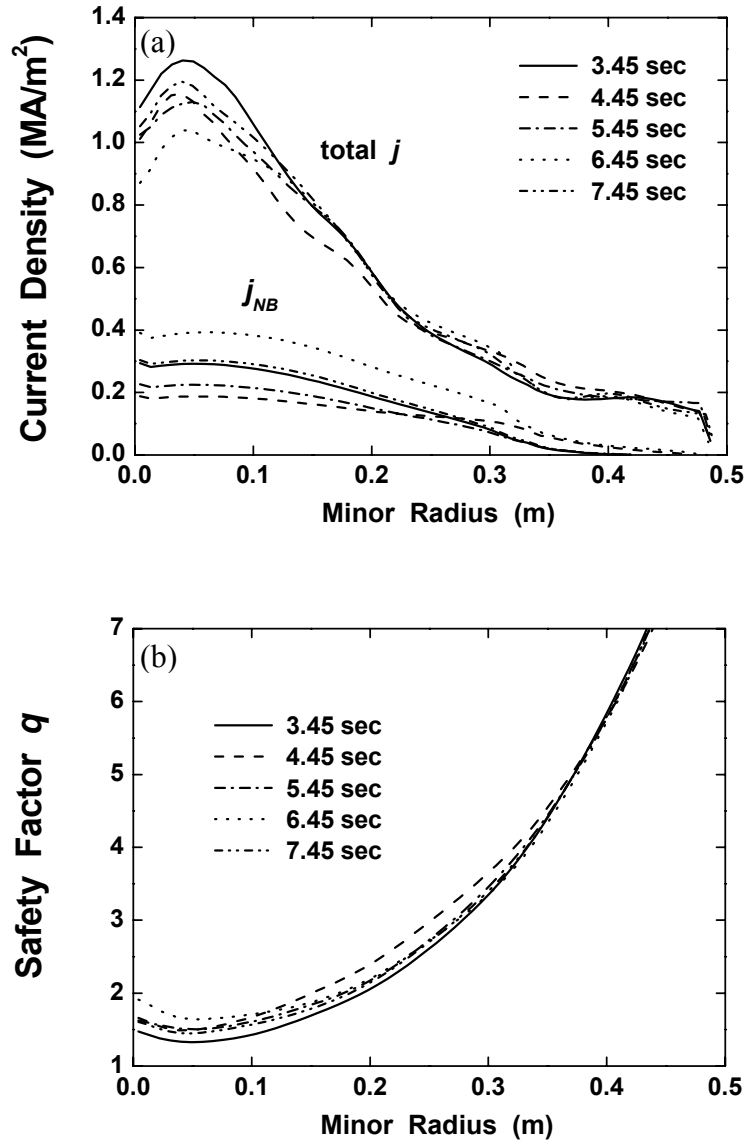
Figure 4.10. Simulated current density profiles (a) and q-profiles (b) at 3.45, 4.45, 5.45, 6.45 and 7.45sec by ASTRA using experimental profiles in pulse 17530.

Shown in figure 4.11 (a) is the time variation of current density values at selected three radial positions, which are used as output signals for modelling. The current density at *r*=0.09m changes most when the beam source is changed. Current density profile can be reconstructed by these three current density values as shown in figure 4.11 (b). Despite having only three radial positions, it is comparable to figure 4.10 (a).
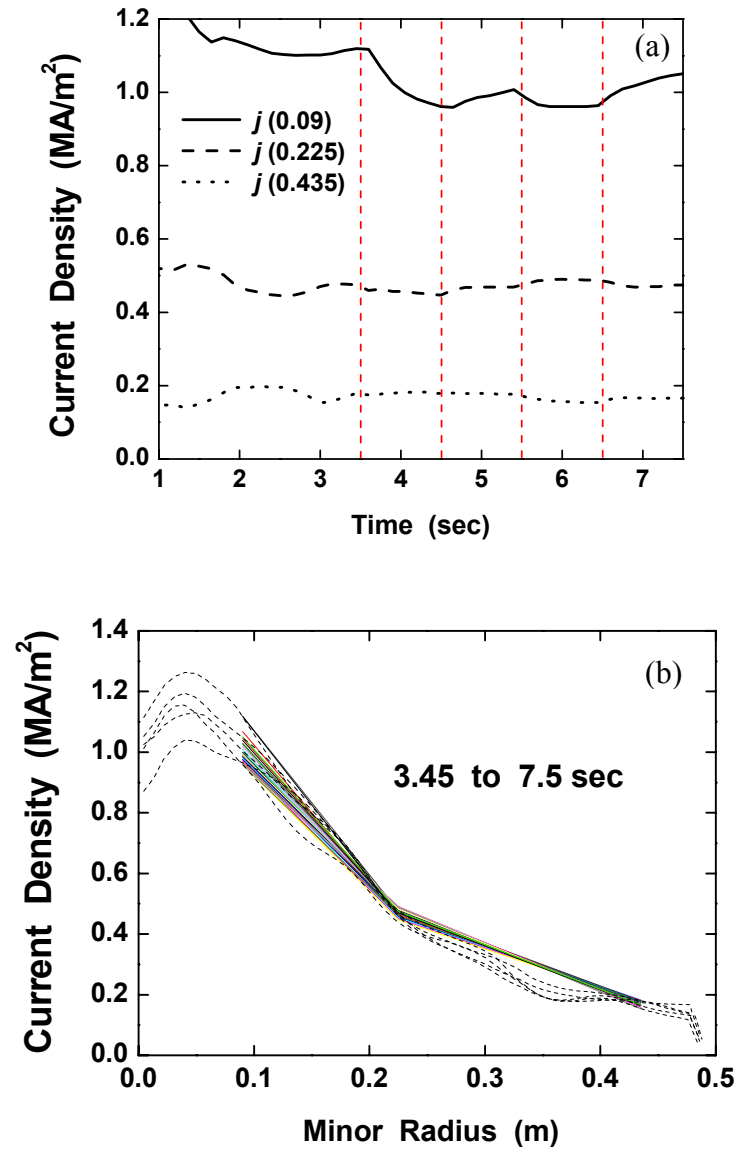
Figure 4.11. (a) Time variation of current density at selected three radial positions (r = 0.09m, 0.225m, 0.435m). (b) Time variation of current density profile, which is reconstructed with selected three radial positions. Here, current density profiles at 3.45, 4.45, 5.45, 6.45 and 7.45 presented in figure 4.10 (a) are shown in dashed lines. All presented results are from ASTRA simulations using experimental profiles for pulse 17530.

4.4 The Effect of Neutral Beam Current Drive

The effect of local neutral beam current drive has been under discussion in ASDEX Upgrade after the NB geometry was modified [58]. To investigate the effect of NB current drive in pulse 17530, ASTRA simulations are carried out excluding the NB current calculation, but keeping the beam heating of the plasma. The simulated MSE angles without local NB current drive in ASTRA are compared to the measured MSE angles.
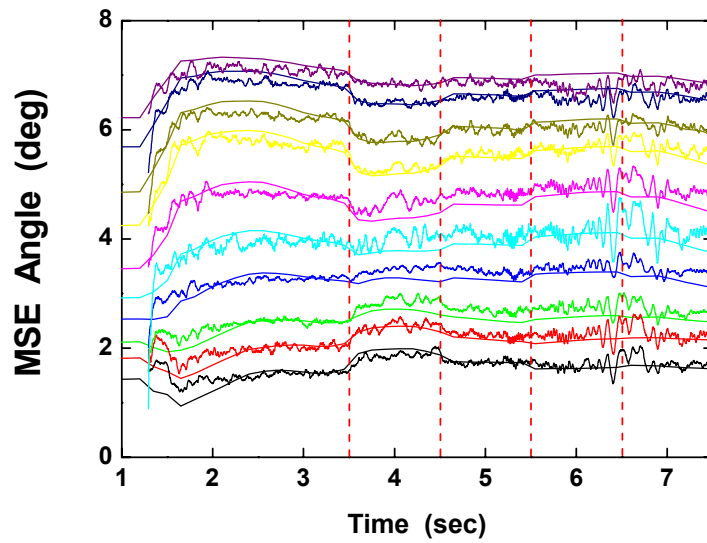

Figure 4.12. MSE angles from experimental measurements (with small oscillations) and the ASTRA simulation without beam current drive.

As shown in figure 4.12, the results of these simulations generally agree with experimental measurements like the simulations including the beam current drive, presented in figure 4.9 (b). However, offsets used here (so the simulations are equal to the experiment at $t = 3.1$sec) are different from that used in figure 4.9 (b). In figure 4.13, MSE angles from experimental measurements, simulations with and without local beam current drive are compared for channel 4, 5 and 6 of the MSE system. The NB driven current density profile has a maximum around the region where MSE channel 4, 5 and 6 are located, when off-axis beam sources are applied. Here, offsets used for the non-calibrated experimental data are the same as in figure 4.9 (b) including the beam current drive. As one can see in figure 4.13, differences are observed between the two simulations particularly from 3.5 to 5.5 sec where beam source 6 and 5 are applied,

respectively. The time evolution of the simulated MSE angles with beam current drive could fit the experimental data better, compared to simulations without beam current drive. However, these differences are in the range of experimental error bar. Furthermore, the offset given here is not the real one, thus it is essential to calibrate MSE measurement in order to investigate the effect of local beam current drive more exactly.
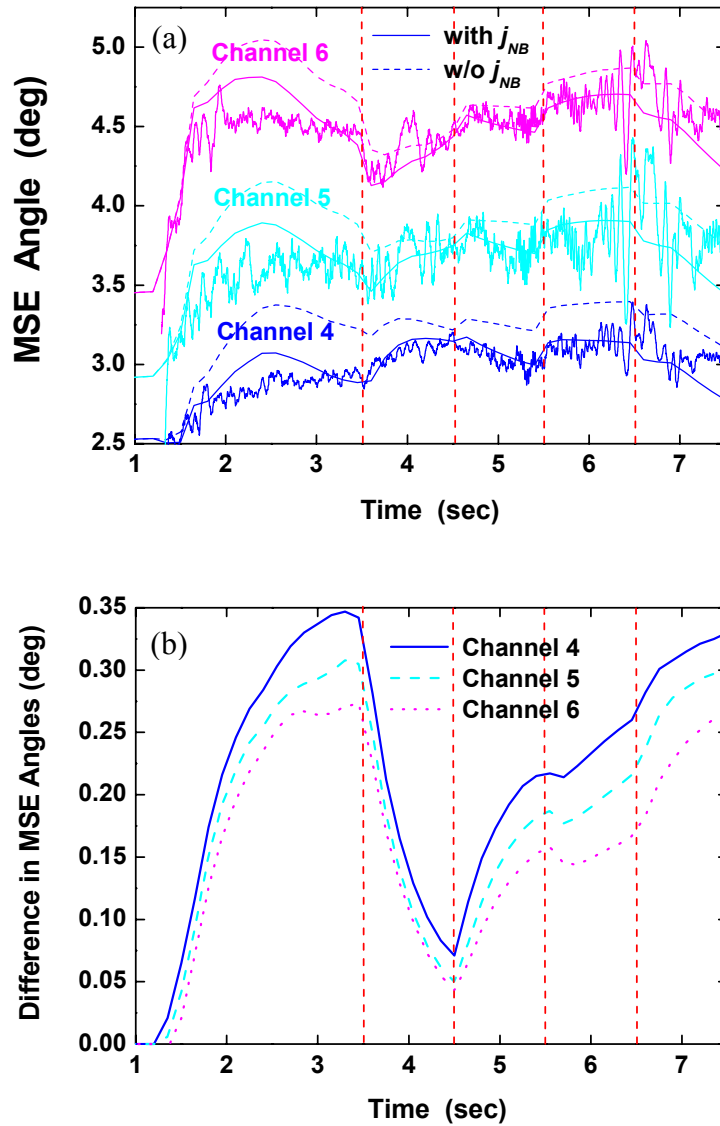
Figure 4.13. (a) MSE angles from experimental measurements (with small oscillations), ASTRA simulations with (solid line) and without (dashed line) beam current drive calculation at channel 4, 5, 6. Note that the offset for experimental data is given to match the ASTRA result with beam current drive (the same as in figure 4.9 (b)). (b) Difference in MSE angles between ASTRA simulation with and without including NB current drive calculation for channel 4, 5, 6.

As mentioned in §4.3, the dominant effect that changes the MSE signals is the change of total stored energy in the plasma. In this experiment, when the beam source is changed from on-axis to off-axis or vice versa, the stored energy changes. As a result, MSE signals change. Changing the beam sources also changes the ion and electron temperature and electron density profiles. Variation in pressure gradients gives rise to changes of the bootstrap current profile and changes the current density profile. In figure 4.14, this effect is presented. The contributions to the total current density in the plasma show different behaviours when the beam sources are changed. Corresponding measured ion and electron temperature and electron density profiles are shown in figure 4.15 at several time points when different beam sources are applied. Ion and electron temperature profiles are obtained from CXRS measurements and from ECE measurements, respectively. Here, electron temperature profiles after 6sec are not shown since ECE diagnostic could not take data in this discharge after this time point. Electron density profiles are from interferometry data combined with Li beam diagnostic data. As shown in figure 4.15, similar result is observed for temperature profiles as in the simulations using the Weiland transport model presented in figure 3.6. For electron density profiles, such changes when beam sources are changed cannot be predicted by ASTRA simulations using the Weiland transport model as no particle transport model is included for simulations (experimental electron density profiles are used).
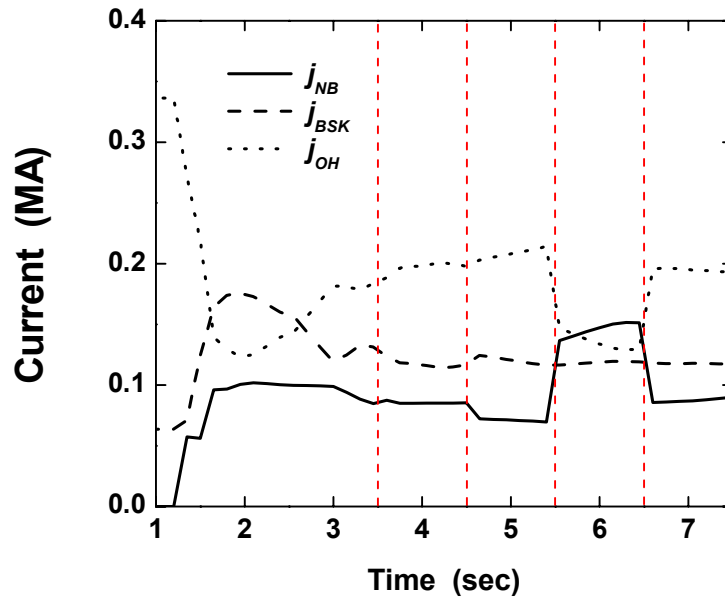
Figure 4.14. Time evolution of NB driven current, bootstrap current and ohmic current for pulse 17530 from ASTRA simulations. Time points where the beam source is changed are presented in vertical dashed lines.

Figure 4.15. (a) ion temperature profiles at 3.46 (when source 8 is applied), 4.45 (source 6), 5.44 (source 5), 6.43 (source 7) and 7.42sec (source 8 again). (b) electron temperature profiles at 3.45 (source 8), 4.45 (source 6), 5.45 (source 5) and 6.00sec (source 7). (c) electron density profiles at 3.45 (source 8), 4.43 (source 6), 5.45 (source 5), 6.49 (source 7) and 7.47sec (source 8 again).

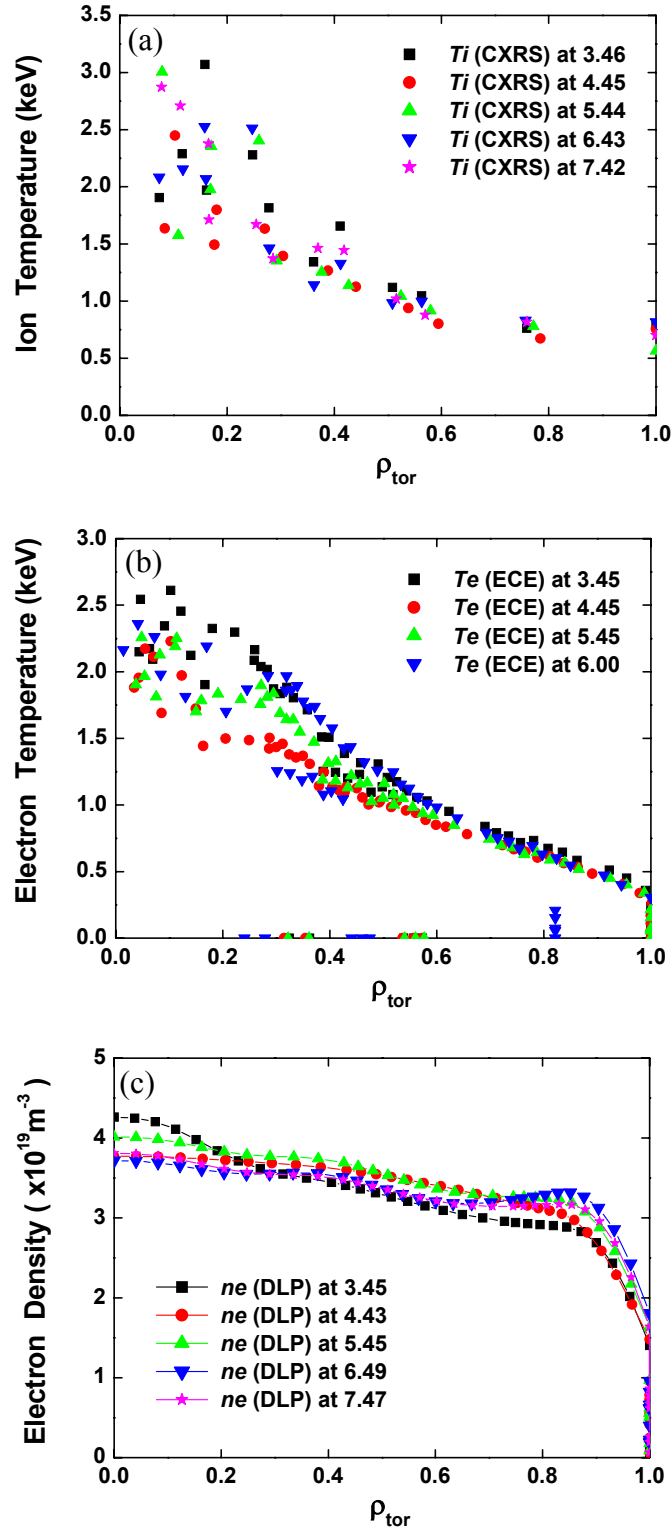As presented above, MSE signals are clearly varied during the experiment when the beam source is changed, though change of stored energy plays a main role to change the MSE signals. However, in other experiments, no significant changes are observed in the MSE signals (at fixed stored energy) when beam source is changed from on-axis to off-axis or vice versa (see figure 4.16) [58].
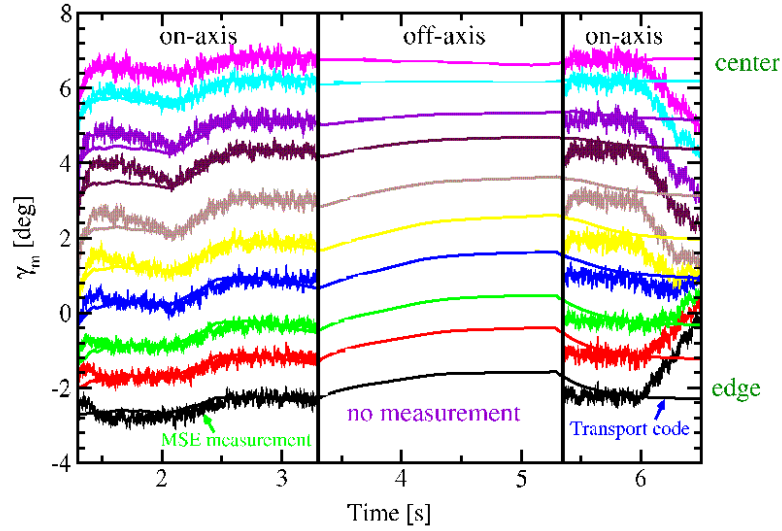

Figure 4.16. MSE angles from experimental measurements (with small oscillations) and the ASTRA simulation including beam current drive calculation in pulse 14513.

Plasma current in this discharge (pulse 14513) is 800kA and two beam sources are used. First, two on-axis beam sources are switched on and then they are replaced by two off-axis beam sources around 3.3sec. Off-axis beam sources are replaced by on-axis sources around 5.4sec again. As shown in figure 4.16, ASTRA predicted that MSE polarisation angles evolve while off-axis sources are used and change their trends after on-axis sources are switched on again. It shows 1 degree difference between start of off-axis injection and end for outer channels. It is not observed in measured MSE angles (during the off-axis phase the MSE angles cannot be measured). Moreover, temperature profiles do not change significantly when sources are changed.

Two other experiments are performed and compared with two beam sources and 800kA of plasma current; one uses two off-axis beam sources (pulse 15884) and the other uses two on-axis beam sources (pulse 15887) during the entire discharge. Ohmic transformer currents for both discharges are presented in figure 4.17.
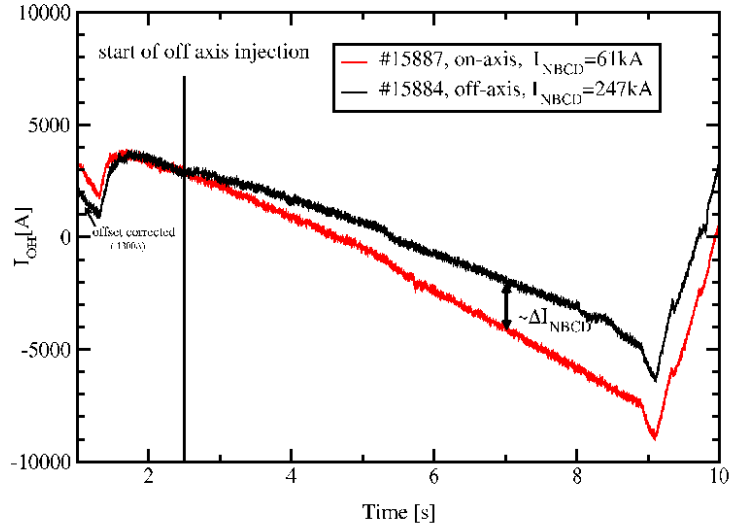
Figure 4.17. Ohmic transformer currents for on- and off-axis injection for pulse 15884 and pulse 15887, respectively.

As shown in figure 4.17, significant change is observed between two discharges. It implies that NB current is driven in the plasma and the observed difference (change in dI_{OH}/dt) results in NB current drive.

Therefore, in some experiments at ASDEX Upgrade, off-axis current drive is seen, while in other experiments this is not observed, although the total current drive is in agreement with simulations. It could depend on the heating level applied. At higher input power, transport in the plasma is dominated by ITG turbulence, which could play a dominant role to redistribute fast particles. However, more work is needed to investigate this.

4.5 Summary of the Results and Discussion

In chapter 3, models for current profile control system at ASDEX Upgrade are calculated with a given database (training dataset). Then, it is necessary to test them with a different database (test dataset), which was not used for calculating the models. To produce a test dataset, a simple step response is applied to input signals of the system (variation of NB powers from four beam sources) and the reaction of output signals of the system (variation of poloidal beta and current density values at three radial positions) are simulated by ASTRA code and stored. These output signals are also calculated by the models. The calculated output signals by identified models are

good in agreement with the calculated output signals by ASTRA code. Among the models, one, appropriate in view of controller during the controller design stage, will be selected for current profile control at ASDEX Upgrade (not part of this thesis).

A discharge is designed to validate identified models experimentally by switching the four NB sources in sequence. Comparing current density profiles from the experiment to those from ASTRA simulations, calculation of current density profile with ASTRA code can be verified. Experimentally obtained MSE signals are directly compared to MSE signals calculated by ASTRA code. The experimental set-up for the discharge is similar to the discharge used for producing training dataset in chapter 3 but the beam power in the stationary phase is reduced to 5MW (two NB sources) from 7.5MW (three NB sources). The time trends of non-calibrated MSE signals from 10 channels are compared to those calculated by ASTRA code. In these conditions, good agreement is found between them. It is clearly observed in this discharge that the MSE signals change when beam sources are changed. Moreover, it is also observed that not only electron temperature profiles and ion temperature profiles but also electron density profiles are changed when beam source is changed. Therefore, a particle transport model is also required for simulations for modelling as well as the energy transport model (the Weiland model).

The effect of local current drive by NBI is investigated by comparing ASTRA simulations with the MSE measurements for (i) an ASTRA simulation including the NB current calculation and (ii) an ASTRA simulation excluding the NB current calculation. Although, simulations with beam current drive fit the experimental data better compared to simulations without beam current drive, the differences are in the range of experimental error bars. The effect of local NB current drive using off-axis beam sources is still under investigation. In other experiment with plasma current 800kA, no significant change is observed in MSE angles when two beam sources are changed from on-axis to off-axis during the discharge. However, when ohmic transformer current is compared for two discharges, one with two on-axis sources, the other with two off-axis sources, a clear difference is observed.

From the results presented in this chapter, it is concluded that the method applied here to find models describing the relation between input and output signals can be used for real-time current profile control at tokamak experiments. Although using NBI as an actuator to control current density profile is arguable since its local current drive effect is not clear yet, the method to find a model described in the thesis can be applied to any other current profile control system if a transport code is available to produce training and test dataset.

Chapter 5

Summary and Conclusions

Motivation

The world's energy consumption will increase significantly due to the population explosion and increases in standards of living. Thermonuclear fusion is proposed to help energy production. As a magnetic confinement technique, a tokamak shows the best results in fusion research today. However, a tokamak is inherently pulsed as the confinement comes by combining a toroidal magnetic field with a poloidal field from a plasma current driven by a transformer. So-called advanced tokamak scenarios are developed to maximise the self-generated current (bootstrap current) in the plasma with the aim of achieving steady state operation. However, control of the current density profile is essential in these advanced scenarios to sustain the high fusion performance and high bootstrap current as the shape of current density profile is a key to improve confinement and stability of the plasma.

Scope of the Thesis

In this thesis, (i) the evolution of the current density profile in advanced scenarios is modelled and compared to experimental observations in the ASDEX Upgrade tokamak and the JET tokamak, (ii) modelling of current profile control is performed to prepare a system for real-time feedback control and (iii) the models for current profile control are verified by simulations and dedicated experiments for ASDEX Upgrade using current drive by neutral beam injection.

Transport Simulations of Advances Scenarios

For the duration of the work presented here, experimental measurements of the current density profile were not routinely available at ASDEX Upgrade, hence the majority of the work presented here is based on simulations with a transport code. To validate the models used in the transport code (ASTRA) for energy transport and current diffusion in the plasma, advanced scenarios at ASDEX Upgrade are modelled. By comparing the results with magnetic measurements and instabilities in the plasma, calculated current density profiles have been verified. The modelling of the current density profile requires a model for the ohmic current, a model for bootstrap current and a model for the current driven by external actuators (neutral beam injection). For energy transport, the Weiland transport model is used and simulated temperatures are compared to experimental measurements. These types of simulations have also been applied to advanced scenarios at JET. The simulated results are in good agreement with the experimental observations.

Modelling of Current Profile Control

For real-time current profile control, neutral beam injection has been proposed as an actuator in ASDEX Upgrade. For modelling of a system used for real-time control, a database is required to calculate transfer functions that describe relationship between input and output signals. The ASTRA code is used for the simulations. These simulations show that different current density profiles can be achieved when different beam sources are applied as the different neutral beam sources change the ohmic, the bootstrap and the neutral beam driven current density profiles due to changes in the temperature profiles, density profiles and tangential beam injection angle. Therefore, the input signals for the system are variations of neutral beam power from four beam sources with different injection trajectories in the plasma. The output signals are chosen: The variation of total plasma pressure (poloidal beta) and the variation of current density values at three radial positions. Using simulated beam modulations and storing the computed changes of the current density profile and plasma pressure, a database is created. Model structures can be defined which are well suited for systems with many input and output signals. This method is used to calculate a model describing the relationship between input and output signals and has been applied to ASDEX Upgrade and JET. For JET, six beam sources are used as input signals and the variation of total plasma pressure (poloidal beta) and the variation of current density values at five radial

positions as output signals. Due to the slower current diffusion time scale in JET compared to ASDEX Upgrade, different frequencies of modulation for input signals is used to ASTRA simulations.

Model Validation and Comparison to Experimental Observations

A validation of identified models is carried out using on the one hand, a different database produced by simulations calculating a step response to the neutral beam sources and on the other hand, dedicated experiments with measurements of the current density profile. The simulations confirm that the accuracy of the models obtained from the training dataset to predict the changes in the current density profile and total plasma pressure from changing neutral beam power or beam sources. Also the experiments show that current density profiles change when beam sources are changed from on-axis to off-axis or vice versa. This is again in agreement of the modelling by the ASTRA transport code or models computed for the use of current profile control.

However, observations in other experiments at ASDEX Upgrade show that theoretically predicted (computed by ASTRA simulations) off-axis current drive by off-axis neutral beams is not achieved in some plasma conditions; the current density profile remains similar despite changing the neutral beam injection from on-axis to off-axis sources. As a result, the effect of neutral beam current drive is specifically investigated for the experiments performed to validate the models for current profile control.

Discussion and Recommendations

The thesis mainly uses transport simulations including a model for neutral beam current drive. Experiments have put the validity of the models used for neutral beam current drive into question. Experiments show that in some conditions off-axis deposited fast ions (by off-axis neutral beam heating) do not lead to significant off-axis current drive. Therefore, the fast ion population must be redistributed (towards centre, not described in the theory). The main reason for differences between simulations and experiments, is still under investigation. However, it is clear that the initial fast ion population is determined by the neutral beam injection geometry and plasma parameters. One possible candidate for the redistribution of the fast ions could be the plasma turbulence, which determines the anomalous energy transport in the plasma. The differences

between the simulated current density profile changes with off-axis heating and experiments are most pronounced when turbulence dominates the energy transport. The effect of this turbulence can be observed by a resilience of the temperature profiles in the plasma to variations of the heating power (stiff profiles). Future experiments are planned at ASDEX Upgrade and JET to investigate this hypothesis.

The use of neutral beams as a real actuator for current profile control can be put into question. However, it is observed that neutral beam injection can modify the current density profile when temperature profiles are not stiff. This implies that neutral beams could still be used for the control of the current density profile in current ramp-up phase and in plasmas with internal transport barriers, where turbulence is suppressed. In this context, it would be very useful to be able to identify plasma phases of tokamak discharges, which are turbulence dominated or not. This would enable an adaptive controller for current profile control to change gains for corresponding plasma conditions.

The method presented in this thesis could be applied for any other current drive method, for example radio-frequency heating methods, if models for these current drive actuators are available in ASTRA. Furthermore, other transport codes and transport models can be employed instead of ASTRA and the Weiland transport model. Seeing the results for JET, the method developed for ASDEX Upgrade can be used directly for current profile control in other tokamak experiments, provided the modulation time is adjusted to typical current diffusion time scale of the experiment. In addition, the method is applicable to pressure profile control simply by replacing current density profile to pressure profile.

It is worthy to note that the approach developed here appears to have widespread applicability for plasma profile control in existing and future experiments.

Bibliography

[1] J. D. Lawson 1957 *Proc. Phys. Soc.* **B70** 6

[2] R. J. Bickerton *et al* 1971 *Nature Phys. Sci.* **229** 110

[3] M. Kikuchi 1990 *Nucl. Fusion* **30** 265

[4] K. Okano *et al* 1989 *Fusion Tech.* **16** 73

[5] F. Wagner *et al* 1982 *Phys. Rev. Lett.* **49** 1408

[6] ITER Physics Basis 1999 *Nucl. Fusion* **39** 2137

[7] H. Zohm 1996 *Plasma Phys. Control. Fusion* **38** 105

[8] M. Greenwald *et al* 1988 *Nucl. Fusion* **28** 2199

[9] The JET Team 1997 *Plasma Phys. Control. Fusion* **39** B353

[10] Y. Koide *et al* 1996 *Plasma Phys. Control. Fusion* **38** 1011

[11] F. M. Levinton *et al* 1995 *Phys. Rev. Lett.* **75** 4417

[12] E. J. Strait *et al* 1995 *Phys. Rev. Lett.* **75** 4421

[13] O. Gruber *et al* 1999 *Phys. Rev. Lett.* **83** 1787

[14] A. C. C. Sips *et al* 2003 *Proc. 30th Europ. Phys. Soc. Conf. on Control. Fusion and Plasma Phys., St. Petersburg*

[15] Y. Kamada *et al* 1999 *Nucl. Fusion* **39** 1845

[16] M. R. Wade *et al* 2001 *Proc. 28th Europ. Phys. Soc. Conf. on Control. Fusion and Plasma Phys., Montreux*

[17] A. C. C. Sips *et al* 2002 *Plasma Phys. Control. Fusion* **44** B69

[18] A. C. C. Sips *et al* 2003 *Fusion Tech.* **44** 605

[19] G. Federici *et al* 2003 *Plasma Phys. Control. Fusion* **45** 1523

[20] O. Gruber *et al* 2000 *Nucl. Fusion* **40** 1145

[21] A. C. C. Sips *et al* 2002 *Plasma Phys. Control. Fusion* **44** A151

[22] T. Ohkawa 1970 *Nucl. Fusion* **10** 185

[23] N. J. Fisch *et al* 1978 *Phys. Rev. Lett.* **41** 873

[24] F. M. Levinton *et al* 1989 *Phys. Rev. Lett.* **63** 2060

[25] P. J. McCarthy *et al* 1999 IPP-Report IPP 5/85

[26] H. Wind 1972 *Proc. CERN Computing and Data Processing School, CERN 72-21,* p 53

[27] G. Pereverzev *et al* 1991 IPP-Report IPP 5/42

[28] J. Weiland *et al* 1989 *Nucl. Fusion* **29** 1810

[29] S. P. Hirshman *et al* 1977 *Nucl. Fusion* **17** 611

[30] M. Kotschenreuther, W. Dorland *et al* 1995 *Phys. Plasmas* **2** 2381

[31] S. -I. Itoh, K. Itoh *et al* 1996 *Plasma Phys. Control. Fusion* **38** 1743

[32] V. Parail, B. Balet *et al* 1998 *Plasma Phys. Control. Fusion* **40** 805

[33] R. E. Waltz *et al* 1997 *Phys. Plasmas* **4** 2482

[34] Y. B. Kim *et al* 1991 *Phys. Fluids B* **3** 2050

[35] G. Tardini *et al* 2002 *Nucl. Fusion* **42** 258

[36] G. Pereverzev *et al* 1999 *Proc. 26th Europ. Phys. Soc. Conf. on Control. Fusion and Plasma Phys., Maastrict* **23J** 1429

[37] T. S. Hahm, K. H. Burrell *et al* 1995 *Phys. Plasmas* **2** 1648

[38] H. Meister 2000 IPP-Report IPP 10/16

[39] W. Suttrop *et al* 1998 IPP-Report IPP 1/306

[40] H. Murmann *et al* 1992 *Rev. Sci. Instrum.* **63** 4941

[41] J. Schweinzer *et al* 1995 *Proc. 22nd Europ. Phys. Soc. Conf. on Control. Fusion and Plasma Phys., Bournemouth* **19C** 253

[42] K. F. Mast *et al* 1991 *Rev. Sci. Instrum.* **62** 744

[43] Yong-Su Na *et al* 2002 *Plasma Phys. Control. Fusion* **44** 1285

[44] S. Günter *et al* 2001 *Phys. Rev. Lett.* **87** 275001

[45] A. Kallenbach *et al* 1991 *Plasma Phys. Control. Fusion* **33** 595

[46] G. M. Stäbler *et al* 1997 *Nucl. Fusion* **37** 287

[47] B. B. Kadomtsev 1975 *Fiz. Plazmy* **5** 710

[48] C. D. Challis *et al* 1989 *Nucl. Fusion* **29** 563

[49] R. J. Goldston *et al* 1981 *J. Comput. Phys.* **43** 61

[50] R. C. Wolf *et al* 2001 *Nucl. Fusion* **41** 1259

[51] A. G. Peeters *et al* 2002 *Nucl. Fusion* **42** 1376

[52] J. Hobirk *et al* 2001 *Phys. Rev. Letter* **87** 085002

[53] *System Identification Tool Box for Use with MATLAB*, The Math Works, 1995

[54] D. Moreau *et al* 2003 *Nucl. Fusion* **43** 870

[55] D. Mazon *et al* 2003 *Plasma Phys. Control. Fusion* **45** L47

[56] F. Crisanti *et al* 2003 *Proc. 30th Europ. Phys. Soc. Conf on Control. Fusion and Plasma Phys., St. Petersburg*

[57] R. Dux *et al* 2003 *Jour. Nucl. Mat.* **313** 1150

[58] J. Hobirk *et al* 2003 *Proc. 30th Europ. Phys. Soc. Conf. on Control. Fusion and Plasma Phys., St. Petersburg*

et cognoscetis veritatem et veritas liberabit vos

John 8:32